SORPTION STUDIES OF

THE SURFACE MODIFIED ACTIVATED CARBON

WITH β-CYCLODEXTRIN

A Thesis Submitted to the College of

Graduate Studies and Research

In Partial Fulfillment of the Requirements

In the Department of Chemistry

University of Saskatchewan

Saskatoon

By

Jae Hyuck Kwon

Permission to Use

In presenting this thesis in partial fulfilment of the requirements for a Postgraduate degree from the University of Saskatchewan, I agree that the Libraries of this University may make it freely available for inspection. I further agree that permission for copying of this thesis in any manner, in whole or in part, for scholarly purposes may be granted by Professor Lee D. Wilson who supervised my thesis work or, in their absence, by the Head of the Department or the Dean of the College in which my thesis work was done. It is understood that any copying or publication or use of this thesis or parts thereof for financial gain shall not be allowed without my written permission. It is also understood that due recognition shall be given to me and to the University of Saskatchewan in any scholarly use which may be made of any material in my thesis.

Requests for permission to copy or to make other use of material in this thesis in whole or part should be addressed to:

Head of the Department of Chemistry
University of Saskatchewan
Saskatoon, Saskatchewan
Canada S7N 5C9

ABSTRACT

Activated Carbon (AC) is an amorphous carbon-based material characterized with a large surface area (~ 1,000 m^2/g) and consists primarily of graphitic (sp^2 hybridization) layers. Its amphoteric chemical property results because of the chemical treatment of the surface of AC with oxidizing agents, reducing agents, and grafting agents. β-cyclodextrin (β-CD) is a very interesting carbohydrate oligomer that provides very strong binding ability for small organic guest molecules in its inner cavity (6.0 ~ 6.5 Å) by van der Waals interactions and hydrogen bond formation between the guest molecules and the host.

Surface modification of AC with β-CD was synthesized by chemical methods: oxidation with HNO_3, reduction with $LiAlH_4$, and grafting β-CD onto the surface of AC via organic linkers such as glutaraldehyde and 1,4-phenylene diisocyanate. This surface grafted AC with β-CD, then, was evaluated for its surface area and sorption performance by using a solution dye sorption method using dye adsorbates.

Surface functional groups produced from oxidation (carboxylic acid, lactone, quinine, phenol, and nitro groups), reduction (alcohol and amine groups), and grafting (imine, hemiacetal, and urethane bonds) methods including microscopy of untreated, surface modified, and grafted ACs were characterized by various surface characterization methods: Diffuse Reflectance Infra-red Fourier Transform Spectroscopy (DRIFTS), Scanning Electron Microscopy (SEM), Raman spectroscopy, X-ray photoelectron spectroscopy (XPS), Thermogravimetric analysis (TGA), Differential thermogravimetry (DTG), Matrix Assisted Laser Desorption Ionization Time of Flight mass spectrometry (MALDI TOF MS), and Electron spin resonance (ESR) spectroscopy. A chemical method, the Boehm method, was used for identifying surface bound acidic and basic functional groups. Nitrogen porosimetry was used to analyze the surface area and pore structure characteristics of AC, surface modified ACs, and grafted ACs.

p-nitrophenol (PNP) and methylene blue (MB) were used as adsorbates for the dye sorption method. PNP and MB were used to measure the sorption performance of grafted ACs at equilibrium using UV-vis spectrophotometry in aqueous solution. Sorption capacity (Q_e), surface area (m^2/g), and binding affinity characteristics [K_F (L/g), K_L (g/mol), and K_{BET} (L/g)] were determined at equilibrium conditions using fundamental sorption models such as Langmuir, Freundlich, and BET isotherms. The sorption performance of grafted ACs and granular AC were different according to the difference in surface area and pore structure characteristics of each material.

ACKNOWLEDGEMENTS

First of all, I would like to sincerely thank my supervisor, Professor Lee D. Wilson, who has guided my research and coached my research attitude on chemistry. I would like to thank the members of Research Committee, Professor Stephen Foley, Professor Dale Ward, Professor Robert Scott, Professor Matthew Paige, and Professor Stephen Urquhart, who corrected my research work when it was astray in the track. I would like to thank all faculty in the Department of Chemistry for their teachings. I would like to thank my laboratory colleagues, Mohammed Hamid Mohammed, Olubumi Fadeyi, Sarker Mahmud for their kind help in filling the knowledge gaps between theory and experiment. I would like to thank the Department of Chemistry for their provision of Teaching Assistantship and also NSERC for their research support.

During the past two years, while I was studying here at the University of Saskatchewan, Gloria, John, David, and Daniel have encouraged me to work wise and hard and all Korean church members have prayed consistently for my study. I would like to thank them from the bottom of my heart.

Finally, I always thank God because He is such a good shepherd to me.

TABLE OF CONTENTS

LIST OF TABLES

LIST OF FIGURES

LIST OF SCHEMES

LIST OF ABBREVIATIONS

AC: Activated carbon
ACAMID: Amidizied ACOXID
AC-β-CD: Grafted activated carbon with β-cyclodextrin via glutaraldehyde
ACCDP: Physisorbed β-CD onto AC
ACF: Activated carbon fiber
ACGAP: Physisorbed GA onto AC
ACOXID: Oxidized AC
ACOXID: Oxidized activated carbon
ACPDICD: Surface modified AC with β-CD via 1,4-phenylen diisocyanate
ACREDUCT: Reduced ACOXID
Ar: Argon
BET: Brunauer, Emmett, and Teller
CAS: Chemical Abstract Service
CD: Cyclodextrin
CGT-ase: cyclodextrin glucosyl transferase enzyme
CHCA: α-cyano-4-hydroxycinnamic acid
CNT: Carbon nanotube
DCC: Dicyclohexylcarbodimide
DMF: N,N-dimethyl formamide
DMSO-d_6: Perdeuterated dimethyl sulfoxide
DRIFTS: Diffuse Reflectance Infrared Fourier Tranform spectroscopy
DTG: Differential thermogravimetry
EDA: Ethylenediamine
EPI: Epichlorohydrin
ESR: Electron spin resonance
eV: Electron volts
GA: Glutaraldehyde
Gpa: Giga Pascal
HPLC: High pressure liquid chromatography
ICP AES: Inductively coupled plasma atomic emission spectrometry
IEP: Isoelectric point
IR: Infrared
M.W.: Molecular weight
MALDI TOF MS: Matrix-assisted laser desorption ionization time of flight mass spectrometry
MB: Methylene Blue
mg: miligram
MHz: Mega Hertz
mM: milli-molar
n/a: Data not available
NLLS: Non-linear least squares
NMR: Nuclear magnetic resonance
PDI: 1,4-phenylene diisocyanate
PNP: Para-nitrophenol
$PNPO^-$: deprotonated PNP

ppb: Parts per billion
ppm: Parts per million
ppt: Parts per trillion
PZC: Point of zero charge
r.b.: Round bottom
SEM: Scanning electron microscopy
SF: Sodium fluorescein
SIMS: Secondary ion mass spectroscopy
SSR: Sum of squares of residuals
SWCN: Single-wall carbon nanotube
TEM: Transmission electron microscopy
TFA: 1,2,3-trifluoro acetic acid
TGA: Thermogravimetric analysis
THF: Tetrahydrofuran
TMS: Tetramethylsilane
TosCl: Tosyl chloride (p-toluenesulfonyl chloride)
TPD: Temperature programmed desorption
UV-Vis: Ultra violet-Visible
VOCs: Volatile organic compounds
W/W: Weight per weight
XPS: X-ray photoelectron spectroscopy
μm: micrometer

CHAPTER 1

INTRODUCTION

1.1 Activated Carbons (ACs)

1.1.1 Introduction

AC [Chemical Abstract Service (CAS) registry number: 7440-44-0 and atomic weight (A.W.): 12.00 g][1,2] is a carbon-based material which has a high surface area and relatively high porosity. Its structure[3] is shown in Figure 1.1 and it is primarily composed of sp^2 graphite crystallites which comprise 3 to 4 parallel hexagonal carbon ring layers separated by 3.44 - 3.65 Å interlayer spacing which is slightly greater than that (3.35 Å) in graphite and are approximately 10 nm in length. However, the major structure in AC is composed of microcrystalline (amorphous) graphitic-like sheets, called "basal planes", which are randomly cross-linked, unevenly stacked, and surrounded by a number of unpaired electrons. These particular architectural features make AC enormously porous and useful for applications in catalysis and adsorption with a wide range of molecules. Moreover, AC contains various heteroatoms such as oxygen, hydrogen, nitrogen, phosphorous, and sulfur. However, the covalently bound atomic or adsorbed molecular oxygen is the major heteroatom which can strongly alter the chemical properties of AC.

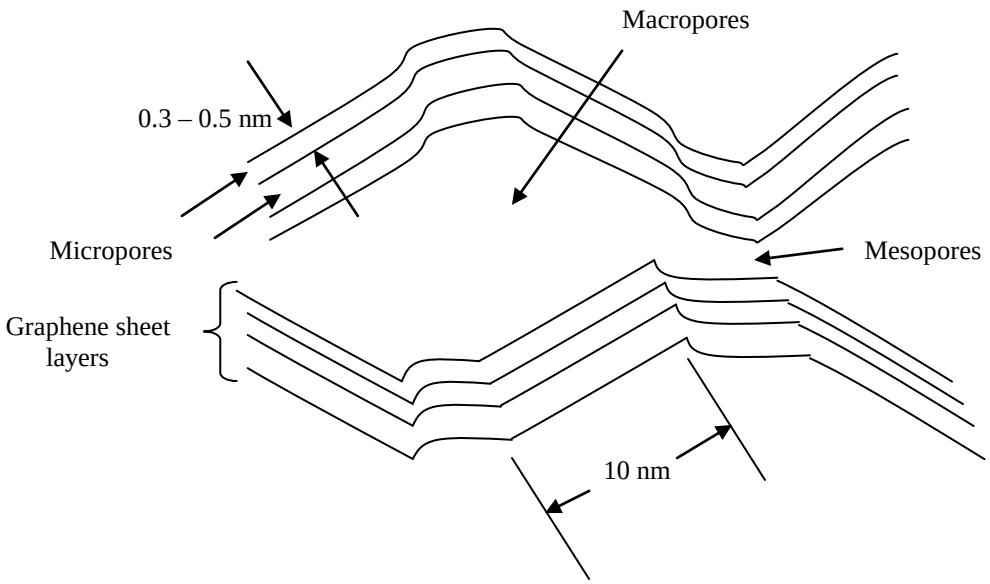

Figure 1.1 Diagram of AC structure. Straight line segments refer to graphene sheets.

The range of pore sizes which is defined according to the International Union of Pure and Applied Chemistry (IUPAC) is shown in Table 1.1.[4]

Table 1.1 IUPAC classification of pore sizes

Pores	Pore width (w)
Ultramicropores	w < 0.7 nm
Supermicropores	0.7 nm < w < 2.0 nm
Mesopores	2.0 nm w < w < 50.0 nm
Macropores	50.0 nm < w

The highly porous AC can adsorb compounds which can be accommodated within the pore structure according to their molecular size or onto the surface of AC. For example, small molecules (< 2 nm) can be captured within the micropores of AC; Abe *et al.*[5] showed that macroporous AC can bind a large molecule such as γ-cyclodextrin, whereas microporous AC can bind different sized molecules on the based of size exclusion, such as α-cyclodextrin, and this occurs by adsorption within the micropores. To determine the porosity of AC by the manufacturer, molecular iodine is mostly used

for measuring internal microporosity content by measuring the adsorbed amount of the standard solution of iodine (0.02 M) treated with a standard AC sample by the American Society for Testing and Materials (ASTM) D 4607-94 (2006). Methylene blue is used for measuring mesoporosity content by measuring absorbance of a decolorized standard solution (1 ppm) of methylene blue with a UV spectrophotometer at 668 nm after treating methylene blue for 48 hours with a standard AC sample.[6] Molasses is used for measuring macroporosity content by measuring the ratio of optical density of the filtrate of molasses solution which is adsorbed by a standard AC sample and the unknown sample.[6] The numbers of iodine (mg/g), methylene blue (mg/g), and molasses adsorbed are approximately equivalent to surface area (m^2/g).

1.1.2 Commercial Production of ACs

AC is produced by carbonizing and subsequent activation of the raw materials. Raw materials are any organic materials with a high carbon content (e.g., sawdust, coconut shells, peat, black ash, charcoal, lignite, bituminous coal, and petroleum coke) and can be properly chosen to have high density for enhancing the structural strength and low ash content for enhancing porous char. Carbonization means that raw materials are converted into a disordered carbon structure with a very low volatile carbon content at high temperature (< 800 °C) in an inert gaseous atmosphere. In this process, non carbon elements (hydrogen and oxygen) are outgassed by pyrolytic decomposition and the free elementary carbon atoms self assemble to form elementary graphite crystallites. The process of activation is achieved by either thermal or chemical means and pore diameters are enlarged by removing any tarry substances, and as a result, some new pores are created. In thermal activation, highly microporous structures with small amounts of surface oxides (approximately 3 - 5 % volatiles) are obtained by oxidizing carbon atoms with an oxidizing agent (e.g., steam and CO_2) around 1,000 °C and followed by exposure to air at 400 °C. At the oxidizing temperature, carbons react with oxidizing agents to form gaseous products endothermically[7] which results in pore formation. Prolonged activation can produce bigger pores. This oxidation process is endothermic and is described in equations (1.1) and (1.2).

$$C_{(s)} + H_2O_{(g)} \rightarrow CO_{(g)} + H_{2\,(g)} \text{ (29 kcal/mol)} \quad (1.1)$$

$$C_{(s)} + CO_{2\,(g)} \rightarrow 2\,CO_{(g)} \text{ (39 kcal/mol)} \quad (1.2)$$

Macropores arising from randomly cross-linked and unevenly stacked basal planes are found on the surface of AC, however meso- and micorpores are found within the structure of AC because those pores are the result of oxidation. A schematic[7] of the porous structure of AC is shown in Figure 1.2. Furthermore, heteroatoms are covalently bonded into the structure of AC during carbonization (e.g., nitrogen from the inert atmosphere) and activation (e.g., oxygen, hydrogen, sulfur, and phosphorous from chemical oxidizing agents).

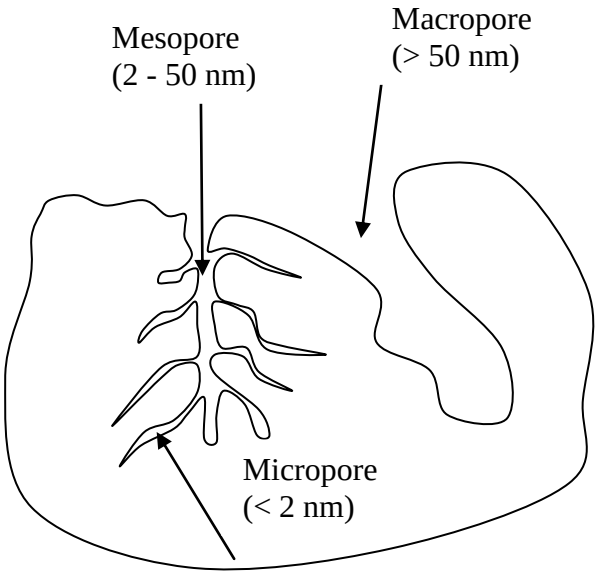

Figure 1.2 Schematic of the pore structure observed in AC

Chemical activation produces mesopores and is a combined process of carbonization and activation at relatively low reaction temperatures (400 °C - 650 °C). Raw materials are wood and any cellulose-based materials and saturated with activating (dehydrating) agents such as sulfuric acid, phosphoric acid, and zinc chloride. These dehydrating agents can facilitate the pyrolytic decomposition by reducing water of hydration, but also which can inhibit the formation of tar by preventing cellulose

material from collapse. Chemically treated material is then heated in the absence of oxygen, cooled, and then washed to remove activating agents which are recyclable.

1.1.3 Physical and Chemical Properties of ACs

The typical properties of NORIT® ROX 0.8 which was used as the AC for this research are shown in Table 1.2. Those properties were obtained from the manufacturer of NORIT® ROX 0.8 from NORIT America Inc.

Table 1.2 Typical properties of NORIT® ROX 0.8 (Literature values obtained from reference 8)

Properties	Values(*)
Methylene blue adsorption, g/100g	22
Surface area (BET), m^2/g	1100
Apparent density, kg/m^3	400
Ash, mass %	3
Calcium, mass %	0.01
Chloride, mass %	0.1
pH	Neutral

(*) based or "as received" NORIT ROX 0.8 activated carbon material

Surface area of BET (m^2/g) is measured by nitrogen porosimetry at 77K to estimate the micropore characteristics. Inorganic materials present in AC originate from the raw materials as essential metals (e.g., Mg, Fe, Zn, etc), but also from the manufacturing processes such as preparation of raw materials from soil or chemical activation and metal-containing solvents which are used for washing of AC materials. Metal containments are typically Fe, Na, Ca, K, Mg, Pb, Zn, and Cu and their content is approximately from 10^1 ppm (Pb, Cu, and Zn) to 10^2 ppm (Na, Ca, and Na). This content is related to the ash contents because their high melting points can make them to be metal oxide residues when they are combusted.

1.1.3.1 Surface modification

Surface modification of AC involves oxidation and further grafting onto the AC surface by chemical, electrochemical, and microwave to introduce organic functional groups (e.g., carboxylic acid, amine, etc) and molecules such as cyclodextrin (CD). Oxidation can be achieved by chemical modification[9,10,11], air oxidation[10,11,12], electrochemical oxidation[13,14,15], and plasma or ozone treatment.[16] Typical oxidizing agents are nitric acid[9,10,11], hydrogen peroxide, hypochlorite, permanganate, and perchlorate. Nitric acid is a major source of nitration (e.g., -NO_2 group), nitrosation (e.g., –N=O group), and oxidation is widely supported by a radical mechanism.[17,18] Nitration for AC is favored by a heterolytic process[19], whereas nitration for aliphatic hydrocarbons is favored by a homolytic process[19] where nitric acid is used as the reagent.

1.1.3.2 Mechanism for initiator

Identifying the mechanism of oxidation is helpful for a better understanding of the structure of surface bound functional groups on AC. Nitrogen dioxide radical formed from the homolytic process can further oxidize AC to produce carbonyl groups at the surface of AC, according to nitration mechanism outlined in equations (1.3) – (1.11).

Nitration for aliphatic: homolytic process $HONO_2 \rightarrow HO\cdot + NO_2\cdot$ (1.3)

Nitration for aromatic: heterolytic process $HONO_2 \rightarrow HO^- + NO_2^+$ (1.4)

(Adapted from reference 19)

$HNO_3 + HNO_2 \rightleftharpoons 2\cdot NO_2 + H_2O$ (1.5)

$\cdot NO_2 + H^+ \rightleftharpoons HNO_2^+\cdot$ (1.6)

$Ph_2CH_2 + HNO_2^+\cdot \rightarrow Ph_2CH\cdot + H_2NO_2^+$ (rate determining step) (1.7)

$Ph_2CH\cdot + \cdot NO_2 \rightarrow Ph_2CHONO$ (1.8)

$Ph_2CHONO + H_2O \rightarrow Ph_2CHOH + HNO_2$ (1.9)

$Ph_2CHOH + HNO_2^+\cdot \rightarrow Ph_2COH\cdot + H_2NO_2^+$ (1.10)

$Ph_2COH\cdot + \cdot NO_2 \rightarrow Ph_2C\text{-}ONO(OH) \rightarrow Ph_2CO + HNO_2$ (1.11)

(Adapted from reference 18)

Surface functional groups[20] commonly found on the surface of AC from oxidation are shown in Figure 1.3.

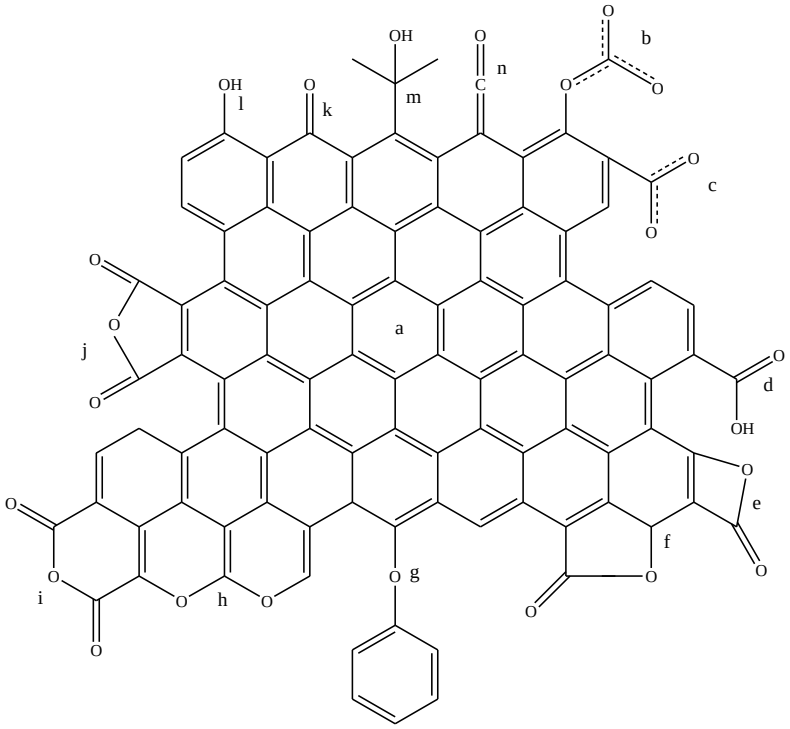

Figure 1.3 Surface functional groups on the surface of AC illustrating aromatic (a), carboxyl-carbonates (b and c), carboxylic acid (d), 4-membered ring lactone (e), 5-membered ring lactone (f), ether bridge (g), cyclic ethers (h), 6-membered ring cyclic anhydride (i), 5-membered ring cyclic anhydride (j), quinone (k), phenol (l), alcohol (m), and ketene (n).

Surface oxidation can produce three types of surface oxides[21] (acidic, basic, and neutral) which are bound to the edges of the carbon layers located at the periphery or defect sites (vacancies[22]), resulting in a more hydrophilic surface structure with surface oxides, which react either as weak acids (e.g., carboxyl acid) or bases (e.g., hydroxyl group) to the surface of AC. Surface oxides also provide chemisorption sites for water or other polar compounds based on their amphoteric behavior,[22,23] whereas an unmodified AC surface is generally hydrophobic. Acidic oxides are formed at high temperatures, and contain variable oxygen contents, which determine their acidity. High oxygen content provides more hydrophilic, acidic, and negative surface charge density, whereas low oxygen content provides more hydrophobic, basic, and positive surface charge density. Basic oxides[24] are formed by contacting oxygen at very low

temperatures (- 40 °C) after which AC was heated up to 1000 °C to remove any surface compounds. The chemisorbed oxygen to the surface of AC can bind to protons available in acidic solution. The Lewis base property of AC originates because of the π-electron system of the basal planes which donate electrons toward any reactive electron deficient functional groups in aqueous solution.

Chemical modification strategies which are shown in Scheme 1.1 begin with surface oxidation and then follow covalent attachment of organic molecules such as amide (I)[25,26,27,28] by a reaction at the carbonyl carbon of an acyl halide on AC employing thionyl chloride with DMF, and a diamine (e.g., ethylene diamine). Covalent attachment of an alkyl group (II)[29] can also occur at a halide moiety on AC by using a Grignard reagent. Microwave assisted modification is also possible for grafting amine, alcohol, and thiol groups.[30,31,32] Dielectric heating effects of microwave radiation can be applied to reduce reaction time and increase yields due to thermal effects resulting from polarization effects caused by dipole-dipole interactions between polar molecules and the electromagnetic field.[33] However, direct modification of organic molecules[34,35,36,37] [e.g., fluorination (III), addition of carbene (IV) and nitrene (V), radicals (VI), etc] which are applied to the functionalization of SWCN are also possible for AC because both SWNT and AC are very similar in terms of their electronic and chemical properties. By using a variation on the amidation mechanism, a dendrimer type of surface modification[36,38] (VII) can be achieved on the surface of AC.

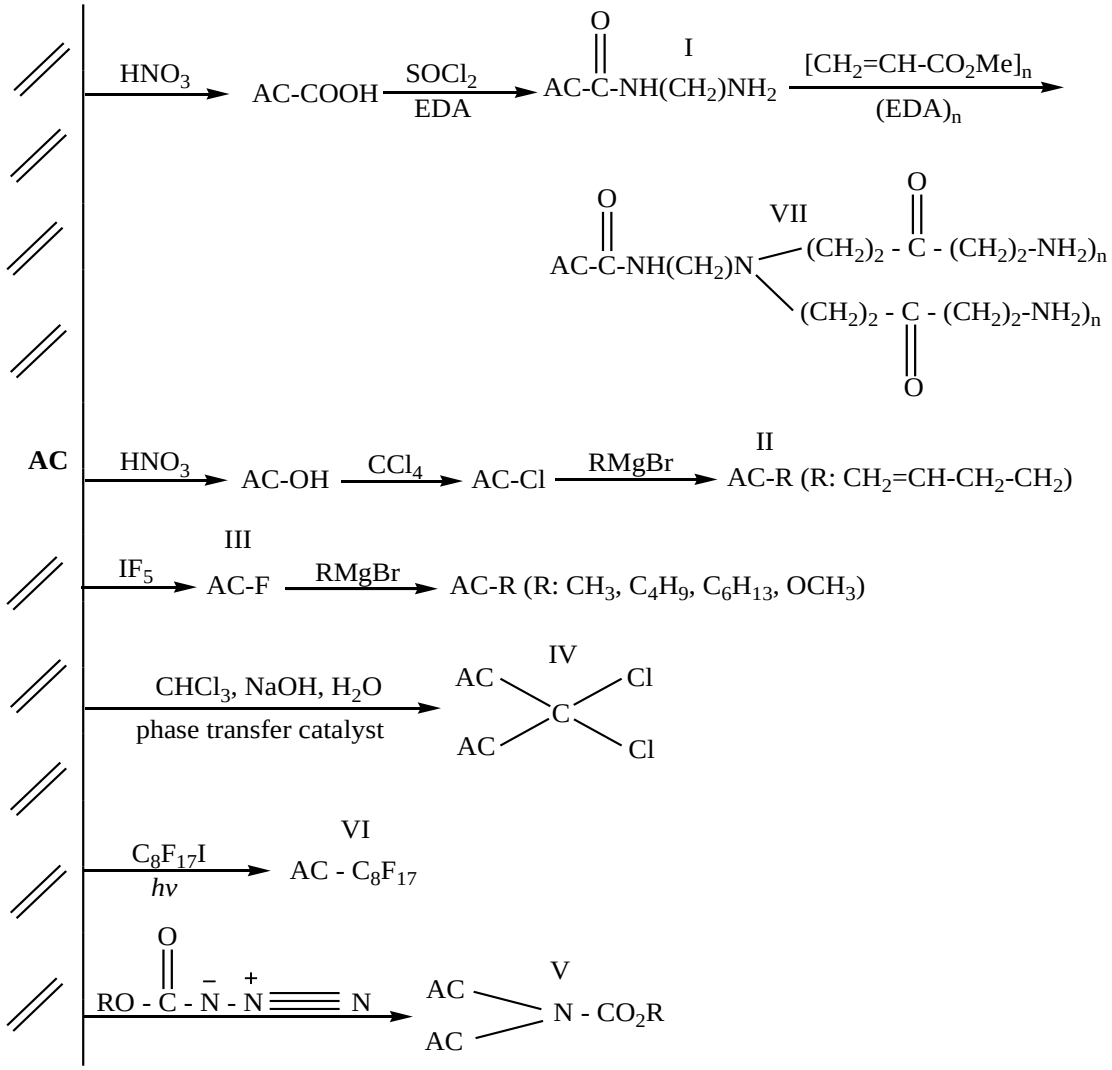

Scheme 1.1 A survey of grafting strategies of chemical modification on the surface of AC, where EDA = ethylene diamine and AC = activated carbon.

1.1.3.3 Grafting CD onto AC and other solid substrates

The grafting of CD onto carbon materials was achieved electrochemically[13] on the surface of carbon fibers by making an ether bond between the hydroxyl group of a carbon fiber and tosylated β-CD (I in Scheme 1.2). Chemical methods for the formation of a carbamate bond between the surface acid group of SWNT[39] and β-CD through 1,4-phenylene diisocyanate (PDI) linker (II in Scheme 1.2) and by forming an hemiacetal bond between an hydroxyl group of poly vinyl alcohol[40] polymer beads or polymeric acrylate microrbeads[41] and the hydroxyl group of β-CD through the

glutaraldehyde (GA) linker (III in Scheme 1.2). Other template solids for grafting CD are silica[42] by reacting tosylated β-CD to the amino functionalized silica and textiles[43] (e.g., polyester, cotton, and polyamide). Grafting was effected by reacting chlorinated or sulfonated β-CD to cyanuric chloride or amine derivatives of polymeric materials.

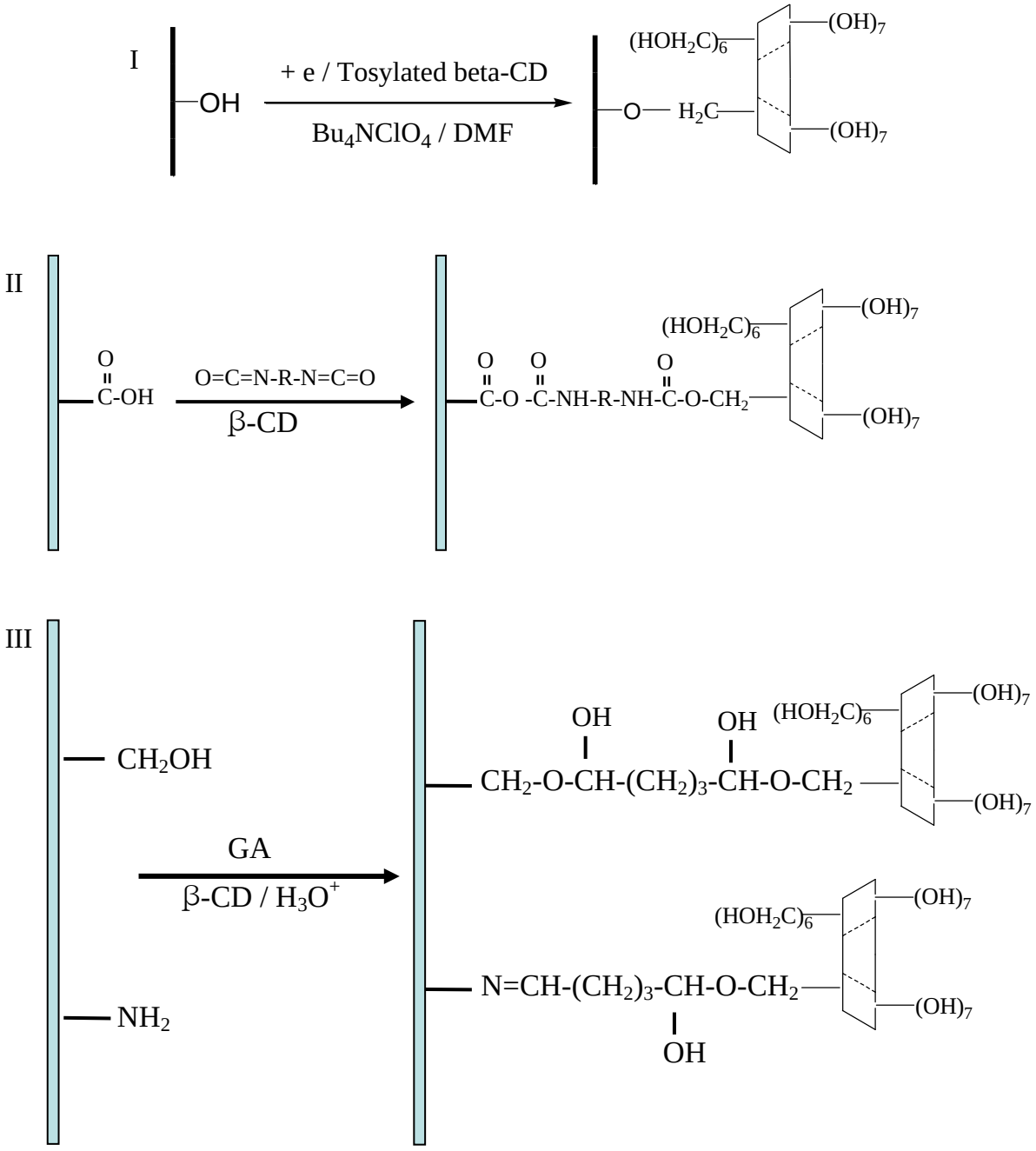

Scheme 1.2 Grafting strategies for β-CD attachment onto AC (the vertical shaded bar = AC surface for II and III and carbon fiber for I)

1.1.4 Application of AC materials

AC is widely used as an adsorbent for catalysis, catalyst support, solvent recovery, gas refining, air purification, exhaust desulfurization, and deodorization.[1,2] These applications are attributed to its porosity (micro-, meso-, and macroporosity) and to its sorption properties for offering better accessibility to reactants.

1.2 Cyclodextrins

1.2.1 Introduction

Cyclodextrins (CDs), (or called Schardinger's dextrins or cycloamyloses), are toroidal shaped (Figure 1.4) cyclic oligomers of glucose consisting of six (α-), seven (β-), or eight (γ-) D-glucopyranose units linked by α (1→4)-glucosidic bonds.[44] (See Figure 1.5) CDs have an apolar and electron-rich hydrophobic cavities[45] arising from their hydrocarbon backbone and polar hydrophilic periphery because of the 21 hydroxyl groups at the periphery of the macrocycle. The cavity can be used as a host receptor for appropriate sized liphophlic guest molecules by van der Waals interaction between the glucosidic oxygen atom and the guest molecule. (Figure 1.5)

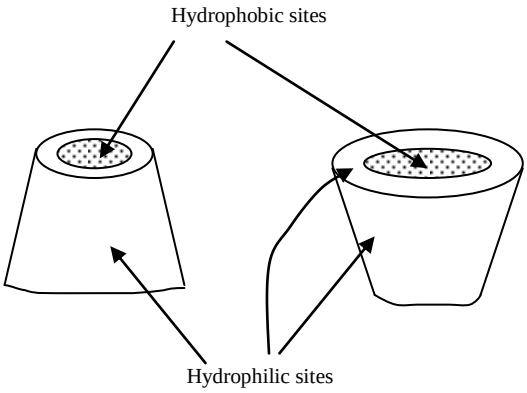

Figure 1.4 The general amphiphilic character of the CD torous is shown according to the presence of hydrophilic hydroxyl groups (not shown here) and the apolar CD interior.

In 1891, A. Villiers first isolated 3 g of α-, β-, or γ-CD and considered its empirical formula to be $(C_6H_{10}O_5)_2 \cdot 3H_2O$ when he digested starch with *Bacillus amylobactor*. Twelve years later, F. Schardinger isolated pure α-, and β-CD by forming a complex with molecular iodine, which was identified as the α-CD/iodine complex. The

complex is blue when it is damp and gray-green when it is anhydrous, whereas the β-CD/iodine complex is always brownish. In 1936, K. Freudenberg and his coworkers elucidated the molecular structure[46] of α-, β-, and γ-CD, which is shown in Figure 1.5 where Glu means glucose.

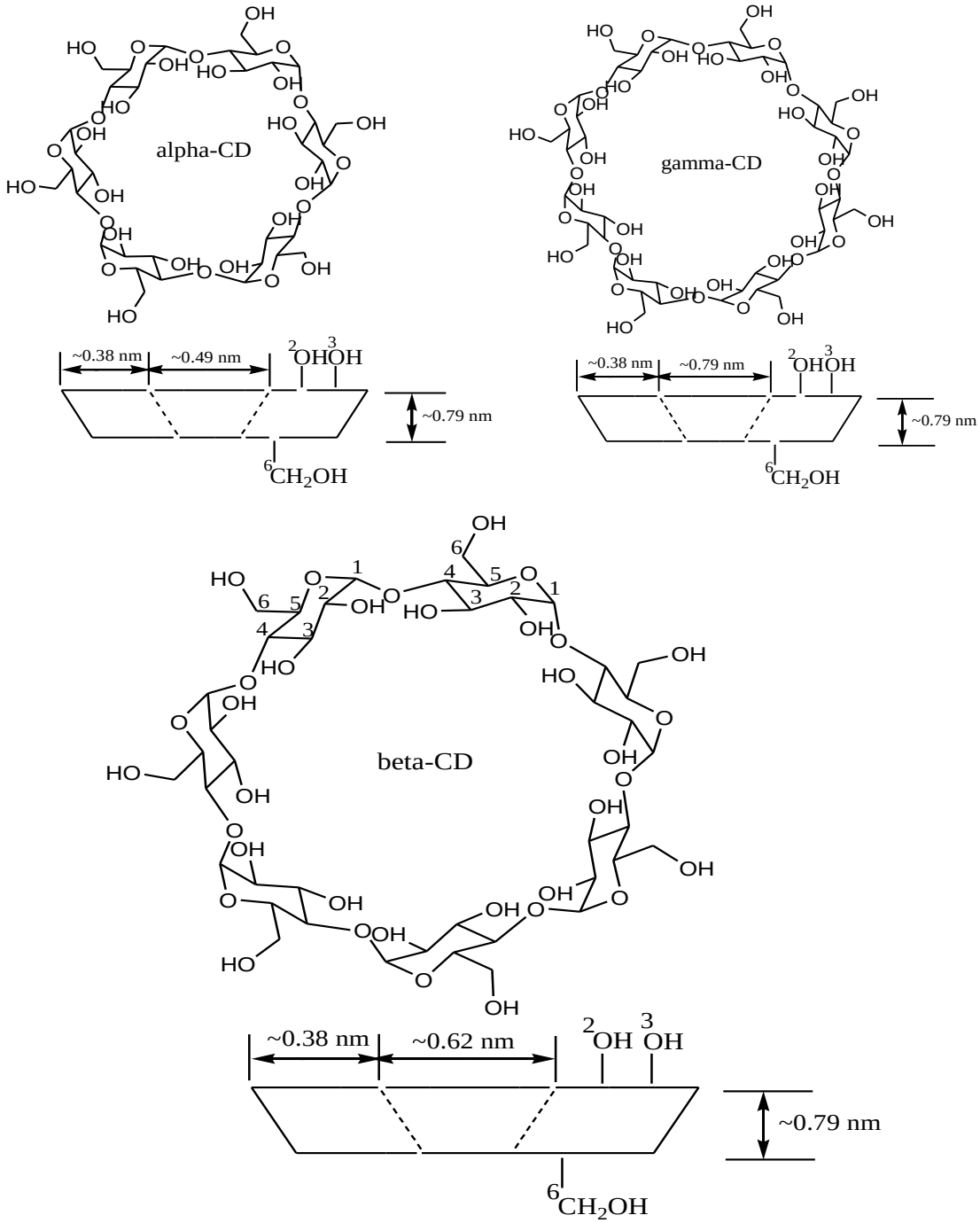

Figure 1.5 Molecular structure of α-, β-, and γ-CD and a schematic of its toroidal shape.

In the structure of β-CD in Figure1.5, there are seven primary hydroxyl groups which are freely rotating at the C6 position and can make its diameter narrow; however, there are fourteen secondary hydroxyl groups which are fixed at the C2 and C3 positions, situated at the wider side of the torus. This cyclic ring structure is stabilized by intramolecular hydrogen bonding between adjacent hydroxyl groups at the C2 and at the C3 positions. The internal CD cavity can include proper sized organic molecules by interacting van der Waals force and hydrogen bond between a CD and guest molecules and serve as Lewis base sites due to the presence of lone pairs of electrons of oxygen in the glucosidic bond framework.

β-CD has the highest inclusion complex formation constant (M^{-1}) with ibuprofen, 1-adamantanecarboxylic acid, and 4-*tert*-butylbenzoic acid, for example, rather than α-CD and γ-CD when it measured by capillary electrophoresis.[45] And also its solubility is the lowest among them due to its unique molecular structure. Therefore, β-CD was chosen as a grafting CD to AC because of its versatile inclusion properties and relative cost.

1.2.2 Manufacturing[45]

Liquefaction of the starch at elevated temperatures is the starting point to make CD in mass production. In the hydrolyzed starch solution, glucose or any low molecular oligosaccharides should not be contained because these carbohydrates can enormously reduce the yield of CD production. After cooling the starch solution, cyclodextrin glucosyl transferase enzyme (CGT-ase) is added to form a mixture of α-, β-, and γ-CDs. A solvent is then added to make a complex with CD, for example, toluene for β-CD complex, 1-decanol for α-CD complex, and cyclohexadecenol for γ-CD. Any insoluble complexes formed during complexation process are removed by filtration and the added solvent is removed by distillation or extraction. Finally, CD is separated with the purity of 99% or higher by crystallization and filtration.

1.2.3 Physical and Chemical Properties

Physical properties of CD are summarized in Table 1.3.

Table 1.3 Physical properties of α-, β-, γ-CDs[45]

Properties	α	β	γ
CAS No.	10016-20-3	7585-39-9	17465-86-0
No. of glucose units	6	7	8
Empirical formula (anhydrous)	$C_{36}H_{60}O_{30}$	$C_{42}H_{70}O_{35}$	$C_{48}H_{80}O_{40}$
M.W. (anhydrous)	972.85	1134.99	1297.14
Solubility in water, g/100mL at room temperature	14.5	1.85	23.2
Cavity diameter, Å	4.7 – 5.3	6.0 – 6.5	7.5 - 8.3
Length of torus, Å	7.9 ± 0.1	7.9 ± 0.1	7.9 ± 0.1
Diameter of outer periphery, Å	14.6 ± 0.4	15.4 ± 0.4	17.5 ± 0.4
Approx volume cavity, $Å^3$	174	262	427
Approx cavity volume in 1 mol CD (mL)	104	157	256
Approx cavity volume in 1 g CD (mL)	0.10	0.14	0.20
Crystal forms (from water)	Hexagonal plates	Monoclinic parallelograms	Quadratic prisms
pK_a (by potentiometry at 25 °C)	12.33	12.20	12.08

The small cavity diameter of α-, β-, or γ- CD as a host can include appropriate size molecules (guests) and the complexes[47] are stabilized by van der Waals interaction, dipole-dipole interaction, and hydrogen bond interactions as shown in Figure 1.6.

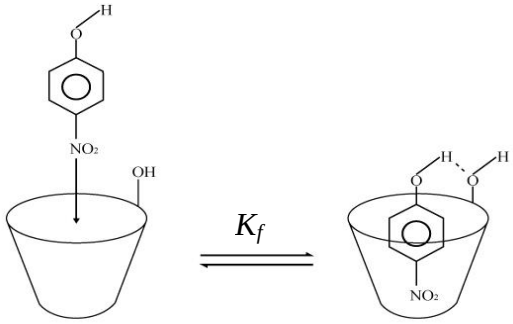

Figure 1.6 A diagram of the formation of a CD-inclusion complex for β-CD with *p*-nitrophenol where K_f is defined according to equation (1.13)

Chemical modification of CD is achieved by polymerization via proper linkers and substitution of hydroxyl groups in CD. CDs are selectively modified at C2-, C3-, and C6-OH positions by substitution with various organic functional groups by chemical and electrochemical methods. The most favorable nucleophilic site is the primary hydroxyl groups at the C6 position because the secondary hydroxyl groups at C2- and C3- positions are sterically crowded by the presence of more hydroxyl groups and intramolecular hydrogen bonding. The C2 and C3 positions are less reactive to nucleophilic substitution. In most cases, tosylation[48,49] of the primary hydroxyl group at the C6 position with tosyl chloride is a starting point for further chemical modification such as amino-derivatized[50] CD. The synthetic strategy is shown in Scheme 1.3, where reaction temperature is ambient.

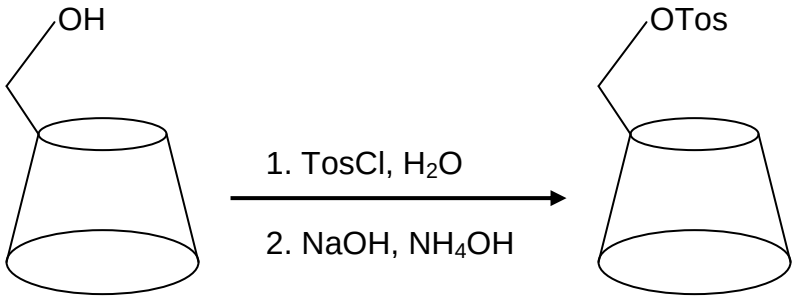

Scheme 1.3 Tosylation of CD, where Tos is tosyl.

Other substitutions at the C6 position involve attaching an acid, aldehyde, imine, and azide functional groups by mono, di, tri, or per-substitution.[51] CDs can be digested at pH < 2 and hydrolyzed into individual glucose units. This digestion property is used for determining the CD content by making a complex with a chromophore (tetrazolium blue[52]) using UV spectroscopic detection.

1.2.3.1 Polymerization

A strategy of polymerization of CDs[47] that is also useful for grating CDs onto AC employs the use of linkers such as isocyanate[39,53] by forming an urethane bond, epoxides [epichlorohydrin (EPI)[47] and ethylene glycol diepoxypropyl ether] by forming a poly-ether bond, and glutaraldehyde[41,40] by forming hemiacetal bond. A

schematic of the polymer is shown in Figure 1.7, where A shows the grafted CD onto the insoluble substrate such as silica or AC. In the case of AC that is already treated with proper functional groups of amine, hydroxyl, and carbonyl groups (herein after referred to as the "grafting to" method). Figure 1.7 B shows the grafted CD reacted with the hydroxyl groups of the coupling agents ("grafting from" method).

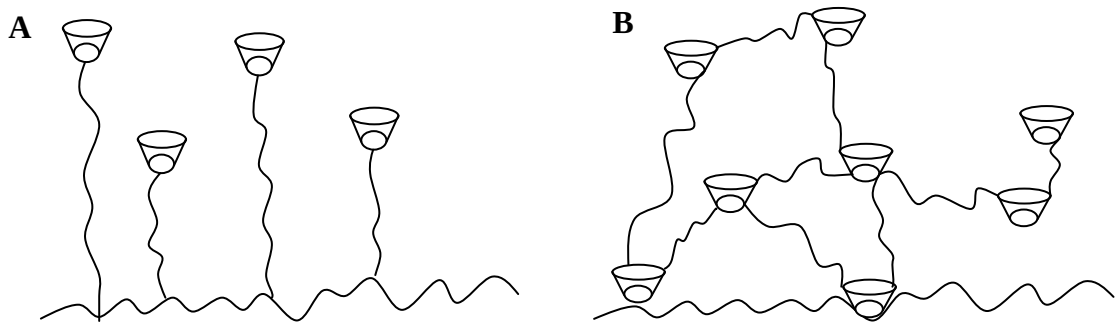

Figure 1.7 A sketch of polymers of CD (A: "grafting to" method and B: "grafting from" method)

Other benefit of these CD polymers can provide a synergistic effect of binding affinity that originates from inclusion by the cavity in CD and by the micropore networks arising from hydrogen bonding between the hydroxyl groups at the periphery of the CD torus and the monomer units.

1.2.3.2 Characterization

Many spectroscopic methods such as NMR,[54,55] IR,[56] circular dichroism (CD), UV,[57] Raman,[58,59] MS, ESR, powder X-ray diffraction (PXRD)[60] and XPS, as well as TGA,[59] are used for characterizing the structure of the CD and its inclusion complexes. Surface morphology is also characterized by microscopy techniques such as SEM[59] and TEM.[61]

1.2.4 Applications of CD based materials

CDs are widely used as adsorbents in the textile industry. CDs are useful as deodorants,[62] slow release agents of perfume scent and insect repellents,[62] and as finishing agents of polyester fabrics[43,63,64] with polycarboxylic acid as the crosslinking

agent.[56,65] It is also used as a food additive[62,66] (cyclodextrin complexes in food for flavors and vitamins. The formation of an inclusion complex with CD alters the physical properties such as increased thermal stability, water retention, stabilization, and taste modificaiton by the sweetness of β-CD and emulsification in cosmetics.[62,66] Inclusion complexes by CDs increase bioavailability and solubility [e.g., retinol/HP (hydroxypropyl) β-CD], oxidation stability (e.g., vitamin and provitamin A), and emulsion stabilizers, reducing toxicity, and avoiding preservatives. Other applications are dye removal[57] from water, purification of soil,[67,68] use as HPLC stationary supports,[59] and use in the area of pharmaceutical drug delivery.[69]

1.3 Sorption

1.3.1 Introduction

Sorption involves absorption and adsorption. Absorption is a completely reversible process defined by capturing smaller molecules in a larger porosity or its analogues on the surface (for example, absorbing water by a sponge), whereas adsorption may be irreversible process when a covalent bond is formed between an adsorbate and an adsorbent. A reversible process occurs when physisorption process occurs between the adsorbate and the adsorbent. Adsorption can be achieved by physisorption or chemisorption. Theoretically, any interaction between adsorbate and adsorbent to produce the change in the energy states of electrons should be considered chemisorption. However, it is impossible to measure all changes in the energy state in a adsorbate-adsorbent system. Therefore, the term of sorption is introduced to represent both physical adsorption (physisorption) and chemical adsorption (chemisorption). Physisorption is achieved by van der Waals interaction (dispersion and dipolar interactions) between the adsorbate and the adsorbent at lower temperatures; for example, N_2 adsorption on an iron metal surface. This reversible interaction can form multilayer sorption with about 40 kJ/mol ($\Delta_{ad}H$) on the substrate. However, chemisorption is achieved by forming a chemical bond (usually covalent bond) between adsorbate and adsorbent at higher temperature: for example, N_2 adsorption on an iron surface at 800 °C to form iron nitride. This irreversible interaction can build monolayer sorption with about 400 kJ/mol ($\Delta_{ad}H$) on the

substrate. Adsorption is a spontaneous phenomenon and decreases the free energy of the system (Gibbs free energy, ΔG). The entropy of the system (ΔS) is also decreased as adsorption occurs. Therefore, the enthalpy (the heat of adsorption, ΔH) is generally negative and exothermic because the Gibbs energy change is negative. All adsorption processes are anticipated to result in a net reduction of Gibbs free energy ($\Delta G = \Delta H - T\Delta S$).

Sorption processes in aqueous solution are different from gas media in that there is a charge-balance interaction between sorption of ions from the adsorbate and desorption of soluble ions from the adsorbent simultaneously. Furthermore, all sorption sites on the surface are non-equivalent as compared to gas sorption due to surface heterogeneity (i.e., a distribution of surface energy of adsorbent). Therefore, localized sorption on the surface of the adsorbent can be possible.

Sorption by CD, or inclusion, is depicted in Figure 1.7 and this complex formation, in case of 1:1 (CD: PNP) complex and assuming activity of H_2O is 1, is described by equation (1.12) and (1.13) at equilibrium, where S is the guest (PNP), K_f is equilibrium formation constant ($\approx K_{equilibrium}$), and [ ] represents the molar concentration of each molecule. The greater K_f value indicates a more stable CD inclusion complex.

$$CD + S \rightleftharpoons CD{\cdot}S \quad (1.12)$$

$$K_f = [CD{\cdot}S] / [CD]\,[S] \quad (1.13)$$

1.3.2 Surface heterogeneity

There are three major surface heterogeneities; physical, chemical, and induced heterogeneity.[70,71] Physical heterogeneities arise from geometrical differences in the size and shape such as porosity, crevices, edges, corners, and step positions on the surface. Chemical heterogeneities are associated with different surface functional groups including contaminants on the surface. Induced heterogeneity is attributed to the induced energy by the first bound molecule to the surface, which can affect the

binding energy of the following molecules. Interaction energy[70] between adsorbent and adsorbates generally decreases as surface coverage increases for the process of chemisorption; however, physisorption occurs between adsorbed molecules on a homogeneous surface and it increases as the degree of surface coverage increases.

1.3.3 Sorption Study

A sorption isotherm is a graphical representation of a sorption experiment in either the gas phase or in solution at a constant temperature. Nonlinear isotherm models can be recast as linear equations. Typical isotherm models include: Langmuir, Freundlich, BET (Brunauer-Emmett-Teller), Dubinin, Temkin, Astakhov, Redlich, Peterson, and so on. Representative linear isotherms that illustrate markedly different behaviors are those of Langmuir, Freundlich, and BET. The best curve fitting of linearized sorption isotherms is accomplished according to the highest correlation coefficients. The Freundlich isotherm (equation 1.14) is useful to identify sorption phenomena with the heterogeneous adsorbent media. The Langmuir isotherm (equation 1.15) is based on the assumption of monolayer surface coverage, equivalent sorption sites, and independent sorption sites. The BET isotherm (equation 1.16) is an extended Langmuir isotherm allowing multilayer surface coverage as well as equivalent sorption sites, and independent sorption sites.

$$Q_e = K_F\, C_e^{\,1/n};\ \ \log Q_e = \log K_F + 1/n \log C_e \qquad (1.14)$$

$$Q_e = K_L\, C_e\, Q_m / (1 + K_L\, C_e);\quad C_e / Q_e = 1 / K_L\, Q_m + (1 / Q_m)\, C_e \qquad (1.15)$$

$$Q_e = Q_m\, C_e\, K_{BET} / \{(1 - C_e)\,[1 + (K_{BET} - 1)\, C_e]\};$$
$$C_e / [(C_s - C_e)\, q_e\,] = 1 / (Q_m\, K_{BET}) + [(K_{BET} - 1) / (Q_m\, K_{BET})]\,(C_e / C_s) \qquad (1.16)$$

Q_m is a monolayer surface coverage at equilibrium (mol/g); K_F (L/g), K_L (g/mol), and K_{BET} (L/g) are equilibrium constants and n is an arbitrary constant evaluated by linearizing the equation. C_e is a concentration at equilibrium (mol/L) and C_s is a saturated concentration of a solute (mol/L). Q_m is the maximum adsorption at monolayer coverage (mol/g) and q_e is the amount of the adsorbate loaded per unit adsorbent at equilibrium, according to equation (1.16).

Useful information that can be obtained from sorption isotherms are the surface areas and sorption capacity. Surface area can be determined from equation (1.17)[72], where Q_m is the maximum adsorption at monolayer coverage at equilibrium (mol/g), N is the Avogadro's number (6.02×10^{23}/mol), σ is the cross-sectional molecular area of the adsorbate (m^2), and X is the coverage factor (X = 1 for PNP, X = 2 for MB). The coverage factor is the number of dye ions in a micelle or the aggregation number of dye ions because monoionic dyes (e.g., MB) can form monolayer of ionic micelle when they are adsorbed at the surface of solid.[72,73]

$$\text{Surface area } (m^2/g) = (Q_m \times N \times \sigma) / X \qquad (1.17)$$

Isosteric enthalpy (ΔH), the enthalpy at the fixed surface coverage, is calculated by equation (1.18) which is rewritten based on a van't Hoff equation when the sorption isotherms are obtained at three or more different temperatures; where T is the temperature in Kelvin, R is the gas constant, K is the equilibrium constant [K_F (L/g), K_L (g/mol), and K_{BET} (L/g)]. The slope is the same as $-\Delta H/R$ as ln K is plotted versus 1/T. Gibbs free energy in case of Freundlich model, ΔG, can be calculated from equation (1.19); where n is the constant [= log $(C_e/(Q_e - K_F)]$ derived from equation (1.14) and K_F is the equilibrium constant.

$$\frac{d(\ln K)}{d(1/T)} = -\frac{\Delta H}{R} \qquad (1.18)$$

$$\Delta G = -nRT \ln K_F \qquad (1.19)$$

The temperature dependence of an equilibrium constant (K) provides the expected isosteric enthalpy; K decreases as T increases in exothermic reaction, however, K increases as T increases in endothermic reaction because ΔS depends on equilibrium condition of adsorption reaction [$\Delta G = \Delta H - T\Delta S$ and $\Delta S = (\Delta H + \Delta G) / T$]. In an exothermic reaction, ΔS will be less favorable as T increases, whereas ΔS will be more favorable as T increases in an endothermic reaction. Therefore, K will increase as ΔS is favored.

1.3.3.1 Types of Sorption Isotherms

Brunauer, Deming, and Teller (BDT) classified sorption isotherms as six different categories (Type I, II, III, IV, V, and VI). Those isotherms are shown in Figure 1.8.[74]

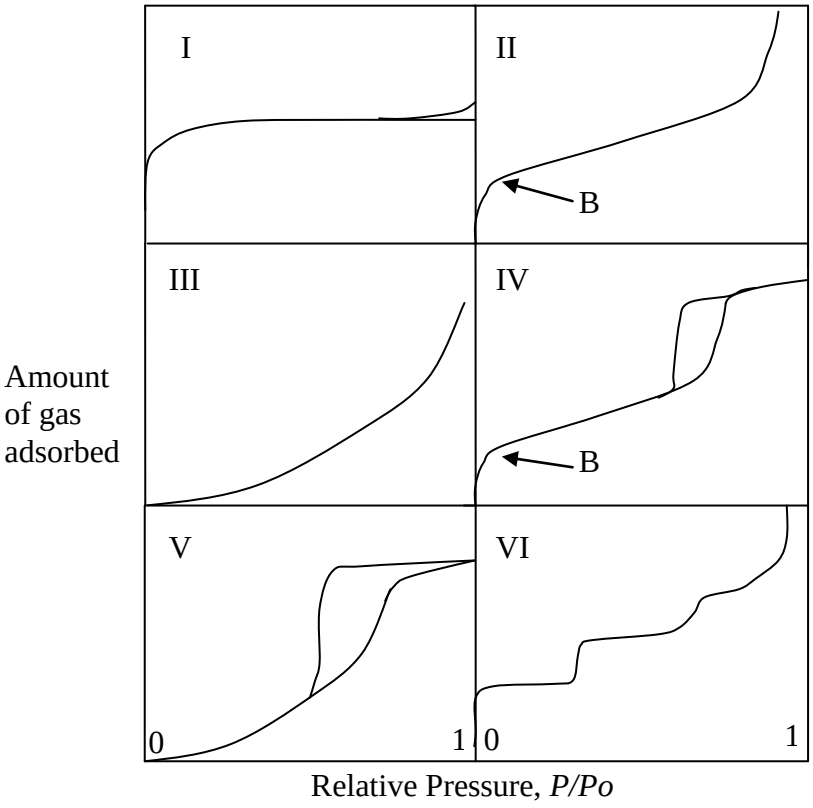

Figure 1.8 The six types of adsorption isotherms, where P = equilibrium pressure and P_o = saturation vapour pressure

Type I Isotherm

These isotherms are used to characterize the sorption caused by predominantly microporous structure because most micropore filling occurs at relative low pressure (< 0.1) and the adsorption process is usually completed at about half relative pressure ($P/P_o \approx 0.5$). Typical adsorptions of this group are the adsorption of nitrogen onto AC at 77 K and ammonia on AC at 273K.

Type II Isotherm

These isotherms involve physical adsorption of gases by non-porous solids. Point B is the end of monolayer surface coverage and multilayer coverage starts right after the point B. ACs with mixed micro- and meso-porosity show Type II isotherms.

Type III Isotherm

These isotherms are favored by weak interactions between adsorbate-adsorbent systems such as non-porous and microporous adsorbents. The weak interactions between the adsorbate and the adsorbent result in low loadings at low relative pressures. However, beyond the first sorption point, much stronger sorption can occur and result in maximum loadings at higher relative pressures. The adsorption of water molecules on AC where the primary adsorption sites are oxygen fall into this category.

Type IV Isotherm

These isotherms show a hysteresis loop attributed to capillary condensation, which is commonly shown for mesoporous materials. Point B is the end of monolayer surface coverage and multilayer coverage starts right after the point B. These sorption isotherms exhibit a limited loading at high relative pressures.

Type V Isotherm

These isotherms are achieved with microporous or mesoporous adsorbents and are convex at the high relative pressure. The driving force of uptake is the same as Type III isotherms. An example is water adsorption on AC at 100 °C.[75]

Type VI Isotherm

These isotherms are associated with extremely homogeneous, non-porous surfaces. The complete formation of a monolayer which corresponds to the step height is fulfilled before progression to a subsequent layer. An example is the adsorption of krypton on carbon black at 90 K which was previously graphitized at 3000 K.[76]

1.3.3.2 Sorption of Dye from Aqueous Solution

As the gas sorption of nitrogen at 77 K, dyes are used as adsorbates in aqueous solution. Examples are *p*-nitrophenol (PNP) as a neutral (non-ionized) dye, methylene blue (MB) as a cationic dye, and sodium fluorescein (SF) as an anionic dye shown in Figure 1.9. However, SF was excluded because it is relatively bulky for inclusion within the cavity of β-CD.

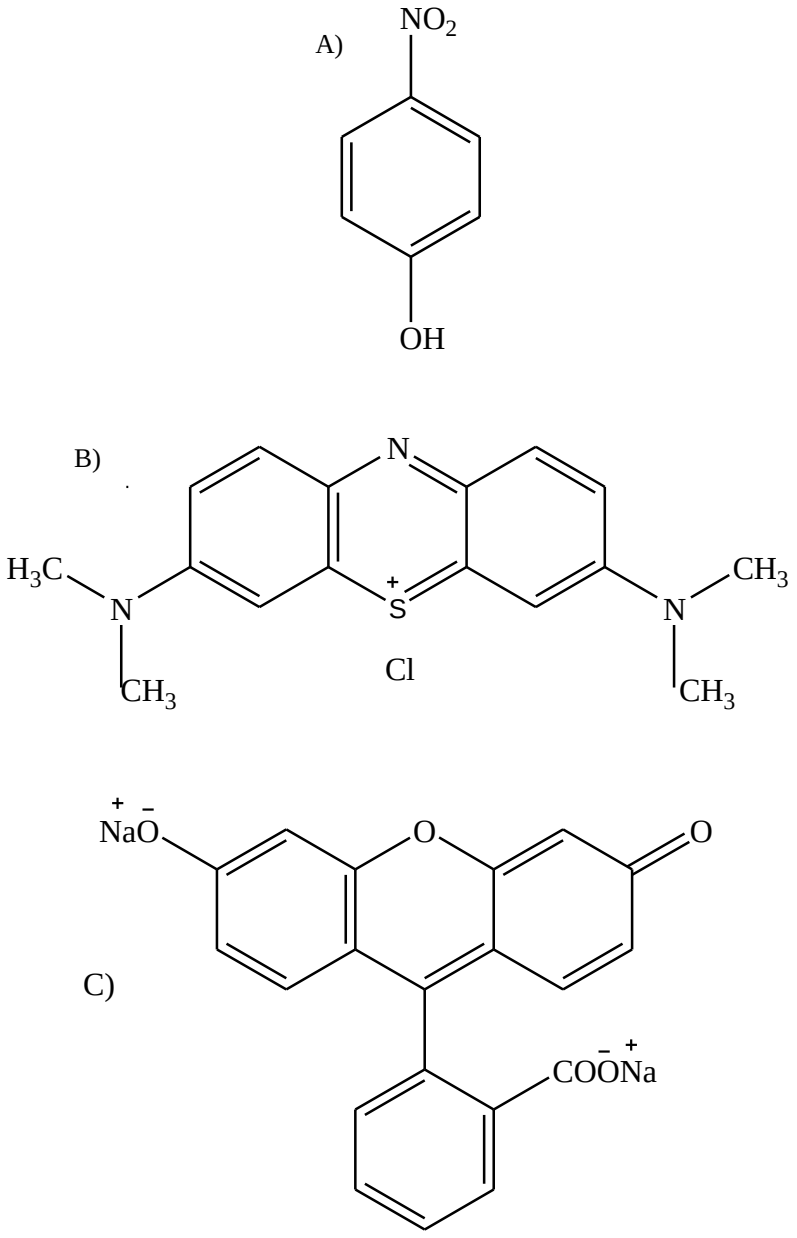

Figure 1.9 Molecular structures of various chromophoric dyes in sorption studies: A) *p*-nitrophenol (PNP), B) methylene blue (MB), and C) sodium fluorescein (SF)

Experimental factors that affect sorption of dye from aqueous solution are pH, temperature, concentration of adsorbate, mass of adsorbent, and shaking conditions such as equilibrium time and shaker speed. The most important factors are pH and temperature of the solution because pH can determine the ionized form of the dye molecule (e.g., PNP) which affects the nature of sorption interactions between the adsorbate and the adsorbent. The reaction rate of sorption depends on temperature; the reaction rate will increase as temperature increases. This phenomenon can be explained by the Arrhenius equation (1.20) as the shape of pores can affect the reaction rate of sorption (fast in macropores and slow in micropores), where k is the rate constant (s^{-1}), A is a constant (s^{-1}), E_a is the activation energy (kJ/mol), R is the gas constant (8.314 x 10^{-3} kJ mol^{-1} K^{-1}), and T is the temperature in Kelvin.

$$k = A \exp^{(-Ea/RT)} \qquad (1.20)$$

PNP has two ionic forms in solution which are shown in Figure 1.10 such as acidic [A) λ_{max} = 318 nm due to $\pi \rightarrow \pi^*$ electronic transition] in acidic condition and anionic [B) λ_{max} = 400 nm due to $n \rightarrow \pi^*$ electronic transition] in basic condition. Its absorption spectrum of UV and the isosbestic point which is 348 nm is shown in Figure 1.11.

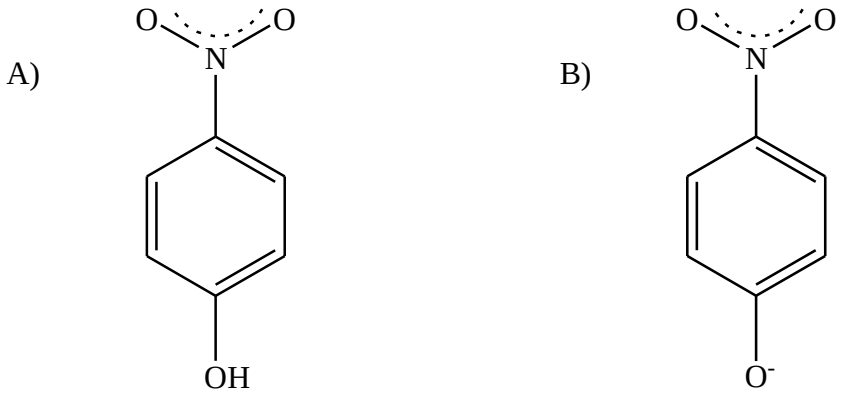

Non-ionized form Ionized form

Figure 1.10 Ionization states of PNP at different pH conditions (pKa for PNP = 7.15)

In its ionized state (form B), the UV absorption arises only from the nitro chromophore, whereas UV absorption by the nitro chromophore disappears in acidic condition because the nitro chromophore is protonated due to the presence of free hydronium ions.

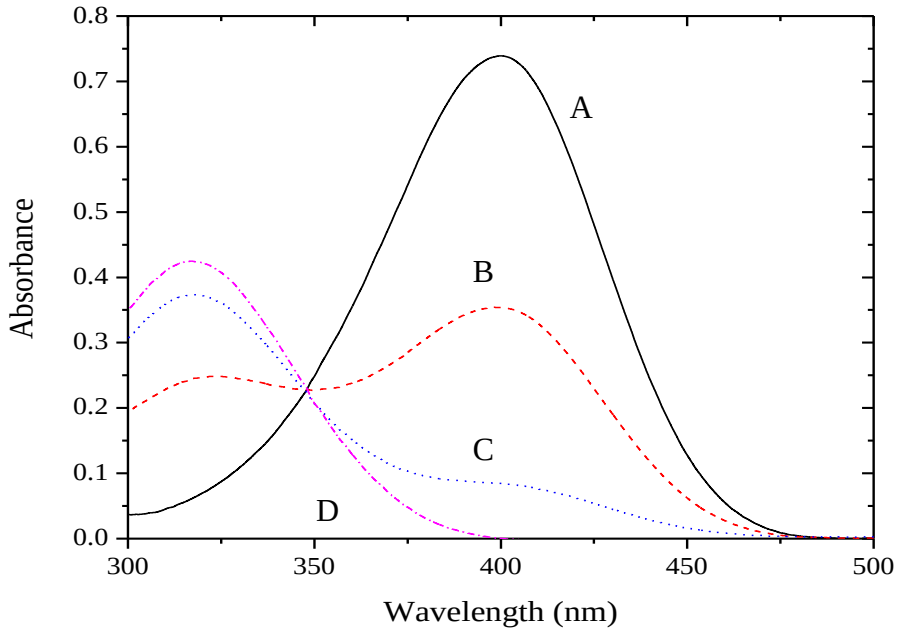

Figure 1.11 Absorbance characteristics of PNP at different pH conditions (A: solid line at pH = 10.00, B: dash line at pH = 7.00, C: dot line at pH = 6.00, and D: short dash line at pH = 2.00)

At pH = 6.00 ± 0.02 with phosphate buffer, the λ_{max} is 318 nm and its molar absorptivity (ε_{max}) is 9.05×10^3 $M^{-1}cm^{-1}$ (Literature value[77] = 9.71×10^3 $M^{-1}cm^{-1}$). At pH = 10.00 ± 0.02 with bicarbonate buffer, the λ_{max} is 400 nm and its molar absorptivity (ε_{max}) is 1.75×10^4 $M^{-1}cm^{-1}$ (Literature value[78] = 1.80×10^4 $M^{-1}cm^{-1}$). The slightly weak acid solution (pH = 6.00) is preferred to avoid contributions from the ionized form of PNP which occurs in basic conditions. In basic condition, deprotonation of the hydroxyl proton in PNP occurs and can make electronic repulsion between the nitro group of the deprotonated PNP (form B in Figure 1.10) and the surface carbonyl oxygen of AC which is electron rich at the surface due to presence of carbonyl oxygen and π-electron system. Hydrogen bonds between the oxygen anion in

the deprotonated PNP in its ionized form (form B in Figure 1.10) and water molecules can be possible and attenuate sorption process between PNP and AC due to strong hydration interactions between PNP and water molecules.

PNP is a well-known organic dye molecule for studying sorption capacity of solid adsorbent from aqueous solution because of its favorable chromopohre characteristics.[79] First, PNP is somewhat polar because of its two functional groups for providing strong sorption to the entire surface of polar solids and also apolar in nature to be adsorbed by non-polar solids. Second, it is a small molecule that its planar close-packed orientation can be preferably stacked by ensuring a monolayer on the surface of the solid. Third, it is also less surface-active for forming three-dimensional micelles at the solid surface because its nature is not an ionic molecule and makes a unity as surface coverage factor. Fourth, it is conveniently observed in the visible region (yellow) for ease of analysis and soluble in water and in non-polar media. Its molecular area is 52.5 $Å^2$ when it orients co-planar and 25.0 $Å^2$ when it orients orthogonally onto polar inorganic solids (e.g. silica).[72]

MB can be used for studying mesoporous adsorbents because its molecular size (120 $Å^2$) is greater than PNP. Its sorption capacity is favored by controlling the pH of the solution with basic condition to reduce competition between hydronium ion and a dye cation with the adsorbent. At basic conditions (pH = 8.40 ± 0.02 with borax buffer), its λ_{max} is 664 nm and molar absorptivity (ε_{max}) is 7.88×10^4 $M^{-1}cm^{-1}$ (literature[80] = 8.42×10^4 $M^{-1}cm^{-1}$).

1.3.3.3 Binding constant of dyes

The binding constant of dyes between the adsorbate and the adsorbent at equilibrium are important because it provides information on the capability of the adsorbent with organic compounds in aqueous solution. As the binding constant increases, the maximum amount of dye adsorption also increases. The Langmuir constant - K_L (g/mol), the BET constant - K_{BET} (L/g), and the Freundlich constant - K_F (L/g) are

referred to as equilibrium constants and are summarized in Table 1.4 for dyes which were used in this research.

Table 1.4 Binding constants of dyes (Literature values obtained from reference 77, 81, and 82)

Dyes	AC[77]		β-CD-HDI(*)[81]	β-CD[82]
	Langmuir (L/g)	Freundlich (L/g)	(M^{-1})	(M^{-1})
PNP	6.2×10^{2}	4×10^{-2}	5×10^{9}	n/a
MB	n/a	n/a	n/a	4.5×10^{3}

(*) β-CD-HDI is an inclusion complex of 1,6-hexamethylene diisocynate (HDI) with 1:1 ratio (n/a – data not available)

1.4 Objectives of the Research

AC is a relatively non-polar material and has high binding affinity for organic adsorbates. Micropores in AC can adsorb lower molecular weight organic compounds which have a wide range of volumes or sizes. AC has a large surface area that it allows for the sorption of organic materials into its pores (pore size, 20 Å ~ 1,000 Å) by physisorption. The equilibrium concentration for sorbates is parts per million (ppm) or parts per billion (ppb) levels because of a moderate formation constant (K = 1×10^{4} M^{-1} ~ 3×10^{5} M^{-1} for *p*-nitrophenol).[81] However, the sorption capacity is attenuated when it absorbs moisture from air. CD polymeric urethane compounds (α-, β-, and γ-) can bind smaller organic materials than AC to parts per trillion (ppt) levels because of its greater formation constant (K = 5×10^{9} M^{-1} for nitrophenol)[81] into its inner cavity (diameter, 7 Å ~ 9 Å). Inclusion binding occurs because of its smaller pore size than that of AC and the larger binding constant for smaller organic materials than AC.

The motivation for this research was to improve the sorption characteristics of AC material by grafting β-CD onto the AC surface. The hypothesis is that the resulting composite material would possess improved sorption characteristics because of the corresponding properties of AC and β-CD, respectively. When CD adsorbent is combined as a hybrid material on the surface of AC, the synergistic effect of its

sorption capacity in combination with the high surface area of AC and strong binding affinity of CD might be maximized toward the sorption of organic compounds from aqueous solution, vapour phase, and soil media. Chemical immobilization of CD onto the surface of AC has not been yet reported. The objectives of this research obtaining surface modification of AC with β-CD were investigated using different synthetic strategies. Therefore, a strategy of grafting β-CD onto AC as the sorbent template by means of organic linker, its characterization with chemical and instrumental analysis, and evaluation of its sorption properties with dye from aqueous solution will be carried out. An outcome of this research is the possibility of industrial application of the grafted AC with β-CD to purify water, air, and soil. An outline of the overall strategy to synthesize the surface modified AC with β-CD is shown in Figure 1.12 and the diagram of the surface modified AC with β-CD that utilizes different types of linker molecules is also provided in Figure in 1.13.

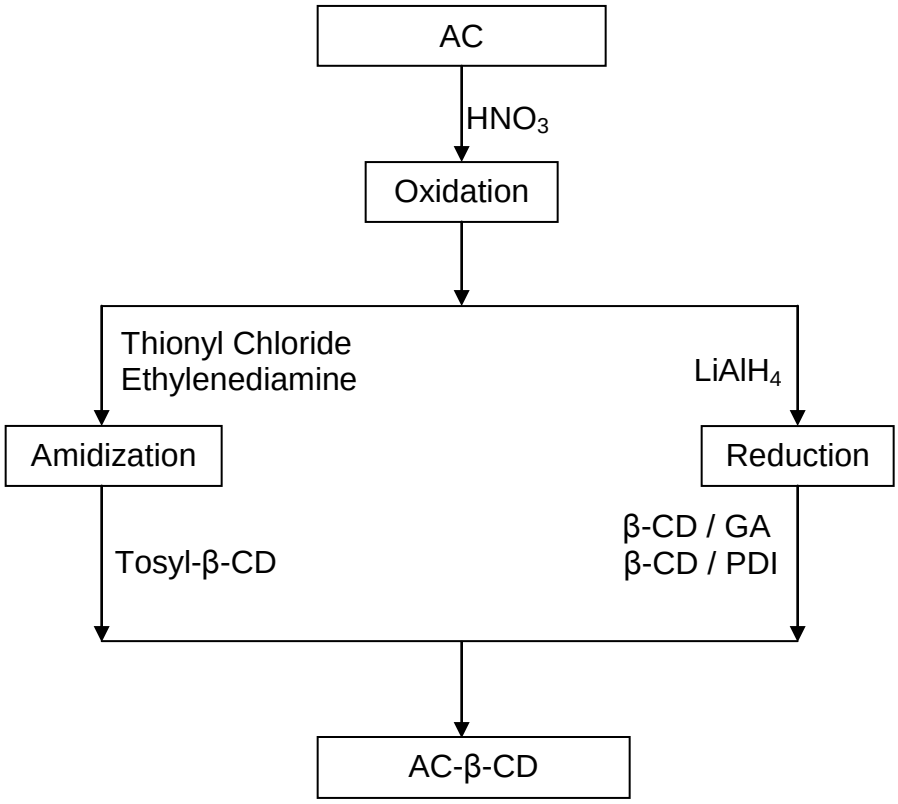

Figure 1.12 Schematic outline of the different synthetic grafting strategies of β-CD onto AC, where GA = glutaraldehyde and PDI = 1,4-phenylene diisocyanate

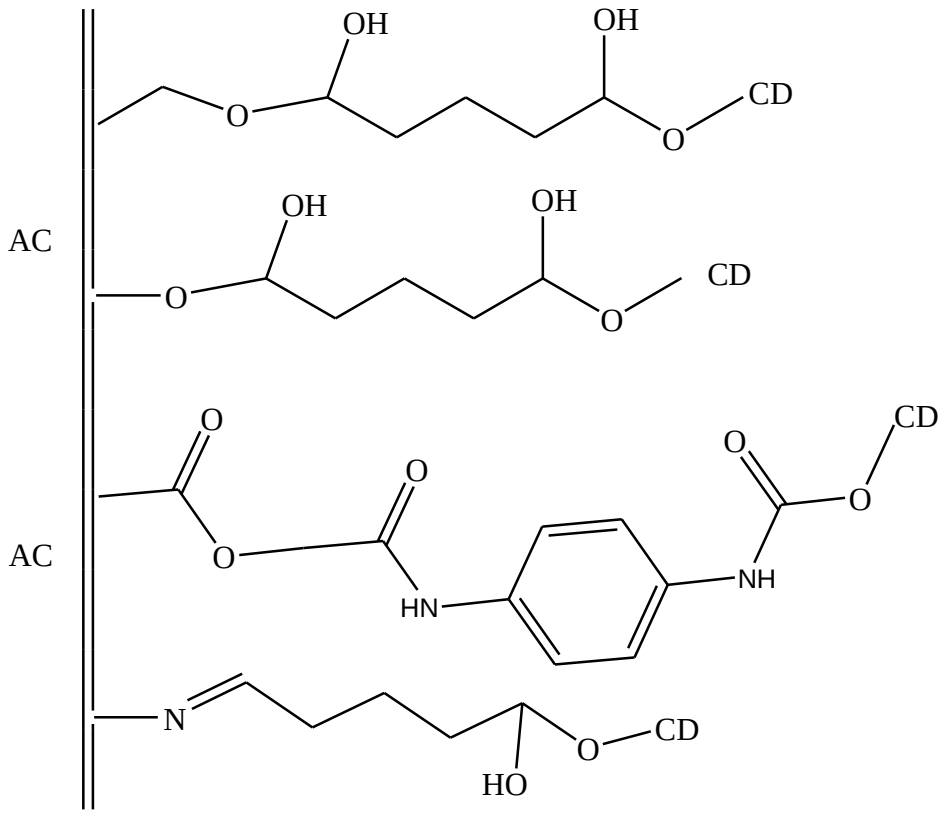

Figure 1.13 A schematic diagram of the grafted AC with CD showing nature of attachment of CD moiety using different linker molecules

CHAPTER 2

EXPERIMENTAL

2.1 Introduction

Chemical modification of AC with β-CD was achieved by the sequential approach of oxidation, reduction and amidization, and finally, grafting of β-CD. First, the oxidized AC (ACOXID) was obtained by reacting AC with nitric acid. The reduced ACOXID (ACREDUCT) was obtained by reacting ACOXID with lithium aluminum hydride and the amidized ACOXID (ACAMID) was obtained by reacting ACOXID to thionyl chloride and followed by reaction with ethylenediamine. Finally, the grafted AC with β-CD was obtained from two different strategies: "grafting to method" (refer to Figure 1.8) by use of linkers and direct covalent bonding by use of tosyl-β-CD. The linkers used were glutaraldehyde (GA) for ACREDUCT and 1,4-phenylene diisocyanate (PDI) for ACOXID. The outline of this synthesis was shown systematically in Figure 1.13 in Chapter 1. In this chapter, materials, instrument analysis, and synthetic methods used for the modification of the surface of ACs are described. As well, the sorption experiments of AC and surface modified AC with β-CD are described.

2.2 Materials

NORIT ROX 0.8 (ultra high purity), a hydrochloric acid-washed extruded AC made by steam activation from peat, was obtained from the company of NORIT America Inc. Hydrochloric, sulfuric, nitric acids, methanol, acetonitrile, NaOH, and acetone were obtained from EMD. Ethylenediamine (EDA) and methylene blue (MB) was purchased from Alfa-Aesar and used as received. Tosyl chloride and β-cyclodextrin monohydrate (β-CD), glutaraldehyde (GA, 50 wt. % solution in water), 1,4-phenylene diisocyanate (PDI), sodium bicarbonate, sodium carbonate monohydrate, dicyclohexylcarbodimide (DCC), dimethylsulfoxide-d_6 (DMSO-d_6), ammonium

hydroxide (NH_4OH), lithium aluminum hydride ($LiAlH_4$), and *p*-nitrophenol (PNP) were obtained from Aldrich. Potassium bromide was obtained from BDH. Molecular sieves (Type 4Å) were purchased from Fisher and anhydrous ethyl alcohol was purchased from Commercial Alcohol Inc. N, N'-dimethyl formamide (DMF, HPLC grade) were purchased from Omni Solv and used after drying over activated molecular sieves (4 Å). Molecular sieves were previously dried in a muffle furnace with the condition of 1 °C increase per minute and maintaining for 4 hours at 232 °C and 316 °C, respectively, and cooled in a desiccator to room temperature before use. All chemicals were of the highest grade commercially available and used as received, unless specified otherwise. Anhydrous tetrahydrofuran (THF) was obtained from MBraun Solvent Purification System with two columns of activated Al_2O_3 to remove trace water.

For Boehm titrations,[83,84,85] 0.2 N hydrochloric acid (HCl) solution and sodium hydroxide (NaOH) solution was obtained from Aldrich and diluted 10 times with Millipore water for further use.

2.3 Instrumentation

2.3.1 Introduction

Characterization of the surface modified AC is achieved by chemical analysis and instrumental analysis, as described below.

For measurement of surface acidity/basicity, the Boehm titration is a typical chemical analysis. This method involves the neutralization of the surface oxides with bases such as sodium hydroxide (NaOH), sodium bicarbonate ($NaHCO_3$), and sodium carbonate (Na_2CO_3) for surface acidic groups and with acid such as hydrochloric acid (HCl) for surface basic group because AC itself shows basic character due to its inherent π-electron system in the basal planes. Boehm made an assumption that $NaHCO_3$ (pK_a = 6.37) neutralizes carboxylic group only, Na_2CO_3 (pK_a = 10.25) neutralizes carboxylic group including lactone group and allows lactone group to open its ring and form carboxylic group which is neutralized, and NaOH (pK_a = 15.74) neutralizes carboxylic

group, lactone group, and phenolic hydroxyl group.[85] The neutralization reaction in aqueous solution of the Boehm titration is described below.[86]

$$R\text{-}COOH_{(aq)} + NaOH_{(aq)} \rightarrow RCOONa_{(aq)} + H_2O_{(\ell)} \quad (2.1)$$

$$2R\text{-}COOH_{(aq)} + Na_2CO_{3(aq)} \rightarrow 2R\text{-}COONa_{(aq)} + CO_{2(g)} + H_2O_{(\ell)} \quad (2.2)$$

$$R\text{-}COOH_{(aq)} + NaHCO_{3(aq)} \rightarrow RCOONa_{(aq)} + CO_{2(g)} + H_2O_{(\ell)} \quad (2.3)$$

(R: a generalized representation for a surface-bound carbon atom)

Other chemical methods are mass titration and potentiometric titration. Mass titration is applied to amphoteric materials such as the surface modified AC from pH = 3 to pH = 11 and uses the concept of the point of zero charge (PZC) based on acid/base titration. PZC is the point of pH at which the net surface charge is zero. If H^+ and OH^- are only adsorbed on the surface where their surface coverage is equal, then PZC is the same as the isoelectric point (IEP). Surface oxides in aqueous solution are ionized at equilibrium, as follows.[23]

$$MOH_2^{+}{}_{(aq)} \rightarrow MOH_{(aq)} + H^+_{(aq)}, \quad K_1 = [MOH]\,[H^+] / [MOH_2^+] \quad (2.4)$$

$$MOH_{(aq)} \rightarrow MO^-_{(aq)} + H^+_{(aq)}, \quad K_2 = [MO^-]\,[H^+] / [MO^-] \quad (2.5)$$

MOH is surface oxide and K_1 and K_2 are the step-wise acid dissociation equilibrium constants. As the oxidation time of AC increases, the PZC value decreases accordingly.[23] Potentiometric titration are used to analyze the surface acidity/basicity and uses a continuous pK distribution of proton binding isotherms in the usual range between pH = 3 and pH = 11 on the surface by smoothening them with a peak deconvolution method, for example, SAIEUS (solution of adsorption integral equation using splines)[87] or CONTIN (a general purpose constrained regularization program for inverting noisy linear algebraic and integral equations).[88] Surface functional groups can interact with strong acids or bases and change their Brønsted acid-base characteristics resulting in overlapping continuous surface acidity – basicity of surface functional groups such as carboxylic acids, lactones, and phenols. This surface property can also be affected by surface heterogeneity. The actual proton binding

isotherms (Θ) which correspond to their continuous p*K* values is given by the overall adsorption integral equation[89] (2.6) and shows the total proton binding sites.

$$\Theta(pH) = \int_{\alpha}^{\beta} \theta(pH, pK)\, f(pK)\, dpK + \Theta o \qquad (2.6)$$

Where *θ(pH, pK)* is the local proton binding sites characterized by the acidic sites in terms of *pK*. *f(pK)* is the distribution of acidic sites in terms of their *pK* values. If the integration limit is slightly broader than the limit of the applied pH range, α goes to pH_1 - 1 and β goes to pH_n + 1 and the constant, Θ*o*, is applied to adjust binding on sites with *pK* values outside of the integration limit. Computing equation (2.6) by SAIEUS or CONTIN represents the continuous p*K* distribution of proton binding isotherms (mol/g) versus pH or pK and the amount (mol/g) of carboxylic acid, lactone, and phenol groups are obtained at pKa < 6.37, 6.37 < pKa > 10.25, and 10.25 < pKa > 15.74, respectively.

Spectroscopic methods used to characterize the surface modified AC are grouped by using vibrational energy [Diffuse Reflectance Infrared Fourier Tranform spectroscopy (DRIFTS) and Raman spectroscopy], photoelectron (X-ray photoelectron spectroscopy: XPS), thermogravimetric analysis (differential thermogravimetry: DTG, temperature programmed desorption: TPD), mass spectrometry (Matrix Assisted Laser Desorption Ionization Time of Flight mass spectrometry: MALDI TOF MS), and electron spin resonance (ESR) spectroscopy.

The theory of DRIFTS is based on the Kubelka-Munk equation for non-transmissive materials so that they can isotropically scatter the incident light and provide diffuse reflectance analogous to Beer's law for transmission measurements.[20,90] A schematic diagram of diffuse reflectance[91] is shown in Figure 2.1, where I is an incident radiation, F is Fresnel reflection which is reflected by a law of reflection, and D is diffuse reflection which does not follow the law of reflection and has not exactly traveled through some finite thickness of a sample as the angle of incident radiation.

The Kubelka-Munk theory is used to apply to convert diffuse reflectance data to an absorption-like spectrum.

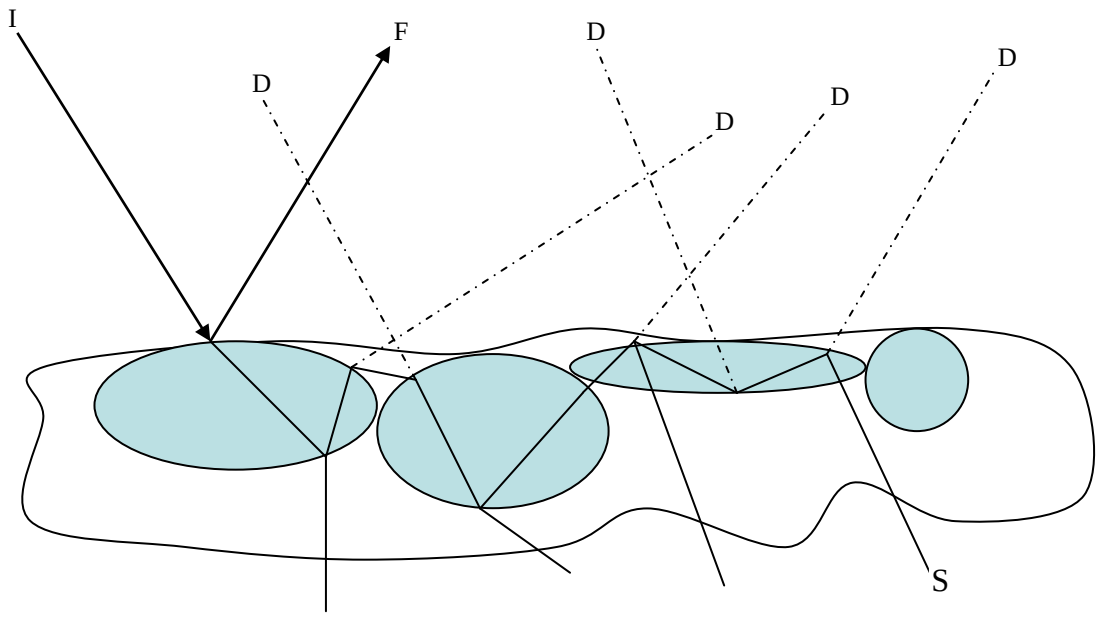

Figure 2.1 Sample geometry of diffuse reflectance where I = incident radiation, F = Fresnel reflection, S = scattered radiation, and D = diffuse reflection

Equation (2.7) is very useful for characterizing the behavior of diffuse reflectance in the mid-infrared region and given by the following, where R_∞ is the diffuse reflectance of the infinitely thick sample, k is the absorption constant, and s is the scattering coefficient.

$$F(R_\infty) = (1 - R_\infty)^2 / 2R_\infty = k / s \qquad (2.7)$$

When the sample is diluted in a nonabsorbing matrix such as KBr, k is proportionally related to the absorptivity, ε ($M^{-1}cm^{-1}$), and the concentration of surface functional groups, c (M), is given by equation (2.8). [92]

$$k = 2.303\ \varepsilon\ c \qquad (2.8)$$

XPS uses soft X-ray (200 – 2000 eV) to break the binding energy of the core 1s electron and excitation into vacuum level: 284.1 eV for C 1s, 409.9 eV for N 1s, and 543.1 eV for O 1s. For obtaining these incident photons, proper X-ray emission lines are used such as Mg $K_{\alpha 1}$ (1,253.60 eV) or Al $K_{\alpha 1}$ (1,486.70 eV). The overall descriptive process of XPS is given by equation (2.9) and Figure 2.2, where E is the total energy, *h* is Plank's constant, *v* is frequency of radiation, BE is the binding energy [Ionization potential (IP) for gases], KE is the kinetic energy, and Φ is the work function of solids (Φ = 0 for gases).

$$E = h\nu = BE + KE + \Phi \qquad (2.9)$$

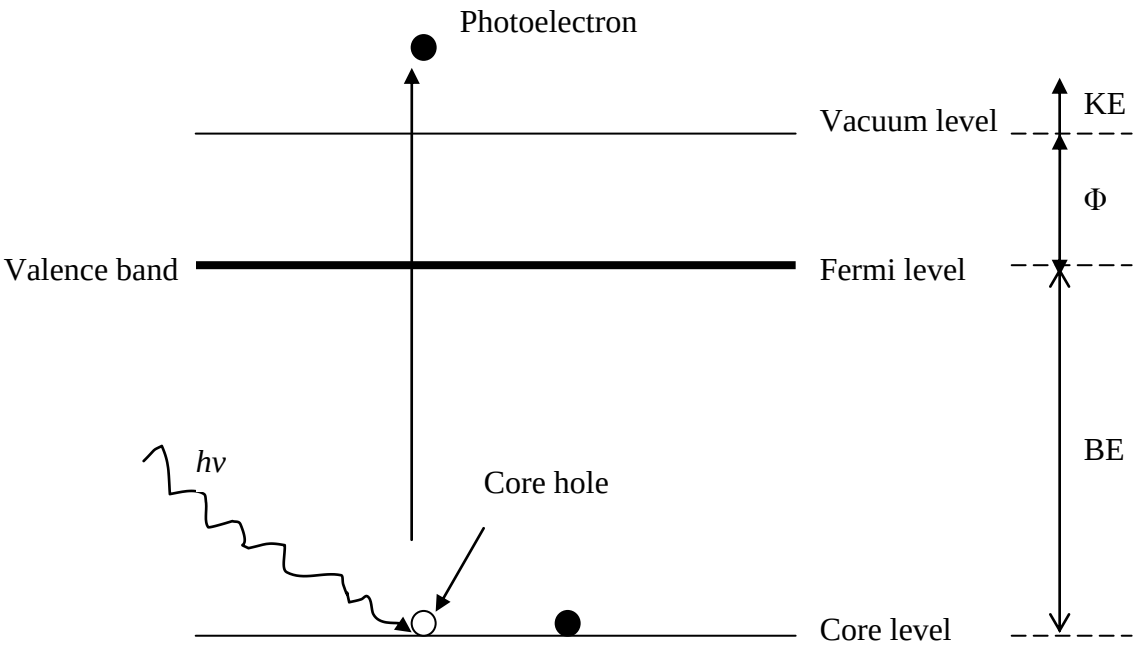

Figure 2.2 A diagram of the photoemission of a core level electron where BE, KE, and Φ are defined in equation (2.9)

The binding energy is altered by the chemical environment of the core electron such as the presence of electron-withdrawing groups and higher oxidation states because these properties can change the net interaction energy between the electrons and the protons and the BE of the core 1s electron increases as electronegtivity or oxidation state increases, resulting in shifting of the XPS peaks to higher energy values.

Therefore, XPS can be used to characterize the nature of surface-bound functional groups on AC.[93,94,95,96]

DTG measures the rate of weight loss upon a constant heating rate versus temperature. Heating rate is the key to good resolution of the curve and good separation of thermal transitions can be obtained by use of a lower heating rate. Air when used as the carrier gas can further oxidize the sample. Typical carrier gases are He and N_2 and mixtures thereof. The heating pan should be selected according to maximum heating temperature. DTG can provide information on the relative surface coverage (w/w, %) over a range of decomposition temperatures of various surface functional groups and information on their thermal stability.[97]

TPD measures decomposition temperature and surface coverage (w/w, %) of bound functional groups when heat is applied, normally up to 1,000 °C. Carbon dioxide can be evolved from decomposition of lactone and anhydrides; however, carbon monoxide can be evolved from decomposition of carbonyl, ethers, and also lactone and anhydrides.[9,10,98]

MALDI is used to identify the mass of constituents on the surface of grafted materials by laser desorption ionization of bound molecules using detection by mass spectrometry analysis.[99] The mechanism of MALDI involves formation of a completely homogenous matrix-analyte-salt solution, irradiation of a laser beam on the surface of the mixture solution which results in ionization of an analyte in the form of $[M+X]^+$, where M is analyte, X = H, Na, K, Li, - CH_3, - OH, and MALDI plate metals and separation of the analyte-salt cluster by its *m/z* (mass/charge) value.

Raman spectroscopy[100] reveals Raman shifts of surface functional groups by Raman scattering or Raman effects which arise from changes in polarizability of molecules when they undergo vibration and rotation during irradiation of a monochromatic laser beam. The magnitude of polarizability, α, is given by equation (2.10) and it increases as the induced dipole moment of molecules (μ) increases and the magnitude of the

applied electric field (E) decreases, such as decreasing electron density, decreasing bond strength, and increasing bond length.

$$\alpha = \mu / E \tag{2.10}$$

Raman (frequency) shifts ($\Delta\upsilon$) are described by equation (2.11) and ν_i is the frequency (cm^{-1}) of the incident radiation and ν_s is the frequency (cm^{-1}) of the particular scattering by the given molecule.

$$\Delta\upsilon = \nu_i - \nu_s \tag{2.11}$$

These shifts are allowed according to the selection rules of vibrational Raman shifts and rotational Raman shifts. For the vibrational Raman shifts, $\Delta\upsilon = \pm 1$ and for the rotational Raman shifts, $\Delta J = 0, \pm 2$, where J is rotational quantum number. In the case of $\Delta J = 0$, the frequency of Raman line is the same as that of the incident radiation which corresponds to Rayleigh scattering (no Raman shift). Typically, AC shows two bands of D [Disordered graphite (C=C stretching); 1,355 cm^{-1}] and G [Graphite (C=C, stretching); 1,575 cm^{-1}] with their associated bands (for details, refer to section 3.2.6 in Chapter 3), whereas pure graphite shows only one peak at 1,575 cm^{-1}.[101,102] Surface modification of AC with molecules shows specific Raman shifts in AC and the grafted AC by Raman scattering[103] because of changes in polarizability due to bound functional groups.

ESR spectroscopy is a result of the absorption of microwave ($10^4 - 10^6$ MHz) energy by unpaired electrons. This technique is sensitive to the paramagnetic property of materials and measures unpaired electrons resulting from inherent structural incompleteness of electronic structures (e.g., basal plane of amorphous AC), some contaminants during manufacturing (e.g., paramagnetic metals) and chemical modification (e.g., incomplete combustion due to radical reaction). As involvement of nuclear spin in nuclear magnetic resonance (NMR), electron spin in ESR involves the applied magnetic field and splitting of energy levels by the Zeeman effect. This

splitting corresponds to a g value which is the exact position of the absorption of microwave radiation and is calculated by equation (2.12), where β is the Bohr magneton, h is Plank's constant, v is the frequency, and B is the applied magnetic field

$$g = hv / \beta \mathrm{B} \qquad (2.12)$$

where the g value for a free electron is 2.0023 and its deviation from 2.0023 is changed by the contribution of orbital angular momentum in the electronic states of spin giving rise to the resonance.[104] The g-value can help us to characterize a sample being measured such as types of transition metals, oxidation states, radical environment, and symmetry. Other information obtained from ESR is spin concentration which is proportional to peak intensity for quantitative analysis, spectral line width which is affected by the interactions of the spins and their interaction with the crystal lattice as electron shielding and deshielding effects in NMR spectroscopy. Hyperfine splitting structure is associated with coupling of the electronic spin with nuclear spins.

The surface morphology of AC and surface modified AC can be studied by scanning electron microscopy (SEM).[11] SEM uses high energy electrons (generally 30 keV) as an incident beam to the surface with a resolution of up to 3 nm and these electron beams can generate various emissions from the sample such as inelastically scattered electrons (backscattered electrons, secondary electrons, X-rays, Auger electrons) and elastically scattered electrons (e.g., electron diffraction). Among inelastically scattered electrons low energy secondary electrons (valence electrons) arising from the surface are mainly used for obtaining surface images for SEM. Backscattered electrons are also used for obtaining surface images when heavy metals are present on the surface where the energy beam can probe the surface. In this case, more bright images can be obtained because many electrons are joined together to produce an image as a charging up effect due to an increased conductivity on the surface.

Proton nuclear magnetic resonance (^{1}H NMR) spectroscopy is a powerful tool to identify function groups. Protons in a surface group can absorb electromagnetic radiation in the radio-frequency region (3 MHz to 30, 000 MHz) at their specific frequency corresponding to atomic nuclear magnetic resonance with the applied electromagnetic field. ^{1}H NMR for ACs was applied to identify functional groups of precursors such as tosyl β-CD in solution. ACs and surface modified ACs are insoluble paramagnetic solids and therefore ^{1}H NMR studies were not pursued in this work.

2.3.2 Chemical Analysis

2.3.2.1 pH measurements

Measurement of pH was done for the total acid or basic components which are dissociated from 2.0 % (w/w) of AC, ACOXID, ACREDUCT, AC-β-CD, and ACPDICD by a Fisher Accumet 620 pH meter for identifying acid and base characteristics of them. Samples (0.4 g, each) were dried in the vacuum oven at 100 °C for 2 hours, added into a 50 mL beaker containing 20 mL of deionized water, stirred overnight to reach equilibrium and to ensure wetting of the carbon surface, and measured at room temperature after one point calibration at pH = 7.00.

2.3.2.2 Boehm titrations[83,84,85]

0.20 g of ACs were dried in the oven at 125 °C for 7hr, added into the bottle containing 25.0 mL of neutralizing agents (0.02 M of HCl, NaOH, Na_2CO_3, $NaHCO_3$), shaken for 48 hr, and filtered with Whatman filter paper No. 4. 5.0 mL of the filtrate was back-titrated with 0.02 M of HCl or NaOH using modified methyl orange as an indicator. The end point was characterized from pink to green (for NaOH titrant) and from green to pink (for HCl titrant). The results are shown in Table 2.1.

Table 2.1 The result of Boehm titration of acidic and basic functional groups at room temperature

Name	Item	Measured Variables			
		Total basicity	Total acidity(*)	Carboxylic acid	Lactone and Carboxylic acid
AC	Titrant	HCl	NaOH	$NaHCO_3$	Na_2CO_3
	Mass (g)	0.2020	0.2011	0.2042	0.2056
	Volume used (mL)	3.58	4.63	4.91	9.71
ACOXID(3)	Titrant	HCl	NaOH	$NaHCO_3$	Na_2CO_3
	Mass (g)	0.2004	0.2006	0.2007	0.2008
	Volume used (mL)	4.75	1.12	2.20	5.79
ACOXID(6)	Titrant	HCl	NaOH	$NaHCO_3$	Na_2CO_3
	Mass (g)	0.2006	0.2007	0.2009	0.2007
	Volume used (mL)	4.65	0.85	1.75	5.20
ACOXID(9)	Titrant	HCl	NaOH	$NaHCO_3$	Na_2CO_3
	Mass (g)	0.2006	0.1999	0.2010	0.2020
	Volume used (mL)	4.50	0.67	1.24	4.65
ACOXID(12)	Titrant	HCl	NaOH	$NaHCO_3$	Na_2CO_3
	Mass (g)	0.2059	0.2093	0.2069	0.2096
	Volume used (mL)	4.41	0.68	4.20	1.10

(*) is the sum of lactone, phenolic hydroxyl, and carboxylic acid groups

2.3.3 Instrumental Analysis

2.3.3.1 Metal contents

The amount (ppm) of metals (Ca, Mg, Na, K, Fe, Cu, Zn, and Pb) was measured by using an atomic absorption spectrometer (AAS, Varian SpectrAA 220). The standard solutions (1,000 ppm) for those metal analyses were from RICCA chemical company and the solvent was 20 % of aqueous nitric acid. Ionization booster (La_2O_3/HCl solution) for the analysis of Na and K was added into both standards and sample solutions. 60.0 mg of AC was added into the beaker and 5.5 mL of concentrated nitric

acid was added and completely dried by heating. The sample was cooled, topped up by the mixture of 5.0 mL nitric acid and 5.0 mL Millipore water, and warmed up again. This solution was further diluted by adding 15.0 mL of Millipore water.

2.3.3.2 Porosimetry

Nitrogen porosimetry for measuring surface area with the accuracy of ± 5 % of ACs, ACOXIDs, ACREDUCTs, AC-β-CDs, and ACPDICD was obtained with Micromeritics (ASAP 2000, V2.05). Approximately 0.2 g of samples, after degassing all volatile molecules from them at 550 μm Hg, was applied to the sample chamber. The degassing temperature for the grafted ACs, ACOXIDs and ACREDUCTs, and ACs were 100 °C, 80 °C, and 200 °C, respectively.

2.3.3.3 TGA and DTG[105,106]

DTG analysis was carried out by using a Perkin Elmer Pyris Diamond TG/DTA. This analysis is a direct method to calculate the amounts of surface bound functional groups by measuring the weight loss resulting from thermal decomposition of the surface bound groups as heat is applied to the sample over a specified temperature range. Heating rate and maximum heating temperature were 5 °C per minute and 600 °C under N_2 flow as the carrier gas. However, the finishing temperature was varied according to the samples. AC, ACOXID, ACREDUCT, AC-β-CDs, and ACPDICD were measured including standards of physisorbed β-CD (1 % and 10 %) and GA (10%) onto AC as reference compounds, which were denoted as ACCDP(1), ACCDP(10) and ACGAP, respectively.

2.3.3.4 Raman Spectroscopy

Raman spectra were obtained using a Renishaw system 2000 whose resolution (= λ/2) is 0.257 μm (laser spot size). Raman shifts were obtained at ambient temperatures by using a 514 nm Argon ion laser with following operating conditions: range of scan (4000 ~ 150 cm^{-1}), power (20 mW with 100 % load), objective lens (x 50), cosmic ray removal (On), detection time (10 seconds), and the number of accumulation scans (40

times). Raman spectra for AC, ACOXID, ACREDUCT, AC-β-CDs, ACPDICD, β-CD, ACCDP, ACGAP, and tosyl-β-CD were obtained.

2.3.3.5 MALDI TOF MS

Mass spectra of solid samples of AC-β-CDs, ACPDICD, β-CD, and ACCDPs were obtained using a MALDI TOF mass spectrometer [Voyager DE STR (Applied Biosystems)]. The matrix used was α-cyano-4-hydroxycinnamic acid (CHCA). Approximately 2.0 mg of sample were placed in an eppendorf tube (a tube for micro-centrifuge) and ground with a 200 µL pipette tip. 50 µL of 75% acetonitrile with 0.1 % 1,2,3-trifluoro acetic acid (TFA) was added to the tube. The sample was sonicated in a sonication bath for 30 minutes. 1 µL of the slurried samples and 1 µL of the matrix solution (5 mg/mL CHCA were mixed on the MALDI plate and air dried) were operated in positive ion linear mode and calibrated with Angiotensin 1 (*m/z* = 1296.6853) and spectra were acquired from *m/z* = 700 to *m/z* = 3000.

2.3.3.6 ESR Spectroscopy

Bruker Bio Spin ESP 300E X-band field swept spectrometer (resonance frequency 9.4 GHZ) equipped with rectangular cavity (model 4108 TMH) was used for measuring the spectra of AC, ACOXIDs, ACREDUCTs, AC-β-CDs, and ACPDICD using 2,2'-diphenyl-1-picrylhydrazyl (DPPH) powder as a *g* standard (g value for DPPH = 2.0037 ± 0.0002)[107], which is shown in Figure 2.3.

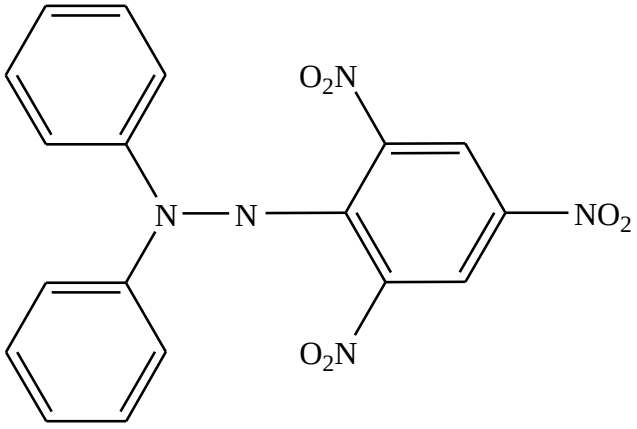

Figure 2.3 A chemical structure of DPPH, *g* standard for absorption of microwave radiation in ESR measurements

2.3.3.7 DRIFT Spectroscopy

Diffuse Reflectance Infrared Fourier Transform (DRIFT) spectra were obtained using a Bio RAD FTS-40 spectrophotometer. The following samples were studied AC, ACOXIDs, ACREDUCTs, AC-β-CDs, and ACPDICD under the following conditions with resolution of 4 cm^{-1} and various scans (30,000 scans for ACs and 256 scans for β-CD and tosyl-β-CD) by preparing samples as 1:1 (KBr/ACs, β-CD and tosyl-β-CD) ratio.

2.3.3.8 Elemental Analysis (C, H, and N)

The content (w/w, %) of carbon (C), hydrogen (H), and nitrogen (N) was measured by Perkin Elmer 2400 CHN Elemental Analyzer and its detection limit is ± 0.3%. AC, ACOXID, ACREDUCT, AC-β-CDs, and ACPDICD were analyzed. The content (w/w, %) of oxygen and hydrogen arising from residual water in ACs was measured by TGA analysis. Elemental analysis data was corrected according to the measured water contents by TGA. (Refer to Table 3.6, Figure 3.2, and Appendices A1 ~ A8)

2.3.3.9 SEM

Scanning electron microscopy images were obtained using a JEOL JSM-840A with maximum resolution of images of 6 nm. The picture of SEM used is shown in Figure 2.4.

Figure 2.4 Picture of SEM instrumentation

The column of the electron gun and objective lens system was maintained by a vacuum of 1.0×10^{-5} to 10^{-6} Torr. The electron gun [Tungsten filament (W) or LaB_6 cathode as thermionic guns] generates monochromatic electrons. The magnetic condenser lens determines smallest illumination spot size on the specimen and reduces the spherical aberration effects. The magnetic objective lens focuses and magnifies the first image which is scanned by scan coils and then detected by various instruments such as a Sample current Detector and a Backscattered Electron Detector. The penetration depth increases with voltage and therefore, contrast can become poorer at higher energies. Charging up effects can be serious for all non-electroconductive samples and also metallic samples which are not electrically grounded during scanning. To avoid electron beam attenuation (beam size) and refraction (beam position) in the air, the specimen chamber was purged with Ar gas at 1 - 20 Torr.

A few granules of AC, ACOXID, ACREDUCT, AC-β-CD, and ACPDICD were coated with gold (200 Å thickness) by an Edwards 505 gold sputter coater using Ar plasma generated with 1 kV and 30 mA for 3 minutes at 7.5 millibars (mb) during the coating after Ar purging through the coating compartment. The purpose of gold coating is to provide electro-conductivity to samples and the gold-coated samples are shown in Figure 2.5.

Figure 2.5 Gold sputter-coated ACs for SEM analysis

Surface morphologies of samples were obtained by magnifying 1,200 times of the real images.

2.3.3.10 XPS

AC, AC-β-CD [1:10:10(9)], and ACPDICD were applied to analyze C 1s, N 1s, and O 1s electron by Shimadzu Kratos AXIX Ultra DLD. The electron gun was fitted with a lanthanum hexafluoride filament that provides 300 W with 15 kV x 20 mA and magnetic lens that are used to obtain high collection efficiency and high spatial resolution. Samples were compounded on a cavity of a stub lined up with aluminum foil and applied to the sample chamber maintained at 1×10^{-10} torr and 25 °C. The source of photoelectron was Al Kα (1,486.6 eV).

2.3.3.11 ^{1}H NMR Spectroscopy

^{1}H-NMR (Bruker; 500 MHz Avance NMR spectrometer) spectra were obtained with 128 scans using DMSO-d_6 as the solvent at 25 °C. Chemical shifts of protons[108] relative to tetramethylsilane (TMS) in various structural environments are shown in Table 2.2 (see next page), where the types of protons of interest are indicated in bold face type.

2.4 Synthesis

Chemical modification of AC with β-CD was carried out by purifying, oxidizing, amidizing, and reduction of AC and finally grafting β-CD to AC via an organic linker group, as outlined below.

2.4.1 Purification[109]

NORIT ROX 0.8 (10.0g) was purified with Soxhlet extraction apparatus by 2.0 M HCl (500 mL) for 15 hours around 97°C, which is the maximum boiling point of 2.0 M HCl (azeotropic temperature), washed continuously and roughly with distilled water first overnight and then deionized water to avoid contamination of unnecessary metals until the filtrate had pH > 6.00 and dried in the vacuum oven at 80°C overnight.

Whatman filter paper No. 4 was used as the filter paper used for washing. Purification by HCl is anticipated to wash some metals, oxides, ashes, organic impurities from the AC surface. The purified NORIT ROX 0.8 (AC) was used for the subsequent surface modification of AC with β-CD.

Table 2.2 Chemical shifts of protons in various structural environments (Literature values obtained from reference 108)

Structural environments	Type of protons	Chemical shift, δ (ppm)
Primary	*R*C**H**$_3$	0.9
Secondary	*R*$_2$C**H**$_2$	1.3
Tertiary	*R*$_3$C**H**	1.5
Vinylic	C = C**H**	4.6 – 5.9
Acetylenic	C≡C - **H**	1.8 – 3.1
Allylic	C = C – C**H**$_3$	1.7
Aromatic	Ar - **H**	6 – 8.5
Benzylic	Ar - C - **H**	2.2 – 3
Alcohols	**H**C - OH	3.4 – 4
Ethers	**H**C - O*R*	3.3 – 4
Esters	*R*COO - C**H**	3.7 – 4.1
Esters	**H**C - COO*R*	2 – 2.2
Acids	**H**C - COOH	2 – 2.6
Carbonyl compounds	**H**C – C = O	2 – 2.7
Aldehydes	*R*C**H**O	9 -10
Aliphatic alcohol	*R*O**H**	1 – 5.5
Phenolic	ArO**H**	4- 12
Enolic	C = C - O**H**	15 – 17
Carboxylic	*R*COO**H**	10.5 – 12
Amino	*R*N**H**$_2$, ArN**H**$_2$	1 – 5
Thiols	*R*S**H**	1.1 – 1.5
Thiophenols	ArS**H**	3 – 4
Amine salts	*R*$_3$N$^+$**H**	7.1 – 7.7

	$ArN^{+}\mathbf{H}_3$	8.5 – 9.5
Amines	**H**C – NR_2	2.1 – 3
Thioethers	**H**C – S*R*	2.1 – 2.8
Fluorides	**H**C – F	4 – 4.5

2.4.2 Oxidation (ACOXID)[10,11,12,28]

Three different concentrations [15.8 M (70%), 5.0 M, and mixture of HNO_3/H_2SO_4 (1:3, v/v)] of nitric acid were used to oxidize AC. The concentrated nitric acid (15.8 M, 100 mL) was introduced to oxidize AC (10.0 g) for 2 hours at different temperatures (room temperature, 70 °C, and 100 °C). The diluted nitric acid (5.0 M) was employed to oxidize AC at its azeotropic temperature for 3, 6, 9, and 12 hr, which were denoted by ACOXID(3), ACOXID(6), ACOXID(9), and ACOXID(12), respectively. The mixture of sulfuric acid (30 mL) and nitric acid (10 mL) was used for oxidizing AC (1.0 g) for 3 hours at 40 °C in an ultrasonic bath[110] and denoted as ACOXID(S). After oxidation, Whatman filter paper No. 4 was used to filter ACs. All oxidized ACs were washed continuously with distilled water first, deionized water until the filtrate had pH > 5.50 and then dried in a vacuum oven at 80°C overnight.

2.4.3 Amidization (ACAMID)[25,26,27,28]

Three different reagents were used for this reaction: ethylenediamine (EDA), ammonium hydroxide (NH_4OH), and dicyclohexylcarbodimide (DCC) with EDA under sonication for 4 hours. 2.2 g of ACOXID dried under vacuum at 105°C for 1 hr was added into the two-necked 250 ml round bottom flask containing with 20 mL of thionyl chloride and 1 mL of DMF. This reaction mixture was refluxed for 24 hours at 60 ~ 80 °C in the presence of Argon (Ar) gas, cooled to room temperature, and filtered with THF in vacuum at room temperature with Ar purging. The residue was dried in vacuum with Ar purging at room temperature for 5 minutes more, added into the new 100 mL round bottom (r.b) flask containing 10 mL of EDA, and refluxed at 90 ~ 100 °C for 44 hours. This reaction mixture was cooled to room temperature, washed with dried ethanol in the Soxhlet extractor for 24 hours to remove free EDA, washed with THF, and dried in the vacuum oven at 50 °C for 12 hours. Ammonium hydroxide

(50 mL of NH_4OH, 30 % of NH_3) was added into a 100 ml of the r.b. flask and ACOXID (1.0 g) was added into the r.b. flask while stirring with NH_4OH. The mixture was then stirred for 24 hours at room temperature, washed with deionized water until the pH of the filtrate was between 6 and 7, and then dried at 40 °C in the vacuum oven. DCC (0.025 g) and EDA (10 mL) were added into a 25 mL Erlenmeyer flask which contained 0.5 g of ACOXID and the mixture was sonicated at 40 °C for 4 hours. Then, it was diluted with 200 mL of methanol, washed and filtered with methanol, and dried at room temperature.

2.4.4 Reduction (ACREDUCT)

Each ACOXID (3.0 g) was, respectively, dried in an oven at 125 °C for 7 hr, cooled in a desiccator to room temperatuere, and transferred to a 100 mL round bottom flasks containing 20 mL of anhydrous THF solution of $LiAlH_4$ [0.33 g for ACOXID(3), 0.35 g for ACOXID(6), and 0.37 g for ACOXID(9)] while stirring under an Ar atmosphere. The amount of reducing agent was calculated as equation (2.13) for ACOXID(3), equation (2.14) for ACOXID(6), and equation (2.15) for AXOXID(9). The amounts of total surface acids (mmol//g) of ACOXIDs were 1.93, 2.07, and 2.17 (refer to Table 3.3 in section 3.2.2 in Chapter 3). The amount of $LiAlH_4$ (g) was added in excess and its molecular weight was 38 mg per mmol.

$$3.0\ g \times 1.93\ mmol/g \times 1.5 \times 38\ mg/mmol = 0.33\ g \quad (2.13)$$

$$3.0\ g \times 2.07\ mmol/g \times 1.5 \times 38\ mg/mmol = 0.35\ g \quad (2.14)$$

$$3.0\ g \times 2.17\ mmol/g \times 1.5 \times 38\ mg/mmol = 0.37\ g \quad (2.15)$$

This reaction mixture of ACOXID and $LiAlH_4$ (1:1.5 molar ratio) was stirred for 24 hours at room temperature, quenched with deionized water in an ice bath, and washed with Millipore water, and then dried in a vacuum oven at 80 °C overnight. The products were denoted as ACREDUCT(3), ACREDUCT(6), and ACREDUCT(9).

2.4.5 Synthesis of p-tosyl-β-cyclodextrin (tosyl-β-CD)[111]

12.0 g (10.6 mmol) of β-cyclodextrin hydrate was placed in the 500 mL round bottom flask and wetted with 100 ml of deionized water. 1.31 g (32.8 mmol) of NaOH dissolved with 4 ml of deionized water was added dropwise into the β-cyclodextrin solution during 1.2 min. The solution was turned clear and slightly yellowish. 2.02 g (10.6 mmol) of p-toluene sulfonyl chloride (tosyl chloride) dissolved in 6 ml of acetonitrile was added dropwise into the β-cyclodextrin solution during 1.6 min. The solution became opaque and started to form precipitate upon adding p-tosyl chloride. The reaction mixture was stirred for 3 hr at room temperature, filtered by Whatman filter paper No. 4 for removing any precipitates, the filtrate was kept in a refrigerator maintained at 4°C overnight, and filtered the cold solution. The white solid residue was dried in the vacuum oven at room temperature overnight and the filtrate was re-filtered again at 4°C after re-crystallization with water. The twice recrystallized sample after filtration and vacuum drying was combined with the once recrystallized sample for the purpose of increasing the amount of material for subsequent chemical reactions with AC.

2.4.6 Grafting of tosyl-β-CD on ACAMID[42]

0.8 g of ACAMID dried in the vacuum oven at room temperature overnight was placed in a two-necked 250 ml round bottom flask. 17 ml of dry DMF was added into the flask via a syringe. 0.10 g of tosyl-β-CD was dissolved in the dry DMF and then added into the flask via a syringe. The reaction mixture of tosyl-β-CD and ACAMID (0.08:1.7 = mole ratio) was refluxed for 24 hr under a nitrogen atmosphere at 60°C, left for 2 days more at room temperature, washed with 100 ml of DMF followed by 100 ml of acetone, and then dried in the vacuum oven at room temperature overnight.

2.4.7 Grafting of tosyl-β-CD on ACREDUCT

Tosyl-β-CD and ACREDUCT were dried in a vacuum oven at 40 °C overnight for 7 hr. 0.5 g of ACREDUCT was added into a two-necked 250 mL round bottom flask and purged by N_2 gas. 15 mL of acetonitrile was added by a syringe into the reaction mixture. 5 ml of DMF containing tosyl-β-CD (0.063 g) was added by a syringe and

the reaction mixture of tosyl-β-CD and ACREDUCT (0.05:1 = mole ratio) was refluxed at 60 °C ~ 70 °C for 24 hr. The reaction was then left for 48 hr at room temperature under atmospheric condition, washed with a 100 mL portion of DMF, CH_3CN, and acetone, followed by drying in the vacuum at 40 °C overnight.

2.4.8 Grafting of β-CD on ACREDUCT via the linker of GA[40,41]

ACREDUCT (0.50 g) was dried in an oven at 125 °C for 2 hr and added to a 500 mL round bottom flask. GA (2.0 mL), deionized water (270 mL), and β-CD (11.5 g) were added while stirring to the reaction mixture. H_2SO_4 (9.0 M) was added dropwise to adjust pH of the solution (pH ~ 2.5). Then, the solution was refluxed at 100 °C for 2 days, and washed with methanol in the soxhlet extractor for 2 days to remove free GA and β-CD. The surface modified AC with β-CD was denoted by AC-β-CD (1:10:1)(3) AC-β-CD (1:10:5)(6), AC-β-CD (1:10:10)(9), AC-β-CD (1:10:20)(9), AC-β-CD (2:10:0.9)(3), AC-β-CD (1:20:2)(3) AC-β-CD (1:20:2)(6), AC-β-CD (1:20:20)(9), according to the mole ratio of ACREDUCT:GA:β-CD, as shown in Table 2.3. The numbers in the parentheses are the mol ratios and the hours of reduction time of ACOXID sample.

Table 2.3 The mole ratios for grafting β-CD on ACREDUCT via the linker of GA

AC-β-CD	Used amounts (g or mL) of reactants			
	ACREDUCT (g)	GA (mL)	β-CD (g)	Water (mL)
[1:10:1(3)]	0.5	1.8	1.2	270
[1:10:5(6)]	0.5	1.9	6.0	270
[1:10:10(9)]	0.5	2.0	11.5	270
[1:10:20(9)]	0.5	2.0	22.7	270
[2:10:0.9(3)]	1.0	1.8	1.0	270
[1:20:2(3)]	2.0	14.0	8.5	400
[1:20:2(6)]	2.0	15.0	9.1	400
[1:20:2(9)]	2.0	16.0	9.5	400

2.4.9 Grafting of β-CD on ACOXID via the linker of PDI [39,53]

1.0 g of ACOXID(9) was dried in an oven at 125 °C overnight and added into a 250 mL round bottom flask containing PDI (0.336 g). DMF (50 mL) was added by a syringe under an inert Ar atmosphere and a dropping funnel containing β-CD (4.768 g) solution dissolved in DMF (50 mL) was fitted to the reaction flask. The reaction mixture was heated to 60 °C ~ 70 °C, stirred for 8 hr at this temperature, and then, the β-CD solution with DMF (50 mL) was added dropwise into the reaction mixture for 1hr. The reaction mixture (mole ratio of ACOXID:PDI:β-CD = 1:1:2) was stirred for 36 hr, washed with methanol in the soxhlet extraction unit for 48 hr, and dried in the vacuum oven at 60 °C overnight. The product was denoted as ACPDICD.

2.5 Sorption Study

Sorption studies are an efficient way to evaluate surface areas of solid materials and can provide information on sorption of foreign materials by any porous or non porous solids. Sorption studies can be achieved by either gas (e.g., N_2, CH_2Cl_2, and NH_3) sorption at the surface of solids using porosimetry or solution sorption using dyes. The sorption of dyes (e.g., PNP and MB) from aqueous solution is measured with a UV spectrophotometer. UV absorbance and molar absorption coefficients of dyes were obtained with a UV-Vis spectrophotometer (Varian Cary 100 SCAN) with a spectral band width of 2 nm and data interval of 1 nm. The 50 mL Qorpak Bottles filled with 20 mL of dye solution was shaken by the mechanical shaker [Heto Birkeroder, Denmark (Type: TBSH02, RPM: 1500)] for sorption equilibrium. Here, typical organic dyes are used as adsorbates; PNP and MB for aqueous sorption was introduced for characterizing sorption properties of ACs. The buffered pH solution of PNP was adjusted to 6.00 ± 0.02 for ACs and grafted ACs and 10.00 ± 0.02 for ACs at room temperature, while the buffered pH solution of MB was adjusted to 8.40 ± 0.02 for grafted ACs at room temperature. To avoid any interfering results, a study on the selection of a proper filter medium and equilibration time are also discussed.

2.5.1 Selection of Filter media

Various filter media [Acrodisc syringe filter, Glass micro-fiber filter 696, Sintered glass filter funnel (M), Whatman No. 40 filter paper, and Whatman No. 42 filter paper] were used to get the best filtration of activated carbon. 5.0 mL of PNP solution was taken and measured its absorbance at 400 nm. The results are shown in Table 2.4 and Figure 2.6. The acrodisc syringe filter was chosen because it showed the least amount of dye sorption according to the absorbance values obtained from the blank.

Table 2.4 Filtration results with various filter media

Filter Media				Absorbance at 400 nm	Difference (%)
Name	Supplier	Material	Pore size (μm)		
Acrodisc syringe filter	Pall	Polyether Sulfone membrane	0.45	1.755	- 0.1706
Glass micro-fiber filter 696	VWR	Glass fiber	1.20	1.815	+ 3.214
Sintered glass filter funnel (M)	Pyrex	Borosilicate glass	-	1.790	+ 1.820
Whatman No. 40 filter paper	Whatman	Cellulose pulp	8.00	1.735	- 1.308
Whatman No. 42 filter paper	Whatman	Cellulose pulp	2.50	1.731	- 1.536
Blank (PNP)		1.0×10^{-4} M		1.758	0.0000

Note: Difference (%) is relative values to a blank solution and the total amount of filter material may be unequal for a given amount of dye solution.

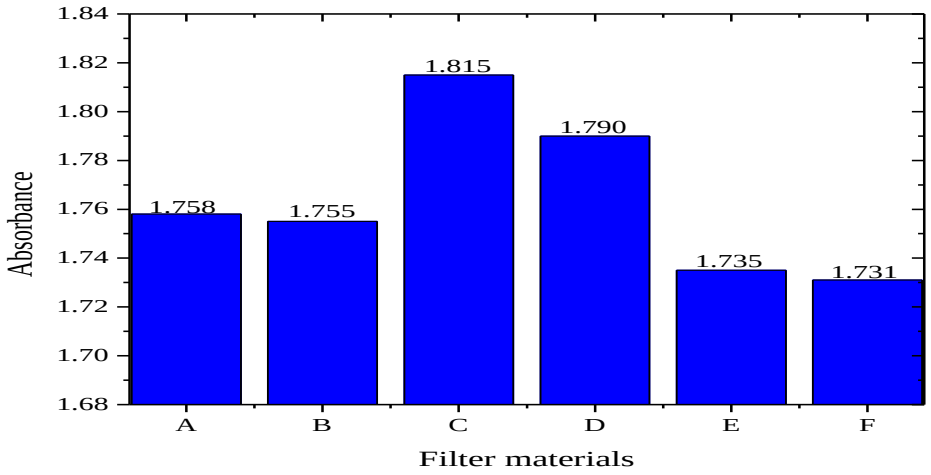

Figure 2.6 Filtration results of PNP (A: Blank, B: Acrodisc syringe filter, C: Glass microfiber filter 696, D: Sintered glass filter funnel (M), E: Whatman No. 40 filter paper, F: Whatman No. 42 filter paper)

2.5.2 Equilibration time

20.0 mL of PNP solutions (8.2×10^{-4} M at pH = 10.00) was added into the bottles containing 40 mg of ACs dried at 105 °C in the vacuum of 1.8 mmHg for 1 hour. The bottles were shaken for 60 hours at room temperature until equilibrium was reached and equilibrium was tested over a 35 hour shaking period. 20.0 mL of MB solutions (9.0×10^{-5} M at pH = 8.40) was added into the bottles containing 1 mg of AC-β-CD[1:10:10(9)] dried at 105 °C in an oven for 7 hours. The bottles were shaken for 31 hours at room temperature until equilibrium was reached and a minimum equilibrium time was concluded over a 5 hour shaking period. The result is shown in Figure 2.7. In the case of MB, the equilibrium time was shortened because it is relatively water soluble hydrophilicity as compared to that of PNP due to its ionic character.

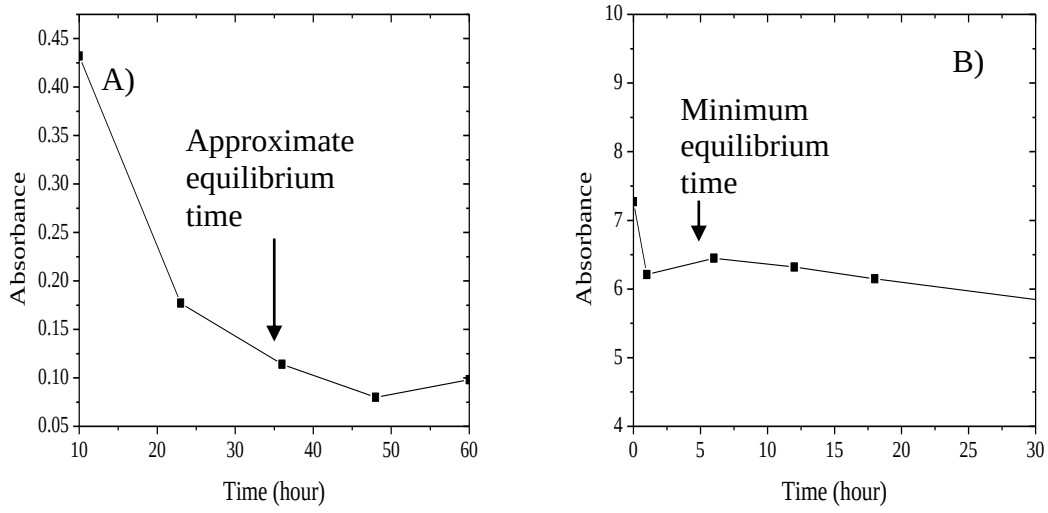

Figure 2.7 Determination of equilibration time of the adsorbates at room temperature A) PNP at pH = 10.00 and B) MB at pH = 8.40 with AC

2.5.3 Standard Curves

Three standard curves were prepared for PNP at pH = 6.00 ± 0.02 (A), PNP at pH = 10.00 ± 0.02 (B), and MB at pH = 8.40 ± 0.02 (C) at room temperature as shown in Figure 2.8. The pH buffer solutions were prepared by the standard method.[112]

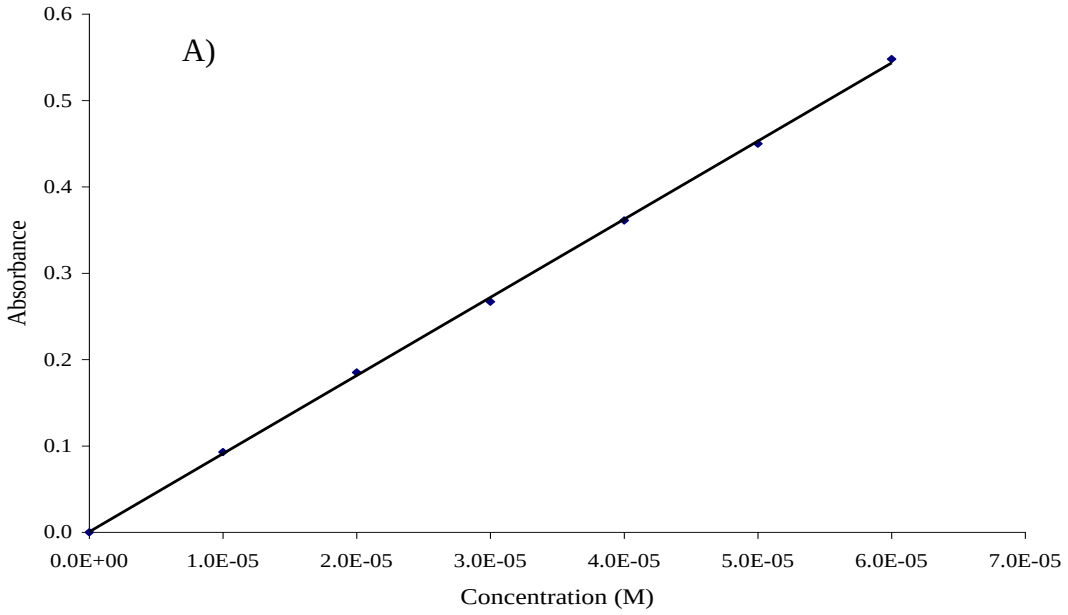

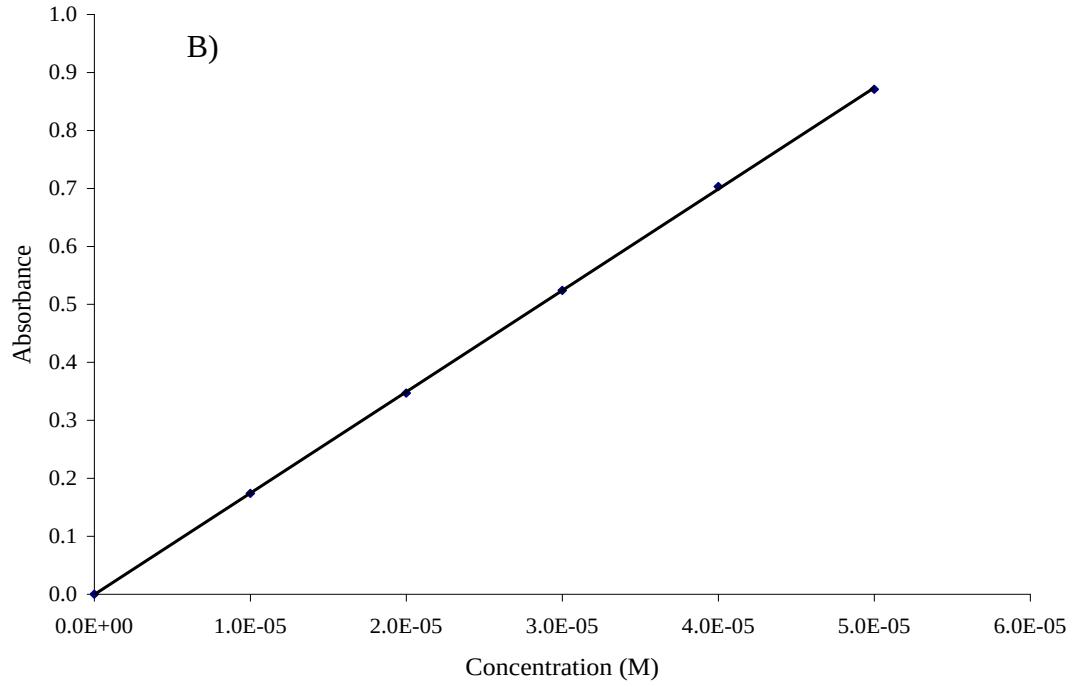

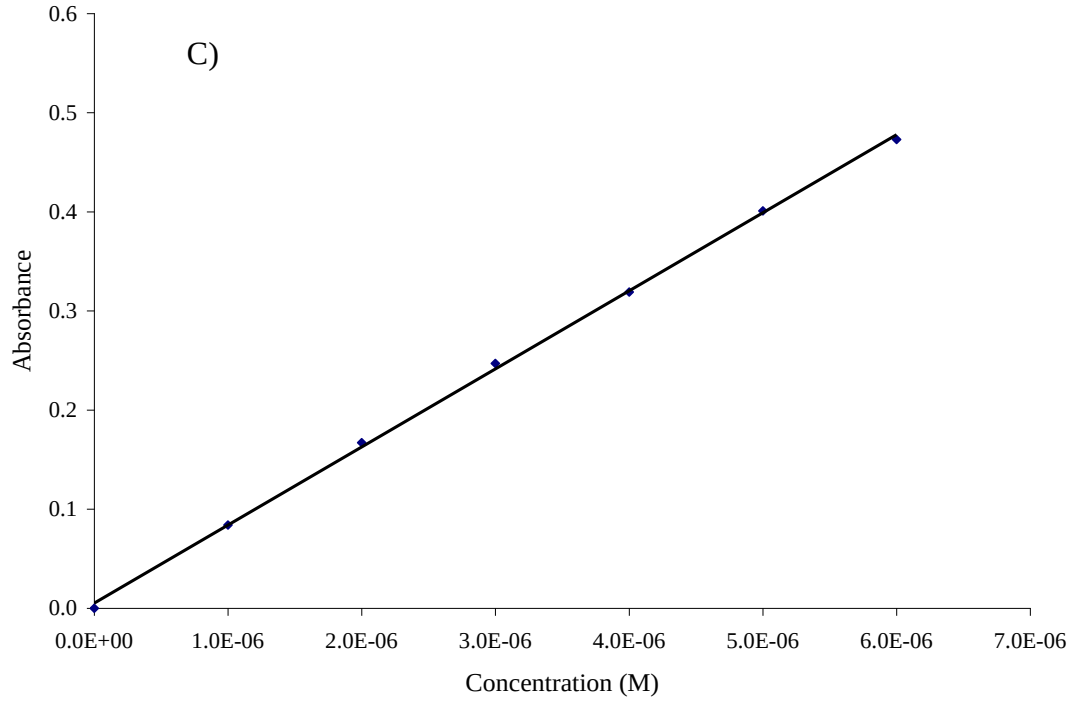

Figure 2.8 Standard absorbance vs. concentration curves of dyes [A) = PNP at pH = 6.00, B) = PNP at pH = 10.00, and C) = MB at pH = 8.40]

ε values for PNP at pH = 6.00, PNP at pH = 10.00, and MB at pH = 8.40 were 9,050 M^{-1} cm^{-1}, 17,483 M^{-1} cm^{-1}, and 78,750 M^{-1} cm^{-1}, respectively. Linear regression coefficients (R^2) for all dyes were > 0.999.

2.5.4 Sorption Isotherms

2.5.4.1 Sorption Isotherms for AC

PNP was the main dye used for the sorption studies. The grain size of AC was kept uniform (< 40 mesh or 420 μm). The sample was dried at 125 °C for 1 hour and kept in a desiccator for further use. The volumetric flask containing PNP solution was stored in the dark room by wrapping with aluminum foil. 20 mL of the solution of PNP was added in polyvinyl capped glass bottles (the Qorpak Bottles) containing various amounts of ACs. Samples were allowed to reach equilibrium after shaking 24 hours of the sample bottles at room temperature. The conditions of sorption experiments are shown in Table 2.5, where C_o is the initial concentration of the stock solutions of PNP which was determined on the basis of the absorbance of the blank solution.

Table 2.5 Experimental conditions for the sorption study of PNP with AC at 25 °C

Adsorbents		Solutions of PNP adsorbate	
Name	Mass (mg)	(C_o, M)	(C_o, pH)
AC	1 (fixed)	$1.0 \times 10^{-3} \sim 8.0 \times 10^{-5}$	6.00 ± 0.02 (phosphate buffer, 10 mM)
	1 ~ 14	1.0×10^{-3} (fixed)	6.00 ± 0.02 (phosphate buffer, 10 mM)
	1 ~ 9	8.8×10^{-5} (fixed)	10.00 ± 0.02 (bicarbonate buffer, 25 mM)

To plot the sorption isotherm with the results from the sorption experiment after reaching equilibrium, the amount of adsorbed PNP with AC (Q_e) and the equilibrium concentration of PNP (C_e) at equilibrium were calculated according to equation (2.16) and (2.17), respectively.

Q_e (mol) = ($C_o - C_e$) × 20 mL / 1000 (2.16)

C_e (M) = (absorbance – y-intercept in the calibration curve of PNP) / ε (PNP) (2.17)

(According to Beer's Law)

The sorption isotherm can be obtained by plotting Q_e versus C_e. To plot the linearized sorption isotherm, equation (1.14), (1.15), and (1.16), as discussed in Chapter 1, are needed for the Freundlich, Langmuir, and BET models, respectively. However, in the case of the BET model [equation (1.16)]; a saturated concentration of PNP is also needed, which is 8.92×10^{-2} M. A linearized Freundlich sorption isotherm was obtained by plotting log Q_e versus log C_e and the slope and y-intercept were $1/n$ and log K_F, respectively. A linearized Langmuir sorption isotherm was obtained by plotting C_e / Q_e versus C_e and the slope and y-intercept were $1/Q_m$ and $1/K_L Q_m$, respectively. A linearized BET sorption isotherm was obtained by plotting $C_e /[(C_s - C_e) q_e]$ versus Ce/C_s and the slope and y-intercept were $[(K_{BET} - 1)/(Q_m K_{BET})]$ and $1/Q_m K_{BET}$, respectively. The theoretical sorption isotherm models of Freundlich, Langmuir, and BET are determined using the non-linear least squares (NLLS) by Microsoft Excel Solver of real sorption data. These models were introduced in equation (1.14), (1.15), and (1.16), respectively in Chapter 1 and subjected to a non-weighted fitting of those data obtained by plotting theoretical Q_e versus C_e. The best-fit was obtained by minimizing the sum of squares of residuals (SSR = $\sum_{i=1}^{N} (X_{i,experimental} - X_{i,calculated})^2$, where X_i represents data points at theoretical Q_e versus C_e for N data points. The surface areas of AC with PNP for Freundlich, Langmuir, and BET models were calculated using equation (1.17) by applying real Q_m values which were obtained from the NLLS Excel Solver program. Equilibrium parameters (K_F, K_L, K_{BET}, and n) were also obtained as fitting parameters after applying Excel Solver program.

2.5.4.2 Sorption isotherms for grafted ACs

PNP and MB were used for the sorption study of AC-β-CD[1:10:10(9)] and ACPDICD in which the grain size was maintained uniformly (< 40 mesh or 420 μm).

ACs were dried at 125 °C for 1 hour and stored in the desiccator for further use. The solutions of PNP were stored in the dark room by wrapping with aluminum foil. 20 mL of the solution of PNP was added in polyvinyl capped glass bottles containing various amounts of ACs. Sorption equilibrium reached after shaking 24 hours at room temperature. The experimental conditions are shown in Table 2.6, where C_o is the initial concentration of absorbate in solution which was determined from the measured absorbance of the blank solution after applying Beer's Law.

Table 2.6 Experimental conditions for the sorption study of PNP and MB with AC-β-CD [1:10:10(9)] and ACPDICD at 25 °C

Adsorbent	Solutions of Dye Adsorbates			
	Mass amount (mg)	PNP (C_o, M)	PNP (pH)	MB (C_o, M)	MB (pH)
AC-β-CD	1	n/a	n/a	9.0×10^{-5} ~ 3.0×10^{-6}	8.40 ± 0.02 (Borax buffer, 12.5 mM)
AC-β-CD	1	1.0×10^{-3} ~ 9.0×10^{-5}	6.00 ± 0.02 (phosphate buffer, 10 mM)	n/a	n/a
ACPDICD	1	n/a	n/a	9.0×10^{-5} ~ 3.0×10^{-6}	8.40 ± 0.02 (Borax buffer, 12.5 mM)
ACPDICD	1	9.9×10^{-4} ~ 4.0×10^{-5}	6.00 ± 0.02 (phosphate buffer, 10 mM)	n/a	n/a

Plotting of the sorption isotherm and calculation of surface areas were done by same procedures described in section 2.5.4.1, as outlined in Chapter 2.

2.5.5 Error Analysis

The Q_e value is calculated using equation (2.18) below where C_o is initial sorbate concentration, V is volume of solution and m is the mass of sorbent.

$$Q_e = \frac{(C_o - C_e) \times V}{m} \tag{2.18}$$

The error contributions of Q_e, ΔQ_e, are related to uncertainties in concentrations (C_o and C_e) and the mass of sorbent (m). Therefore, it is necessary to differentiate Q_e with respect to each quantity. The following contributions to errors in Q_e are obtained, as shown in equations (2.19 – 2.21)

$$\Delta Q_e = 2\left|\frac{(C_o - C_e) \times V}{m^2} \times \Delta m\right| \tag{2.19}$$

$$\Delta Q_e = 2\left|\frac{V}{m} \times \Delta C_o\right| \tag{2.20}$$

$$\Delta Q_e = 2\left|\frac{V}{m} \times \Delta C_e\right| \tag{2.21}$$

where ΔC_o, ΔC_e, and Δm are the standard errors associated with each measurement. The overall total error in Q_e is obtained from the sum of each of the quantities in equations (2.19 – 2.21). Note that there is both a positive error and a negative error with respect to each data point, hence, the inclusion of the factor of two preceding the absolute value of each quantity in equations (2.19 – 2.21). The standard error in C_e and C_o arises from uncertainties in absorbance and can be calculated based on the straight line equation for the Beer's Law coefficients. The uncertainty in mass arises from uncertainties in consecutive weighing on the electronic balance, i.e., $\pm 1\times10^{-4}$ g or 1×10^{-5} g per weight measurement. If there are 3 weighings to obtain a mass, the standard error is approximately 3×10^{-4} g (assuming the use of a 4-place balance or 3 $\times10^{-5}$ g if you are using a 5-place balance).

CHAPTER 3

RESULTS AND DISCUSSION

3.1 Synthesis

3.1.1 Oxidation (ACOXID)

All samples of AC that were subjected to oxidation reactions with nitric acid solutions [5.0 M, 15.8 M, and mixture of HNO_3/H_2SO_4 (1:3, v/v)] provided ACOXID except those reactions in which concentrated HNO_3 (15.8 M) at room temperature or 70 °C. The main evidence that supports oxidation of the surface of ACs is the DRIFT results according to the appearance of different peak intensities of carbonyl groups (C=O) around 1,760 cm^{-1}. Sonication of ACs also provided good levels of oxidation on the surface of ACs and provided similar IR results.

The most common functional groups which can be found from oxidation conditions with nitric acid are carboxylic, phenolic hydroxyl, and carbonyl (quinone)[113] or lactone groups. Vinke *et al.*[17] confirmed that carboxylic acid and ketone groups were formed on 9,10-dihydrophenanthrene and diphenylmethane, respectively, using nitric acid and these molecules are analogous to fragments of the graphene structure contained with the structure of AC. These reactions are shown in Scheme 3.1.

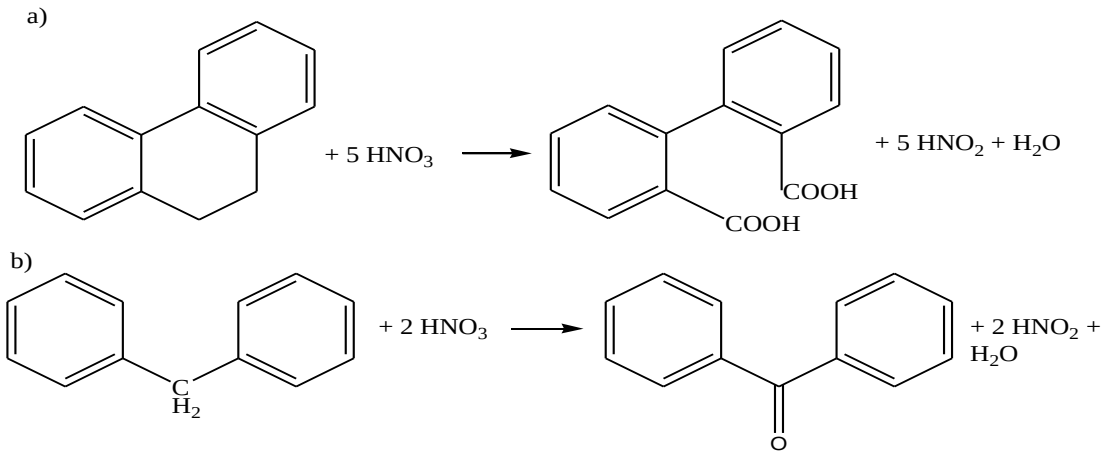

Scheme 3.1 Oxidation by nitric acid with a) 9,10-dihydrophenanthrene and b) diphenylmethane. Reaction condition [b) used 2.5 M HNO_3 in 70 % aqueous acetic acid at 90 °C with the yield of 84%][114]

Furthermore, the nitro group can also be found because the nitronium ion (NO_2^+)[115] is a strong electrophile that can be easily attached onto the rings of AC, as shown in the overall chemical reaction equation (3.1).

$$HNO_{3(aq)} + HNO_{3(aq)} \rightarrow NO_2^+{}_{(aq)} + NO_3^-{}_{(aq)} + H_2O_{(\ell)}$$
$$NO_2^+{}_{(aq)} + AC_{(s)} + H_2O_{(\ell)} \rightarrow AC\text{-}NO_{2(s)} + H_3O^+{}_{(aq)} \quad (3.1)$$

(Adapted from reference 115)

Interestingly, the oxidation of AC may reduce the surface area of ACOXID due to functionalization of the openings of micropores thereby inhibiting access of N_2 for sorption. As well, it can be explained by the fact that severe oxidation can collapse the graphitic ring structure of the micro-pores and also decompose the binders [e.g., cellulose ether or its derivatives (2 to 12 wt. %), clay (2 to 30 wt. %) based on AC, etc] of AC and create blockage within the inner walls of the micro-pores.

3.1.2 Amidization (ACAMID)

ACOXID was acylated by reaction with thionyl chloride and DMF, converted to an amide and imine groups by reacting with EDA. A generalized reaction scheme is shown in Scheme 3.2, where the vertical shaded plane represents the surface of AC.

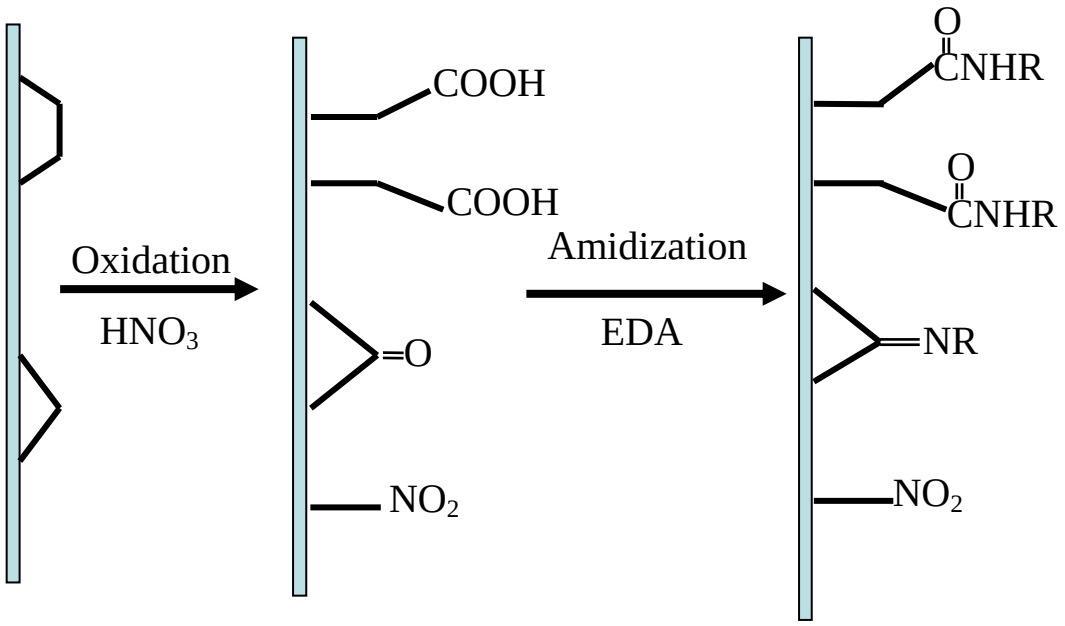

Scheme 3.2 Amidization of ACOXID with EDA (R = $CH_2CH_2NH_2$). The vertical shaded plane represents the surface of AC.

Ammonium hydroxide did not produce amide groups on the surface of AC due to the hydrolysis of the amide group formed on the surface of AC in the reaction mixture. Alternatively DCC/EDA did not provide amide group when the reaction was repeated. The absence of target product materials was concluded on the basis of IR results.

3.1.3 Reduction (ACREDUCT)

The byproducts from reduction of AC with $LiAlH_4$ were alcohol and amine functional groups. The generalized synthetic pathway is shown in Scheme 3.3.

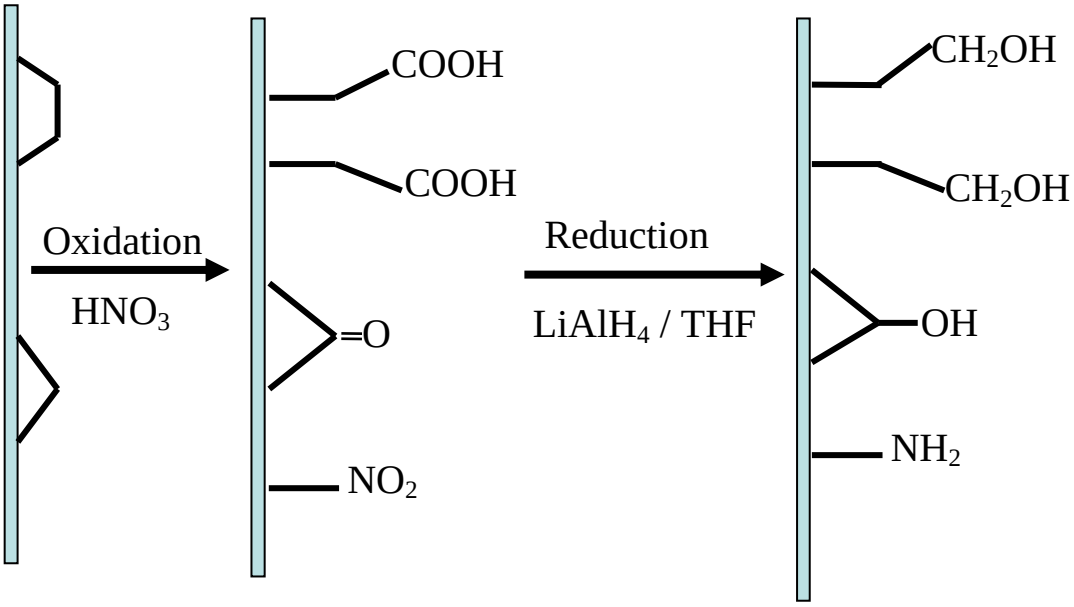

Scheme 3.3 Reduction of ACOXID with $LiAlH_4$. The vertical shaded plane represents the surface of AC.

To complete the reduction reaction, deionized water was added instead of using mild HCl because quenching by deionized water did not show the presence of a grey powder [$Al(OH)_{3(s)}$] which made purification of ACREDUCT more difficult. Lithium and aluminum are byproducts, as shown in equation (3.2) and may be included in the pore structure of AC.

$$LiAlH_{4(s)} + 4H_2O_{(\ell)} \rightarrow Li^{+}_{(aq)} + Al^{+3}_{(aq)} + 4OH^{-}_{(aq)} + 4H_{2(g)} \uparrow \qquad (3.2)$$

Interestingly, the reduction of ACOXID affected the surface area of ACREDUCT by the inclusion of metal ion (Al^{+3}), which was identified by AA results (refer to section 3.2.3) and XPS results (refer to Table 3.12 in section 3.2.12.) in Chapter 3.

3.1.4 Synthesis of p-tosyl-β-cyclodextrin (tosyl-β-CD)

The deprotonated form of β-CD under basic conditions is attacked by the sulfonyl group of tosyl chloride, which resulted in tosyl-β-CD (M.W = 1,288.25 g/mol) and characterized by ^{1}H NMR and IR results. The yield was less than 11 % and consistent with a previous literature value.[111] The reaction scheme is shown in Scheme 3.4.

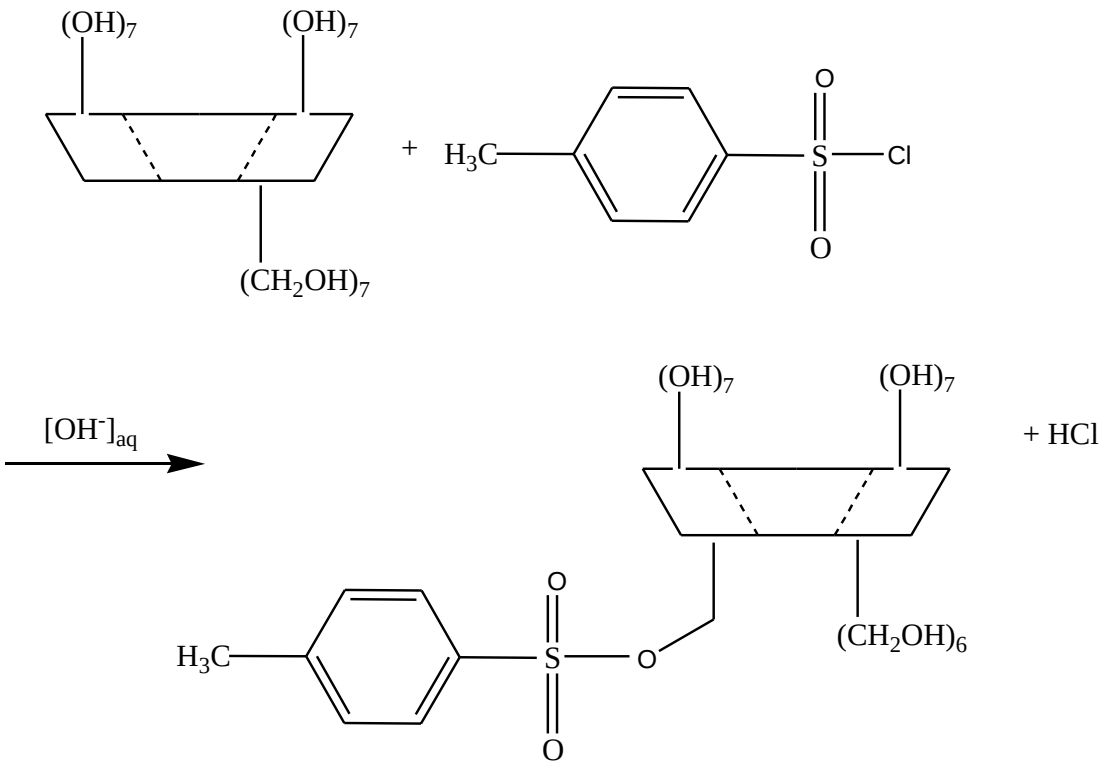

Scheme 3.4 Tosylation of β-CD in aqueous solution (solvent not shown)

3.1.5 Grafting of tosyl-β-CD on ACAMID

The amine group of ACAMID is a strong nucleophile for reaction with tosyl-β-CD resulting in the loss of a tosyl group from tosyl-β-CD and replacing with β-CD because the tosyl group is considered to be a good leaving group. However, the mole ratio of tosyl-β-CD against ACAMID was 0.08:1.7 which was not sufficient to yield the expected chemical reaction. There may have been hydrolysis of the amide into an acid and amine. Therefore, no product was observed according to IR results. The general reaction scheme is shown in Scheme 3.5.

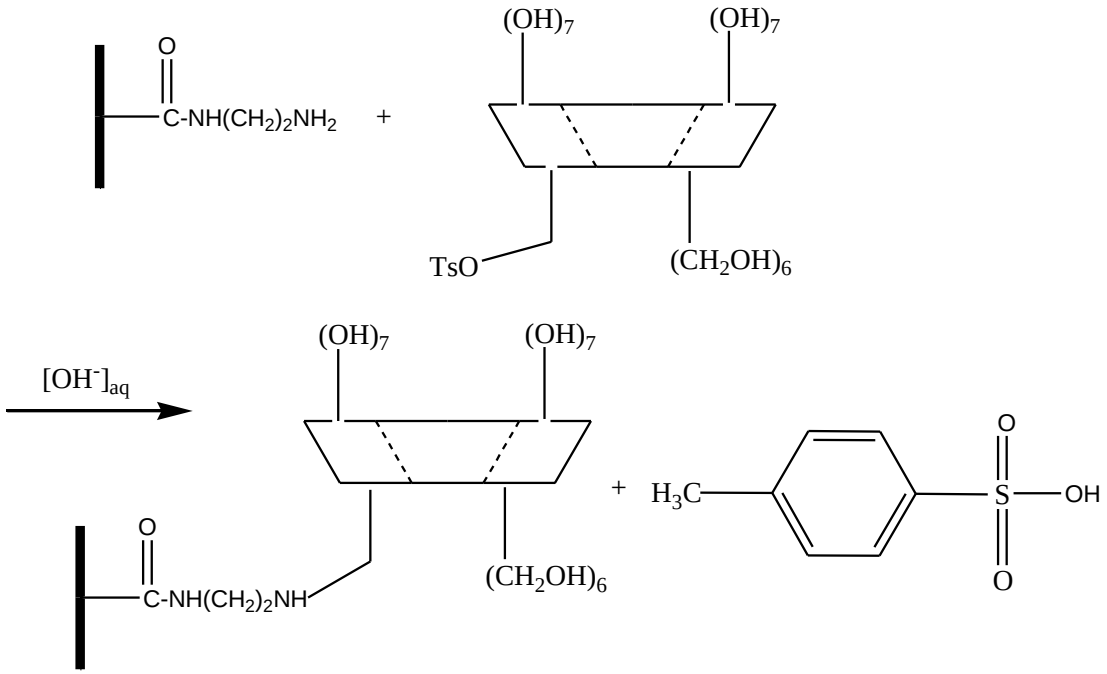

Scheme 3.5 General reaction scheme for the grafting of tosyl-β-CD on ACAMID. The dark vertical bar represents the surface of AC.

3.1.6 Grafting of tosyl-β-CD on ACREDUCT

The reaction mechanism of this grafting procedure is similar to the grafting of tosyl-β-CD on ACAMID because the tosyl group is a good leaving group. However, the mole ratio of tosyl-β-CD against ACREDUCT was 0.05:1 which may have been insufficient to yield the predicted product. Therefore, no product was observed according to the IR results.

3.1.7 Grafting of β-CD on ACREDUCT via the linker of GA

All trials were conducted with β-CD with a chemical selectivity of forming two covalent bonds on ACREDUCT, which are imine bond formation at higher mole ratios of GA and hemiacetal bond formation at higher mole ratios of β-CD. The functional group between GA and β-CD was concluded to be the hemiacetal bond because of the reaction that occurs between an alcohol and aldehyde under acidic conditions (refer to Scheme 3.6). Formation of an acetal bond might be impossible because of the steric hindrance of β-CD. If the mole ratio of GA is much higher than that of β-CD (at least GA > 2 CD), grafting occurs to an amine moiety in

ACREDUCT. However, if the mole ratio of β-CD is greater than that of GA (CD ≥ GA), grafting occurs with an alcohol moiety in ACREDUCT. The crossover ratio from imine to hemiacetal was 1:10:5. The analysis of chemical bond and grafting mole ratios are shown in Table 3.1.

Table 3.1 The analysis of chemical bonds and various grafting mole ratios for surface modified ACs

Mole ratio (AC:GA:β-CD)	Chemical bond(*)
1:10:1(3)	Imine
1:20:2(3,6,9)	Imine
2:10:0.9(3)	Imine
1:10:5(6)	Hemiacetal
1:10:10(9)	Hemiacetal
1:10:20(9)	Hemiacetal

(*) determined according to IR and Raman results

The reaction scheme for the GA based grafting of β-CD onto AC is shown in Scheme 3.6.

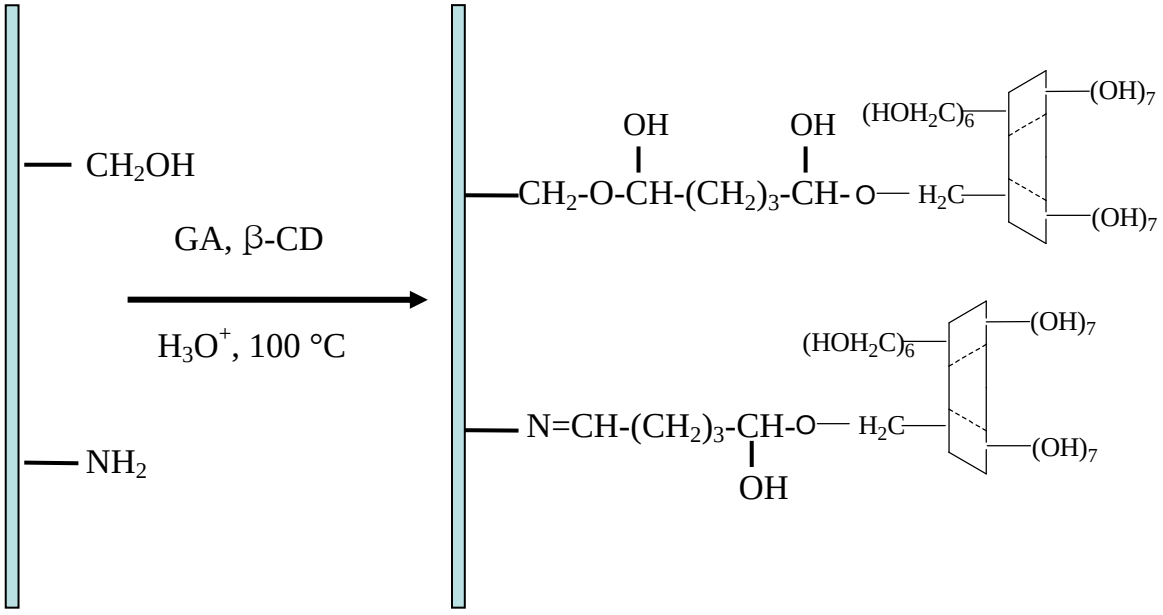

Scheme 3.6 Grafting of β-CD on ACREDUCT via the linker of GA. The vertical shaded plane represents the surface of AC.

Hydrolysis of the hemiacetal grafted AC under acidic condition did not occur because the imine and hemiacetal groups were identified by IR and Raman results and also supported by MALDI results which showed peaks of [β-CD+salt] adducts.

Complete removal of free β-CD and GA was confirmed by measuring the absorbance of washings of the products with a UV spectrophotometer between 190 nm and 200 nm for β-CD and between 200 nm and 300 nm for GA. The λ_{max} for β-CD is below 200 nm and the λ_{max} for GA is 234 nm, respectively.

Interestingly, the grafting of β-CD to ACREDUCT affected the surface area of AC-β-CD by the inclusion of aluminum (refer to Table 3.12 in section 3.2.12.) and mesopore filling with fine ground powder of ACREDUCT which was formed during the stirring of ACREDUCT material in the reaction mixture with a magnetic stir bar for 48 hours and may have resulted in the mechanical damage of the mesopores of ACREDUCT.

3.1.8 Grafting of β-CD on ACOXID via the linker of PDI

β-CD was grafted onto the surface of ACOXID via an urethane bond formed between the carboxylic group in ACOXID and the isocyanate group of PDI. (See Fig 1.13 in Chapter 1) The functional group in the covalent bond between PDI and β-CD is the urethane bond. The carbon in isocyanate group is considered electron-deficient and therefore the electron-rich oxygen of carboxylic group in ACREDUCT and hydroxyl group in β-CD was added resulting in the forming of the urethane bond between them. The general scheme for the addition reaction is shown in Scheme 3.7.

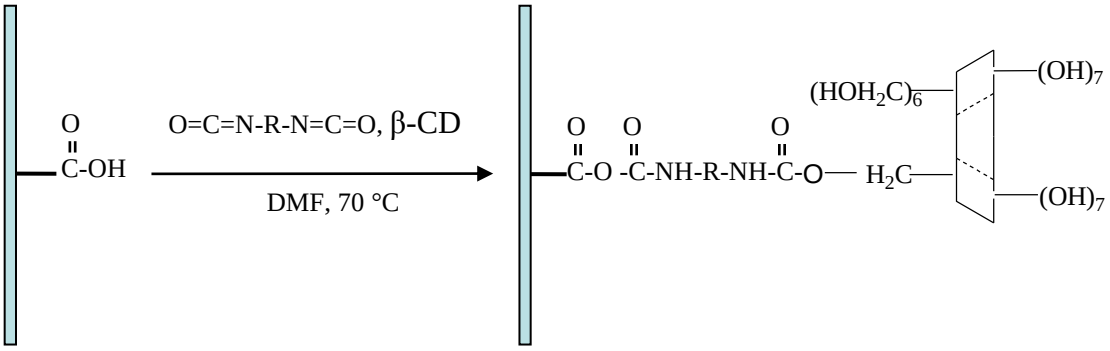

Scheme 3.7 Grafting of β-CD on ACOXID via the linker of PDI, where CD represents β-CD and R = 1,4-phenylene

The complete removal of unbound β-CD was verified by measuring the absence of absorbance from the water washings by UV light between 190 nm and 200 nm.

Interestingly, the grafting of β-CD to ACOXID affected the surface area of ACPDICD by micropore filling with fine ground powder of ACOXID which was formed during the stirring ACOXID in the reaction solution with a magnetic stir bar for 44 hours and may have resulted in the mechanical damage of the micropores of ACOXID. Another possible reason is the absorption of reactant (PDI) into micorpores of the surface-heterogeneous ACOXID.

3.2 Characterization

3.2.1 pH measurements

The results of the pH measurement for total surface functional group of AC, ACOXID(9), ACREDUCT(9), and grafted ACs with β-CD are shown in Table 3.2.

Table 3.2 The results of pH measurement for total surface functional group from AC, ACOXID, ACREDUCT, and grafted ACs at 25 °C

ACs	pH (2.0 %)
AC	7.37
ACOXID(9)	2.97
ACREDUCT(9)	8.29
AC-β-CD(1:10:10)(9)	3.63
ACPDICD	4.78

The surface charge density of AC was changed from neutral to acidic or basic by different surface treatments. Oxidation provided surface acid groups such as carboxylic, carbonyl and hydroxyl groups at the surface of AC. Reduction reactions changed these surface acid groups to surface basic groups such as alcohol and amine groups at the surface and grafting of β-CD to ACREDUCT using GA returned its basicity to acidic characteristic due to the acidic nature of the linker. Grafting of β-CD to ACOXID using PDI decreased its acidity slightly due to the basic nature of the linker and the nitro groups. Therefore, the pH value of the surface modified AC was affected by the nature of the linkers.

3.2.2 Boehm titrations

The total amount of surface acid and base groups were calculated by equation (3.2), where A (mL) was the consumed volume of the titrant and B was the mass (g) of the sample involved in individual calculation.

$$\text{Total acid} = [(0.02\ \text{M} \times 0.005\ \text{mL}) - (0.02\ \text{M} \times \text{A mL})] \times 1000 \times 5 / \text{B} \qquad (3.2)$$

The total amount of hydroxyl groups is the result of subtracting total carbonyl groups from total acid groups. As the degree of oxidation on the AC surface was increased, the amount of surface bound acid groups was also increased in agreement with the results from the Boehm titration. The maximum amount of surface acid groups occurred between 9 - 10 hours of treatment with nitric acid in the solution. The number of hydroxyl groups gradually decreased due to further oxidation to carbonyl groups such as quinone, while the total basicity was increased by an increase of the numbers of nitro groups. The results of the Boehm titrations are shown in Table 3.3 and Figure 3.1.

Table 3.3 The results of the Boehm titrations for oxidized forms of AC

Time of Oxidation (hr)(*)	Carbonyl groups (mmol/g)	Hydroxyl groups (mmol/g)	Total surface acidity (mmol/g)	Total surface acidity groups (mmol/nm^2)(**)	Total surface Basicity (mmol/g)
0	0.0440	0.140	0.184	1.81×10^{-22}	0.703
3	1.40	0.530	1.93	2.59×10^{-21}	0.125
6	1.62	0.450	2.07	3.37×10^{-21}	0.174
9	1.87	0.300	2.17	4.31×10^{-21}	0.249
12	1.86	0.200	2.06	-	0.287

(*) Oxidation according to the conditions given in section 2.4.2
(**) calculated according to surface area (BET) of bare AC from nitrogen porosimetry

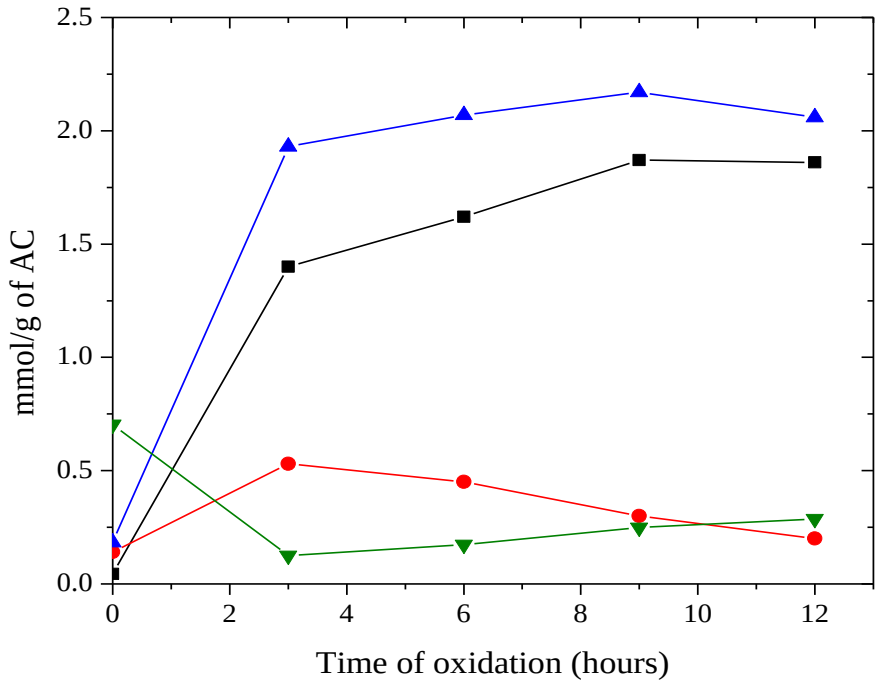

Figure 3.1 The results of Boehm Titrations (Triangle: Total acidity, Rectangle: Carbonyl group, Circle: Hydroxyl group, Inversed triangle: Total basicity)

3.2.3 Metal contents

Many metals were found from the peat[116] with the use of the inductively coupled argon plasma atomic emission spectrometry (ICP AES) technique. Similarly, metals found from AC are alkali metals (Na, K, Ca), transition metals (Fe, Mg), and heavy metals (Cu, Zn, Pb). The analysis of metals is shown in Table 3.4.

Table 3.4 Metal content (ppm) composition in "as received" AC using atomic adsorption spectrophotometry

Ca	Mg	Na	K	Fe	Cu	Zn	Pb
239.5	152.0	677.0	81.8	86.0	45.7	25.5	18.9

The content of aluminum in ACREDUCT(9) which was supposed to block mesopores of ACREDUCT(9) was 6.0 % by atomic adsorption spectrophotometry.

3.2.4 Porosimetry

According to the BET results (refer to Table 3.5), the surface area of modified AC was gradually decreased after oxidation, reduction, and grafting, as compared to that of the "as received" AC. It can be explained by the fact that severe oxidation can weaken the graphitic ring structure of the micro-pores, decompose the binders of AC, and possibly block the inner walls of the micro-pores. Upon reduction of AC, metals (Li and Al) were absorbed in pores in ACREDUCT and its surface area was dramatically decreased. This was demonstrated by increased average pore diameter (Å) and decreased micro-pore volume (cc/g) and micro-pore area (m^2/g). The experimental results of porosimetry are shown in Table 3.5. According to Table 3.5, information concerning the surface area and pore structure are provided for modified ACs measured at 80 °C and 100 °C because there might not be complete dehydration of water molecules captured in micropores of AC.

Table 3.5 The results of nitrogen porosimetry measurements

ACs	Surface Area (m^2/g)		Micropore Area (m^2/g)	Micropore Volume (cc/g)	Average Pore Diameter(*) (Å)
	BET	Langmuir			
AC (Granular)	1,016	1,348	672	0.311	19.1
AC (Powder)	956	1,269	650	0.301	18.5
ACOXID(3)	745	997	429	0.196	18.4
ACOXID(6)	615	823	331	0.153	18.1
AXOXID(9)	503	670	294	0.136	18.9
ACREDUCT(3)	377	507	149	0.068	19.9
ACREDUCT(6)	276	370	110	0.050	22.0
ACREDUCT(9)	135	181	68	0.031	42.0
AC-β-CD [1:10:10(9)]	74	103	9	0.004	39.4
AC-β-CD [1:10:20(9)]	91	131	0	~ 0	31.4
ACPDICD	69	95	22	0.010	39.1
β-CD	1	n/a	0	~ 0	n/a

(*) Average pore diameter based on the BET model

3.2.5 TGA and DTG

The total surface coverage was calculated based on a consideration of weight losses of adsorbed molecules on the surface of ACs and peak deconvolution of their thermograms. Adsorbed water was evaporated from the surface of AC, in the pores of ACs, and in the cavity of β-CD, whereas linkers, such as GA and PDI, were decomposed from the covalent bond decomposition between AC and β-CD which can make their typical T_m higher. Carbon dioxide and carbon monoxide that were formed undergo decarbonylation of C=O and C-O functional groups including hydroxyl groups. β-CD was desorbed and decomposed from the surface of AC at the covalent

bond between the linker and β-CD. The calculation of surface coverage with β-CD and analysis of the decomposition temperature of AC, the surface modified ACs and the grafted ACs are shown in Table 3.6, where T_m is the temperature of maximum decomposition in the corresponded decomposition temperature range with the most possible product from the source of decomposition. Note that the heating pan is always contaminated by water in the air and fingers.

Table 3.6 The results of TGA and DTG measurements

Region	Decomposition Temperature (°C)	Samples A	B	C	D
I	Range	23.0 ~ 127.9	25.0 ~ 137.0	22.0 ~ 116.0	29.0 ~ 79.0
	$T_m^{(*)}$	44.2 (H_2O)	70.0 (H_2O)	65.8(H_2O)	n/a (H_2O)
II	Range	128.0 ~ 285.0	137.1 ~ 350.0	116.1 ~ 183.0	79.1 ~ 144.0
	$T_m^{(*)}$	202.4 (H_2O in micropores)	251.7 (H_2O in micropores and CO_2)	156.0 (H_2O in micropores)	123.5 (H_2O in micropores and physisorbed GA)
III	Range	285.1 ~ 422.0	350.1 ~ 547.0	183.1 ~ 267.0	144.1 ~ 384.0
	$T_m^{(*)}$	335.9 (CO_2)	430.7(CO)	225.3 (CO_2)	205.5 (CO_2)
IV	Range	422.1 ~ 547.0	n/a	267.1 ~ 547.0	384.1 ~ 592.0
	$T_m^{(*)}$	n/a (CO)	n/a	395.0 (CO)	520.3 (CO)

Region	Decomposition Temperature (°C)	Samples E	F	G	H
I	Range	21.0 ~ 117.5	21.0 ~ 164.0	20.0 ~ 160.0	20.0 ~ 123.0
	T_m(*)	34.0 (H_2O)	68.9 (H_2O)	66.4 (H_2O)	44.4 (H_2O)
II	Range	117.6 ~ 247.0	164.1 ~ 244.0	160.1 ~ 246.0	123.1 ~ 266.0
	T_m(*)	206.5 (H_2O in micropores)	231.8 (H_2O in micropores and in the cavity of β-CD)	226.9 (H_2O in micropores and in the cavity of β-CD)	228.4 (H_2O in micropores and in the cavity of β-CD and PDI linker)
III	Range	247.1 ~ 457.0	244.1 ~ 300.0	246.1 ~ 288.0	266.1 ~ 368.0
	T_m(*)	291.3 (β-CD and CO_2)	266.5 (GA linker)	264.3 (GA linker)	312.4 (β-CD and CO_2)
IV	Range	457.1 ~ 592.0	300.1 ~ 357.8	288.1 ~ 389.0	368.1 ~ 547.0
	T_m(*)	513.1 (CO)	323.3 (β-CD)	323.6 (β-CD)	n/a (CO)
V	Range		357.9 ~ 547.0	389.1 ~ 523.0	
	T_m(*)		438.4 (CO)	447.2 (CO_2)	
VI	Range			523.1 ~ 592.0	
	T_m(*)			557.0 (CO)	

Product	Method	H_2O (%)	CO_2 and CO (%)	Linkers (%)	Linkers $T_m^{(*)}$ (°C)	β-CD (%)	β-CD $T_m^{(*)}$ (°C)	Total Surface Coverage (%)	Residual ash (%)
AC	W.L.	3.7	1.8	n/a	n/a	n/a	n/a	5.5	94.5
ACOXID(9)	W.L.	6.0	25.8	n/a	n/a	n/a	n/a	31.8	68.2
ACREDUCT(9)	W.L.	11.5	48.2	n/a	n/a	n/a	n/a	59.7	40.3
ACGAP(10)	W.L.	2.3	13.3	1.7	123.5	n/a	n/a	17.3	82.7
ACCDP(10)	P.D.	3.5	1.7	n/a	n/a	5.0	288.4	10.2	89.8
	W.L.	3.6	1.7	n/a	n/a	4.9	291.3		
AC-β-CD [1:10:10(9)]	P.D.	5.4	23.6	3.0	237.9	3.0	316.4	35.0	65.0
	W.L.	8.8	18.6	3.7	266.5	3.9	323.3		
AC-β-CD [1:10:20(9)]	P.D.	7.4	16.0	4.1	242.3	3.3	311.3	30.8	69.2
	W.L.	8.3	13.7	3.9	264.3	4.9	323.6		
ACPDICD	P.D.	3.3	21.0	4.0	223.4	3.6	305.7	31.9	68.1
	W.L.	6.0	13.3	5.4	228.4	7.2	312.4		

(*) T_m is determined on the basis of analyzing DTG thermograms for Weight Loss (W.L.) method and Peak Deconvolution (P.D.) method by Origin 7.5 [A = AC, B = ACOXID(9), C = ACREDUCT(9), D = ACGAP(10), E = ACCDP(10), F = AC-β-CD [1:10:10(9)], G = AC-β-CD [1:10:20(9)], H = ACPDICD], n/a = not applied

The evolution temperature of CO_2 varies by chemical functional groups; it can occur from 100 °C to 400 °C for carboxylic acid groups, from 200 °C to 600 °C for lactone groups, and over 600 °C for phenol, carbonyl, ether, quinine, and anhydride groups which includes CO.[98] ACOXID from HNO_3 treatment evolves CO_2 in the range of 130 ~ 827 °C with Tm (252 °C).[10]

The peak deconvoluted DTG thermograms are shown in Figure 3.2.

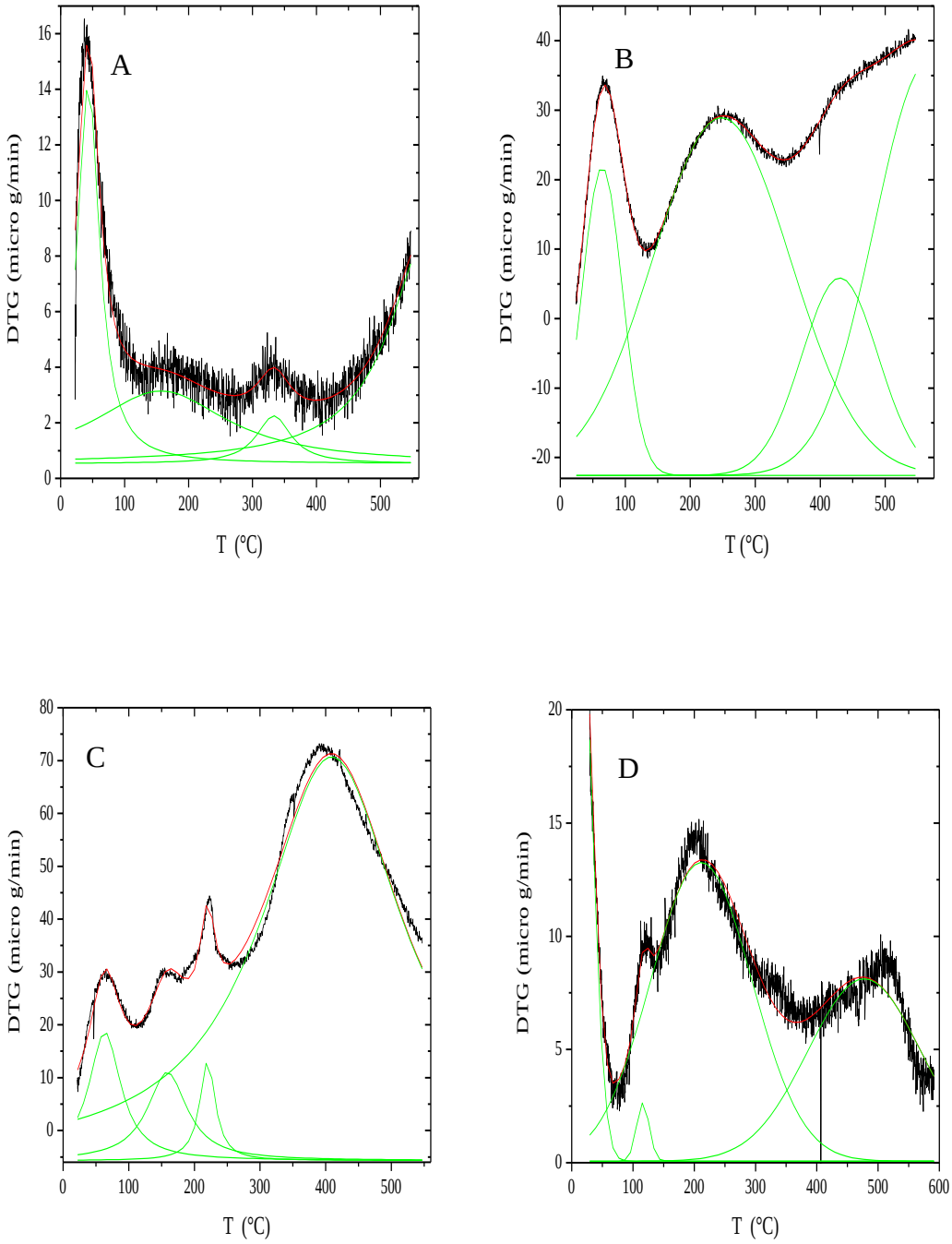
A
B
C
D
DTG (micro g/min)
T (℃)

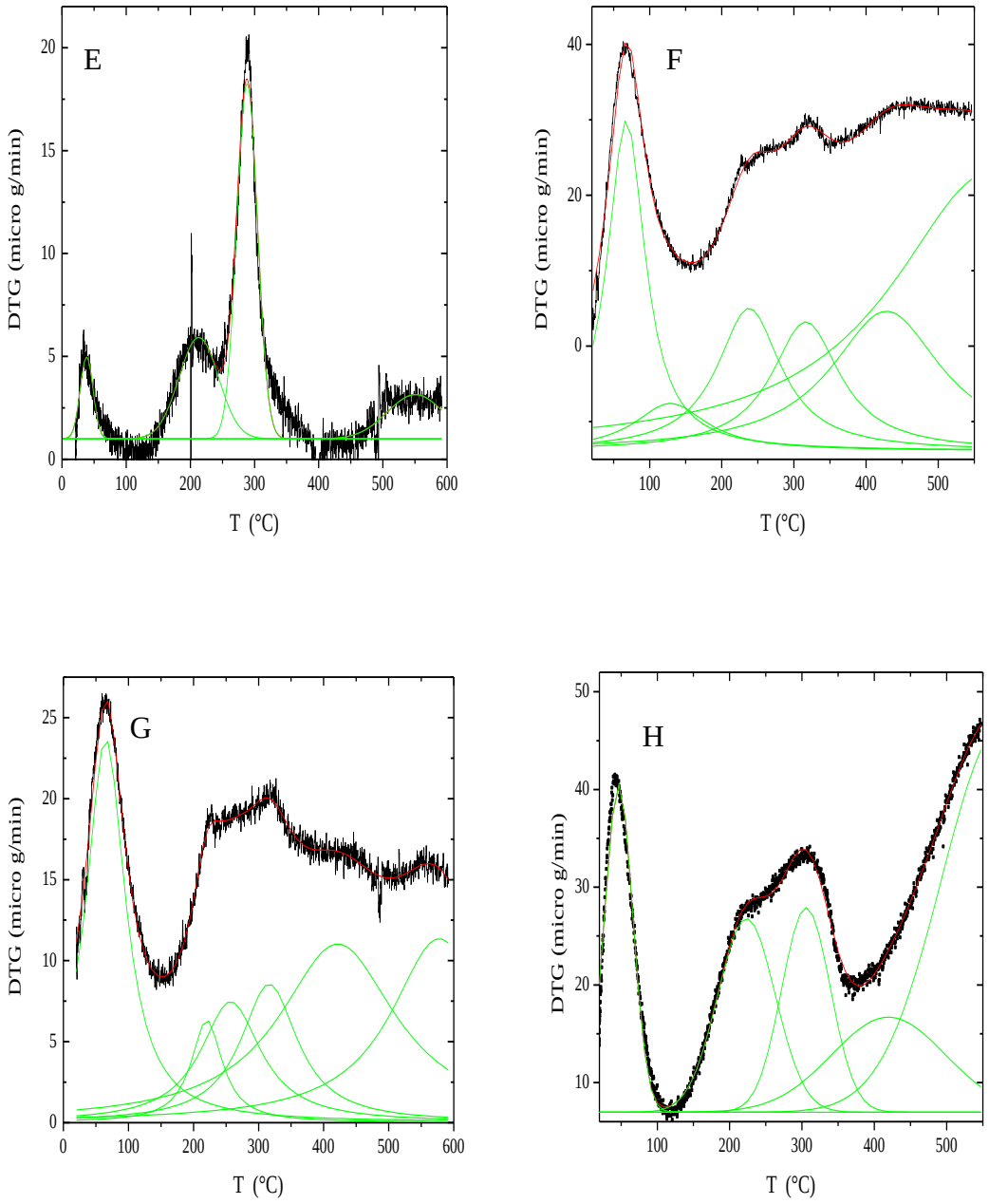

Figure 3.2 The experimental DTG curves and peak deconvoluted DTG thermograms [A = AC, B = ACOXID(9), C = ACREDUCT(9), D = ACGAP(10), E = ACCDP(10), F = AC-β-CD [1:10:10(9)], G = AC-β-CD [1:10:20(9)], H = ACPDICD]

With regard to the calculation of the content of β-CD for ACCDP(10), it also contains CO_2 because carbonyl group is present on the surface of AC. For ACPDICD, the total linker content might include the water content from micropore in ACPDICD and in

the cavity of β-CD. Likewise, the total β-CD content might include the CO_2 content. The T_m of the PDI linker was greatly changed when it is compared to its melting point (~ 100 °C) because the formation of a urethane bond between PDI and β-CD imparted additional thermal stability as shown by T_m values that exceed the melting point temperature for PDI and β-CD (290 °C), respectively. From the analysis of Table 3.6, the stoichiometric ratio between AC:linker:β-CD seems to be reasonably well matched as 1:1:1 although AC-β-CD [1:10:20(9)] showed a slightly higher ratio of β-CD content by the calculation of weight loss of the decomposed materials, which would still remained as free β-CD and some deviation in the calculation of the content of water and β-CD for ACPDICD is proposed. The content of water increased as the amount of surface hydrophilic groups increased. AC is relatively hydrophobic at its surface, however, the relative hydrophobicity decreases as its surface was oxidized, reduced, and grafted with surface functional groups, as evidenced by more bound water in its pores or cavities. (See TGA/DTG thermograms in APENDICES: A1 – AC, A2 - ACOXID(9), A3 - ACREDUCT(9), A4 - ACGAP(10), A5 - ACCDP(10), A6 - AC-β-CD[1:10:10(9)], A7 - AC-β-CD[1:10:20(9)], and A8 – ACPDICD)

3.2.6 Raman Spectroscopy

Activated carbon shows six bands with particular Raman shifts: D band (1,339 cm^{-1}), G^1 band (1,593 cm^{-1}), G^2 band (1,587 cm^{-1}), D+G^1 band (2,932 cm^{-1}), 2D band (2,678 cm^{-1}), 2G^1 band (3,186 cm^{-1}) which are characterized by different structural identity with different vibrational stretching modes from the basal plane (for example, G^1 band from in-plane E_{2g} vibrational stretching and D band from breathing A_{1g} vibrational stretching).[117] D band originates from the structural disorder of amorphous AC such as curvature effects of graphene sheets and defects at the closed ends. G band originates from intramolecular vibration between graphene sheet carbon atoms and in-plane tangential stretching between graphene sheet carbon atoms.

Characteristic Raman shifts[58,118,119] for grafted ACs via GA are –OH (~ 3,300 cm^{-1} from broad H-bond of β-CD, hemiacetal linker, and bound water), $–CH_2$ (3000 cm^{-1}~ 2800 cm^{-1} from β-CD), = CH [~ 3,070 cm^{-1} from N=C-H (imine) stretching], C = N (~

1,650 cm^{-1} from imine), G band (1,593 cm^{-1} from AC, C = C stretch in graphite),[101,102] D band (1,340 cm^{-1} from AC, C = C stretch in disordered graphite),[101,102] and several peaks at 1,450 cm^{-1} ~ 480 cm^{-1} from β-CD). Characteristic regions for grafted ACs via PDI are –NH (~ 3,300 cm^{-1} from urethane), $–CH_2$ (3000 cm^{-1}~ 2800 cm^{-1} from β-CD), amide I [C=O (~ 1,640 cm^{-1} from urethane)], $–C-NO_2$ (1,590 cm^{-1} ~ 1,530 cm^{-1} from asymmetric vibration and 1,380 cm^{-1} ~ 1,340 cm^{-1} from symmetric vibration), G band (1,593 cm^{-1} from AC), D band (1,340 cm^{-1} from AC), and several peaks at 1,450 cm^{-1} ~ 480 cm^{-1} from β-CD. The analysis of Raman shift frequencies are shown in Table 3.7. Characteristic Raman shifts of tosyl- β-CD are also shown in Table 3.7.

Table 3.7 Experimentally obtained vibrational band frequencies for grafted ACs

Name	Functional groups ($\Delta\upsilon$ / cm^{-1})
AC	1,339 (s, D band); 1,593 (s, G^1 band); 1,587 (s, G^2 band); 2,678 (w, 2D band); 2,932 (w, $D+G^1$); 3,186 (w, $2G^1$)
β-CD	3,390 (br, H-bond); 2,939 and 2,903 (s, $–CH_2$); 1,451 , 1,410, 1,387, 1,334, and 1,250 (m, δ_{C-H} and δ_{O-H} in CHOH and CH_2OH); 1,203, 1,126, 1,081, 1,046, 1,001 (m, υ_{C-O-C} in CH-O-CH and υ_{C-OH} in H_2C-OH or HC-OH); 946 (m, skeletal vibration involving α-1,4 linkage); 848 (m, δ_{C1-H} anomeric carbon); 574, 475 (m, skeletal vibration) (reference 58 and 119)
ACCDP(10)	3,390 (br, H-bond); 2,899 (s, $–CH_2$); 1,470, 1,378, and 1,338 (m, δ_{C-H} and δ_{O-H} in CHOH and CH_2OH from β-CD); 1,094 (m, υ_{C-O-C} in CH-O-CH and υ_{C-OH} in H_2C-OH or HC-OH from β-CD); 568 (w, skeletal vibration from β-CD) ➔ no D and G bands
AC-β-CD [1:10:1(3)]	3,304 (br, H-bond); 3,056 (w, from N=C-H stretching); 2,929 and 2,874 (s, $–CH_2$); 1,650 (w, C=N); 1,605 (m, G band); 1,446, and 1,348 (m, δ_{C-H} and δ_{O-H} in CHOH and CH_2OH from β-CD including D band); 1,203, 1,124, 1,028,

	1,002 (m, $\upsilon_{C\text{-}O\text{-}C}$ in CH-O-CH and $\upsilon_{C\text{-}OH}$ in H_2C-OH or HC-OH from β-CD and hemiacetal linker); 935 (br and w, skeletal vibration involving α-1,4 linkage from β-CD); 848 (w, $\delta_{C1\text{-}H}$ anomeric carbon) ➔ imine bond
AC-β-CD [1:10:5(6)]	3,350 (br, H-bond); 2,946 and 2,896 (s, – CH_2); 1,602 (s, G band); 1,478 and 1,338 (br and s, $\delta_{C\text{-}H}$ and $\delta_{O\text{-}H}$ in CHOH and CH_2OH from β-CD and hemiacetal linker including D band); 1,119, 1,093, and 1,052 (m, $\upsilon_{C\text{-}O\text{-}C}$ in CH-O-CH and $\upsilon_{C\text{-}OH}$ in H_2C-OH or HC-OH from β-CD and hemiacetal linker) ➔ hemiacetal bond
AC-β-CD [1:10:10(9)]	3,350 (br, H-bond); 2,966 and 2,893 (s, – CH_2); 1,606 (m and br, G band); 1,475, 1375, and 1,338 (m, $\delta_{C\text{-}H}$ and $\delta_{O\text{-}H}$ in CHOH and CH_2OH from β-CD and hemiacetal linker including D band); 1,149, 1,118, and 1,093 (m, $\upsilon_{C\text{-}O\text{-}C}$ in CH-O-CH and $\upsilon_{C\text{-}OH}$ in H_2C-OH or HC-OH from β-CD and hemiacetal linker); 897 (m, $\delta_{C1\text{-}H}$ anomeric carbon) ➔ hemiacetal bond
AC-β-CD [1:10:20(9)]	3,350 (br, H-bond); 2,963 and 2,894 (s, – CH_2); 1,608 (m and br, G band); 1,474, 1376, and 1,336 (m, $\delta_{C\text{-}H}$ and $\delta_{O\text{-}H}$ in CHOH, CH_2OH from β-CD and hemiacetal linker including D band); 1,147, 1,119, and 1,094 (m, $\upsilon_{C\text{-}O\text{-}C}$ in CH-O-CH and $\upsilon_{C\text{-}OH}$ in H_2C-OH or HC-OH from β-CD and hemiacetal linker); 897 (m, $\delta_{C1\text{-}H}$ anomeric carbon) ➔ hemiacetal bond
AC-β-CD [2:10:0.9(3)]	~ 3,300 (br and w, H-bond); 3,070 (w, from N=C-H stretching); 2,930 and 2,904 (s, –CH_2); 1,599 (m, G band); 1,444, and 1,300 (m, $\delta_{C\text{-}H}$ and $\delta_{O\text{-}H}$ in CHOH and CH_2OH from β-CD); 1,124, 1,084, 1,003 (m, $\upsilon_{C\text{-}O\text{-}C}$ in CH-O-CH and $\upsilon_{C\text{-}OH}$ in H_2C-OH or HC-OH from β-CD and hemiacetal linker); 481 (m, skeletal vibration from β-CD) ➔ imine

	bond
ACPDICD	3,306 (m, –NH); 2,916 and 2,870 (s, – CH_2); 1,633 (m, C=O in urethane); 1,602 (m and br, G band); 1,472, 1,439, 1,380, 1,337, 1,296, and 1,229 (m, δ_{C-H} and δ_{O-H} in CHOH, CH_2OH from β-CD including D band and –C-NO_2); 1,126, 1,060, and 1,044 (m, υ_{C-O-C} in CH-O-CH and υ_{C-OH} in H_2C-OH or HC-OH from β-CD); 953 (m, skeletal vibration involving α-1,4 linkage from β-CD) ➔ urethane bond
Tosyl- β-CD	3,402 (br, H-bond); 3,062 (s, aryl C-H); 2,931 and 2,901 (s, –CH_2); 1,597 (s, $\delta_{C=C,}$ in-plane); 1,455 , 1,406, 1,379, 1,332, and 1,259 (m, δ_{C-H} and δ_{O-H} in CHOH and CH_2OH); 1,175 (s, sulfonate); 1,210, 1,126, 1,099, 1,078, 1,045, 1,000 (m, υ_{C-O-C} in CH-O-CH and υ_{C-OH} in H_2C-OH or HC-OH); 946 (m, skeletal vibration involving α-1,4 linkage); 858 (m, δ_{C1-H} anomeric carbon); 792 (s, para-disubstituted benzene ring); 574, 475 (m, skeletal vibration)

Note: s: sharp, m: medium, br: broad, w: weak, δ: bending, and υ: stretching

A Typical Raman spectrum for AC-β-CD [1:10:10(9)] is shown in Figure 3.3.

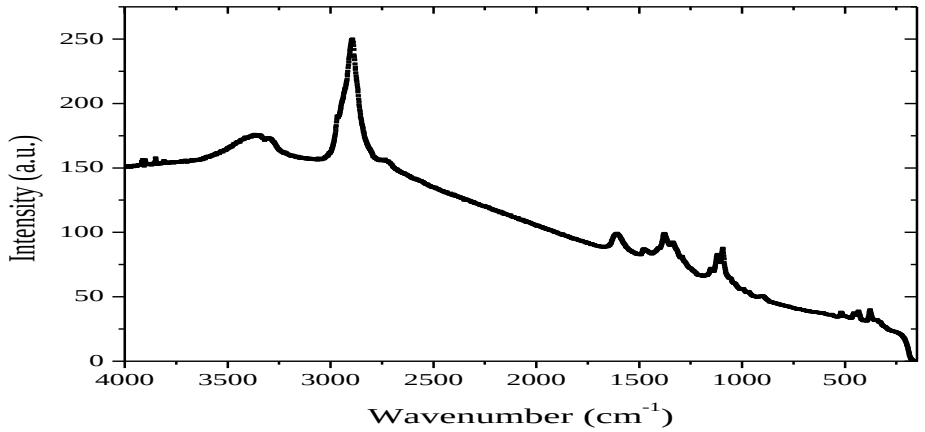

Figure 3.3 A typical Raman spectrum for AC-β-CD [1:10:10(9)]. λ_{ex} = 514 nm, T = 25 °C, and the base line is uncorrected.

β-CD was found as an image of white aggregates which was grafted at the surface of AC via linkers, whereas the surface of AC was shown as black regions. A metal such as Zn is also shown as white image, but its intensity was very strong at ~ 470 cm^{-1}. Those images taken by a charge-coupled device camera (CCD) camera fitted with Raman microscope [× 500 times: objective lens (× 50 times, fitted with 0.5 numeric aperture) × eyepiece lens (× 10 times)] are shown in Figure 3.4. The dimension of images are 95 μm x 65 μm.

A)

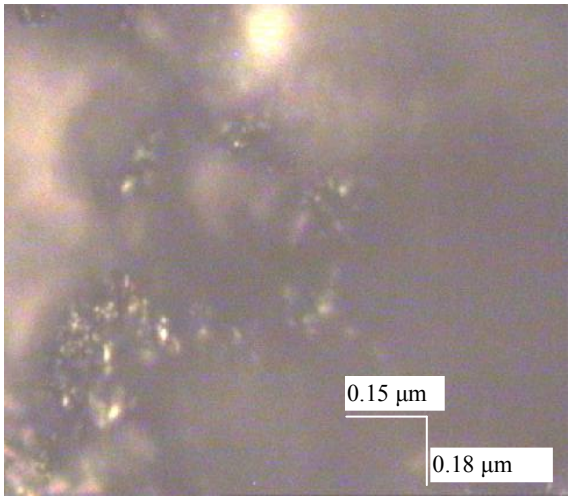

B)

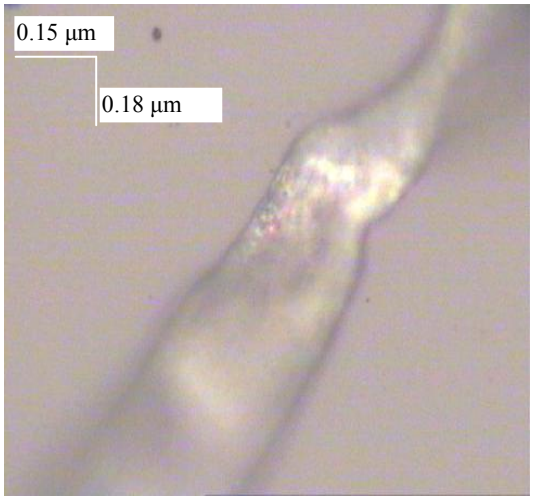

C)

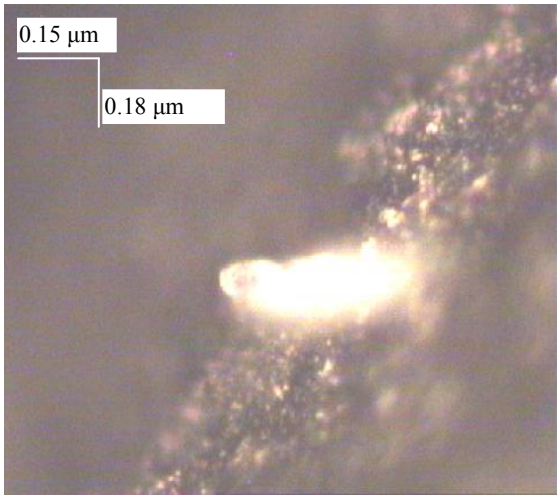

D)

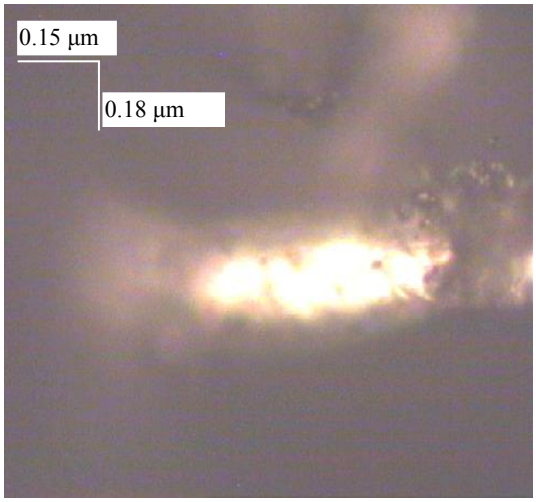

E)

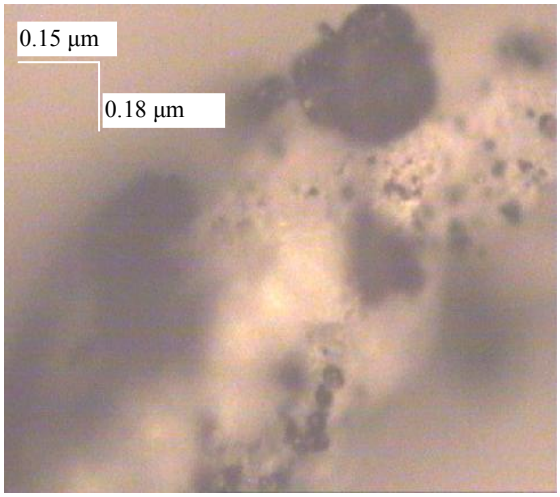

F)

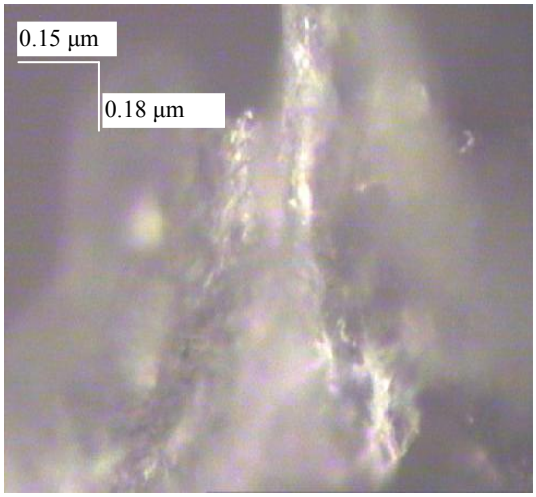

G)

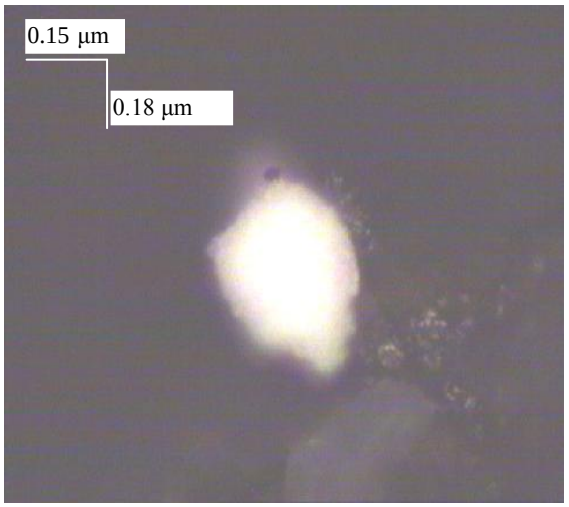

H)

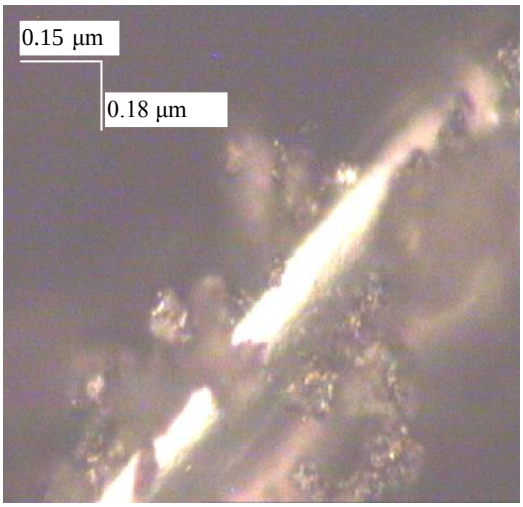

Figure 3.4 Raman microscopic images recorded at λ_{ex} = 514 nm and T = 25 °C {A) AC, B) ACCDP(10), C) AC-β-CD [1:10:1(3)], D) AC-β-CD [1:10:5(6)], E) AC-β-CD [1:10:10(9)], F) AC-β-CD [1:10:20(9)], G) AC-β-CD [2:10:0.9(3)], and H) ACPDICD}

(See Raman Spectra in APENDICES: A9 - AC, A10 - β-CD, A11 - ACCDP(10), A12 - AC-β-CD[1:10:1(3)], A13 - AC-β-CD[1:10:5(6)], A14 - AC-β-CD[1:10:10(9)], A15 - AC-β-CD[1:10:20(9)], A16 - AC-β-CD[2:10:0.9(3)], A17 – ACPDICD, and A-18 – Tosyl- β-CD)

The key features of Raman images are explained in Table 3.8.

Table 3.8 Key features of Raman images (cf. Figure 3.4)

Name	Grain		
	Color	Size (l × w, μm)	Shape
AC	Black	-	Shiny; amorphous
ACCDP(10)	white	95 × 7~20	Plate-like aggregate groth with lustrous appearance; stretched out from the surface of AC
AC-β-CD [1:10:1(3)]	white	20 × 15	Bright oval; embedded in the surface of AC
AC-β-CD [1:10:5(6)]	white	30 × 15	Bright oval; embedded in the surface of AC
AC-β-CD [1:10:10(9)]	white	95 × 15~45	Opaque aggregates; stretched out from the surface of AC
AC-β-CD [1:10:20(9)]	white	95 × 7~50	Coupled aggregates; stretched out from the surface of AC
AC-β-CD [2:10:0.9(3)]	white	15 × 36	Bright oval; embedded in the surface of AC
ACPDICD	white	85 × 9	Long bright oval; embedded in the surface of AC

Grain size gradually increases from imine bond to hemiacetal or urethane bond as the mole ratio of β-CD increases or urethane bond forms. The dwellings of the grafted β-CD on the surface of AC seem to be localized by forming aggregates. Brightness of the image is affected by the angle of the sample and its surface condition (hardness and crystallinity) because the resulting signal arises from scattered laser light.

3.2.7 MALDI TOF Mass Spectrometry

All samples showed the molecular ion (*m/z*) at 1,157 which represents $[M+Na]^+$ and 1,173 refers to $[M+K]^+$, where M is β-CD. However, AC-β-CD [1:10:1(3)] and AC-β-CD [1:10:5(6)] showed [M+X+H] for $[M+K]^+$ and [M+X-H] for $[M+Na]^+$ and

$[M+K]^+$, respectively. ACPDICD additionally showed fragment ion peaks at 1,324, 1,572 and higher molecular ion fragments besides at 1,157 and 1,173 which may be attributed to further adducts forming of [M±X], where X = metals, H, H_2O, organic functional groups, or organic acids and matrix elements which may form inclusion and non-inclusion complexes with β-CD. Similar observations were made in CD grafted silica materials.[120] The analysis of MALDI TOF MS results are provided in Table 3.9.

Table 3.9 Molecular ions (*m/z*) determined from MALDI TOF MS analysis

Name	$[M+Na]^+$	$[M+K]^+$	Other Ions
AC-β-CD [1:10:1(3)]	1,157	1,174	
AC-β-CD [1:10:5(6)]	1,156	1,172	
AC-β-CD [1:10:10(9)]	1,157	1,173	
AC-β-CD [1:10:20(9)]	1,157	1,173	
AC-β-CD [2:10:0.9(3)]	1,157	1,173	
ACPDICD	1,157	1,173	1,324, 1,572, etc
ACCDP(10)	1,157	1,173	
β-CD	1,157	1,173	

Note: M = β-CD molecular ion

A typical MALDI TOF MS spectrum for AC-β-CD [1:10:5(6)] is shown in Figure 3.5.

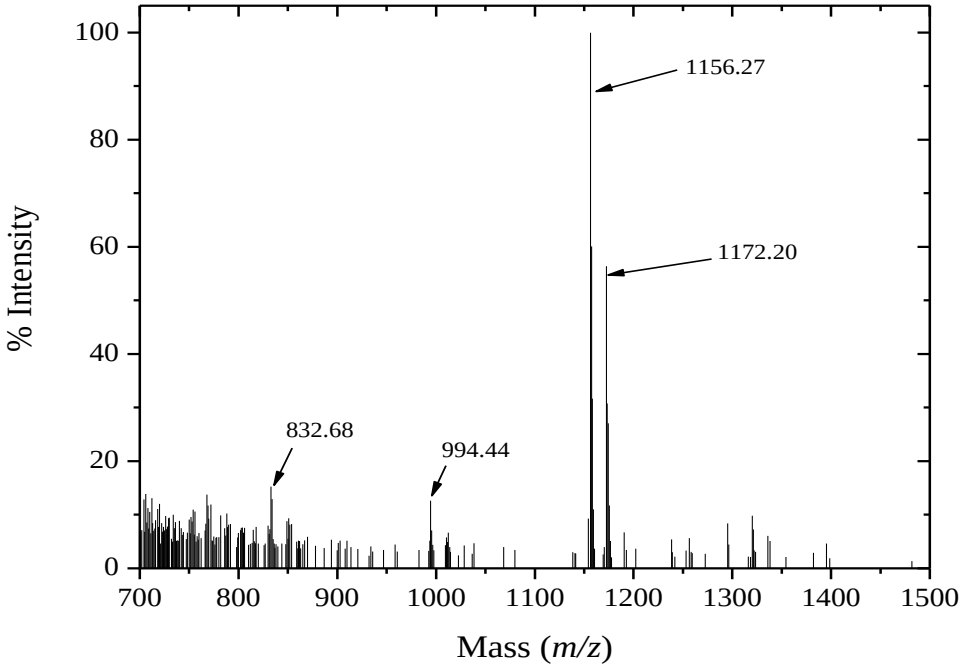

Figure 3.5 A typical MALDI TOF MS spectrum of AC-β-CD [1:10:5(6)]

Lower molecular ion fragmentation of CD which is ionized by the energy beam and its adduct, [M±X], also appeared below 1,157 (*m/z*). For example, [M±X] = 832.68 is [5 glucose units + Na] and [M±X] = 994.44 is [6 glucose units + Na - H] in Figure 3.5. Higher mass molecular ion above 1,172 (*m/z*) for ACPDICD, for example, 1,324 (*m/z*) and 1,572 (*m/z*) are adducts of [CD+3COOH+2CO-H] and [CD+9CO_2+Ca+2H], respectively. The origins of the alkali metal ions (e.g., Na^+ and K^+) are the deionized water used to prepare the matrix prior to analysis. (See MALDI TOF MS Spectra in APENDICES: A19 - AC-β-CD[1:10:1(3)], A20 - AC-β-CD[1:10:5(6)], A21 - AC-β-CD[1:10:10(9)], A22 - AC-β-CD[1:10:20(9)], A23 - AC-β-CD[2:10:0.9(3)], A24 - ACPDICD, A25 - ACCDP(10), and A26 - β-CD)

3.2.8 ESR Spectroscopy

The analysis of ESR spectra is shown in Table 3.10, where k is a constant ($k = h/B_e$), B_{actual} for DPPH is calculated from $\{\nu_{dpph}\ k\ /\ [g\ (2.0037\ \text{for DPPH}) \times 1000]\}$, B_{corr} for DPPH is calculated from (B_{actual} - $B_{experimental}$), B_{corr} for a real sample is calculated from

[center field (CF, sample) + B_{corr} (DPPH)], and the *g* value for the sample is calculated from [v_{sample} *k* / B_{corr} (DPPH) × 1000)]. CF can be measured at which the first derivative line of the absorption spectrum is passes through the zero point of the axis of the peak intensity. The above terms are defined as outlined in section 2.3.1 (ESR) in Chapter 2.

Table 3.10 Analysis of ESR parameters

Name	Line Width (G)	*v* (GHz)	CF (G)	*k*	B_{actual} (G)	B_{corr} (G)	*g* value
DPPH	1.1120	9.8415	3510.0329	0.7145	3509.2577	- 0.7752	
ACOXID (6)	2.7550	9.8193	3501.3157			3500.5405	2.0042
ACOXID (12)	3.2780	9.8930	3514.3469			3513.5717	2.0118
DPPH	1.0650	9.8445	3506.6719	0.7145	3510.3356	3.6637	
AC PDICD	2.5130	9.8205	3503.1131			3506.7768	2.0009
AC-β-CD [1:10:20 (9)]	3.1850	9.8410	3520.6049			3524.2686	1.9951
AC REDUCT (6)	4.7740	9.8166	3501.4099			3505.0736	2.0011
DPPH	1.0790	9.8357	3516.2892	0.7145	3507.2002	- 9.0890	
AC REDUCT (9)	4.7590	9.8295	3510.7027			3501.6137	2.0057
AC-β-CD [1:10:10 (9)]	4.0240	9.8561	3509.9906			3500.9016	2.0115
DPPH	1.1120	9.8279	3505.1868	0.7145	3504.4193	- 0.7675	
ACOXID (9)	3.1510	9.8540	3514.8000			3514.0325	2.0036

As the total surface acidity in ACOXID or oxidation time for AC increases, the *g*-value decreases due to the increased oxidation state of the surface functional groups. However, it again sharply increases at which the total surface acidity decreases. Likewise, it increases as the total surface basicity in ACREDUCT increases. ACPDICD shows a lower g-value than ACOXID due to its lower content of oxygen. Likewise, AC-β-CD[1:10:10(9)] shows a higher g-value than ACREDUCT due to its higher content of oxygen (refer to Table 3.12 and 3.13). However, AC-β-CD[1:10:20(9)] shows much decreased g-value for an unknown reason. In general, the ESR data provides information, both quantitative and qualitative about the presence of free radicals whose origin is from AC itself or paramagnetic metals as impurities. (See ESR Spectra in APENDICES: A27 - DPPH, A28 - ACOXID(6), A29 - ACOXID(12), A30 - ACPDICD, A31 - AC-β-CD[1:10:20(9)], A32 - ACREDUCT(6), A33 - ACREDUCT(9), A34 - AC-β-CD[1:10:10(9)], and A35 - ACOXID(9)

3.2.9 DRIFT Spectroscopy

The tabulation of DRIFTS data for various ACs are shown in Table 3.11. The DRIFT spectra for ACOXIDs (A), ACREDUCTs (B), and grafted ACs (C) are shown in Figure 3.6.

Table 3.11 Characteristic infrared bands peaks of ACs and modified ACs

Name	Functional groups (cm^{-1})
Tosyl- β-CD	3,357 (br, hydrogen bond); 1,600 (w, aromatic C=C); 1,363 and 1,153 (s, sulfonates)
ACOXID(3,6,9)	1,852 (w, C=O); 1,760 (s, cyclic ketone or lactone); 1,604 (s, aromatic or C=O with highly conjugated with aromatic: quinone)[121]; 1,334 (w, nitro)[115] and 1,250 (w, C-O); maximum C=O peak at 9 hour oxidation
ACRREDUCT(3,6,9)	3,653 (w, Hydroxyl); 3,553 & 3,486 (w, amine stretching); 1,612 (s, quinol type); Reducing C=O peak at 1, 852 and 1,760; Increasing quinol peak at 1,612
AC-β-CD [1:10:1(3)]	C=N peak[122] at 1,677 (m ~ w)
AC-β-CD [2:10:0.9(3)]	Refer to accompanying text
AC-β-CD [1:20:2(3,6,9)]	Refer to accompanying text
AC-β-CD [1:10:5(6)]	Disappearing C=N peak at 1,677
AC-β-CD [1:10:10(9)]	Refer to accompanying text
AC-β-CD [1:10:20(9)]	Refer to accompanying text
ACPDICD	3,390 (m, Free NH); 3,306 (br, Bonded NH); 1,698 (m, C=O stretching - urethane); 1,512 (m, NH deformation - Amide II); Disappearing N=C=O peak at 2,250; Decreasing C=O peak at 1,852 and 1,763

Note: The following abbreviations are defined as follows: broad (br), sharp (s), medium (m), weak (w).

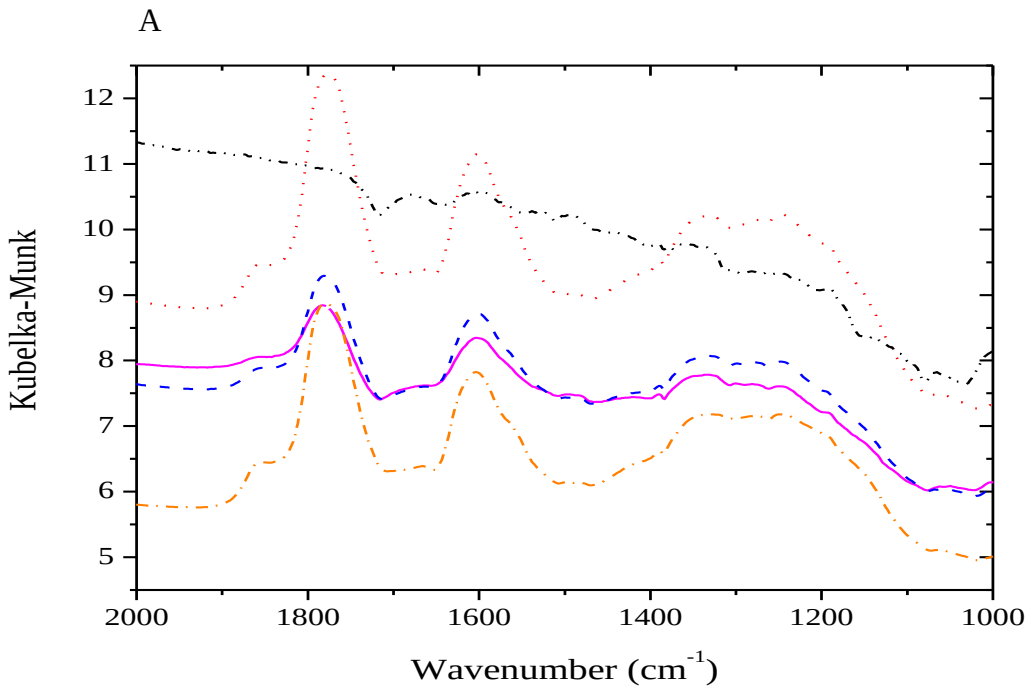
A
Kubelka-Munk
12
11
10
9
8
7
6
5
2000
1800
1600
1400
1200
1000
Wavenumber (cm-1)

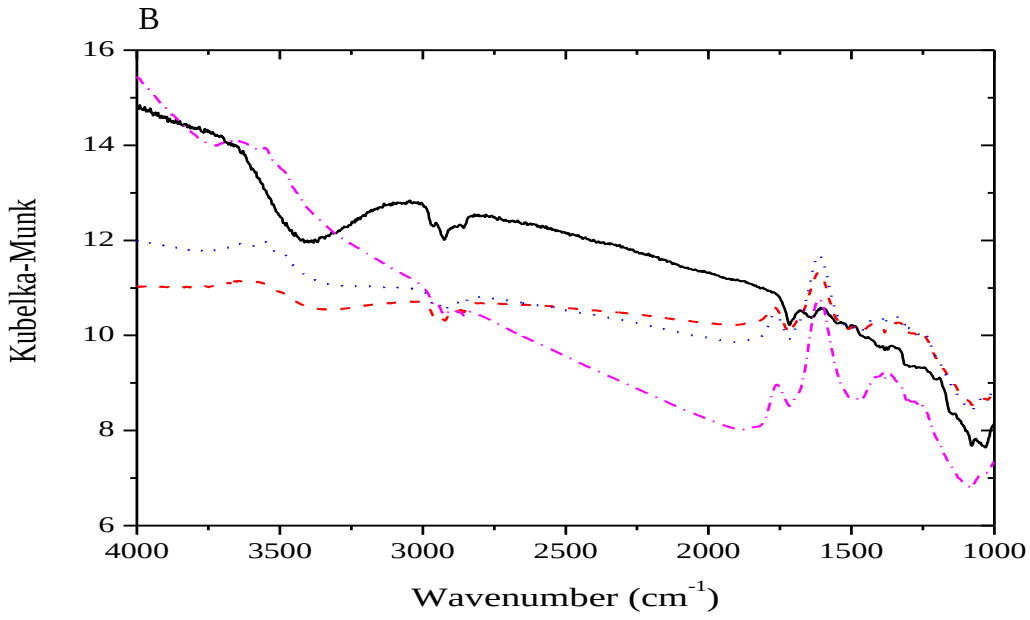
B
Kubelka-Munk
16
14
12
10
8
6
4000
3500
3000
2500
2000
1500
1000
Wavenumber (cm-1)

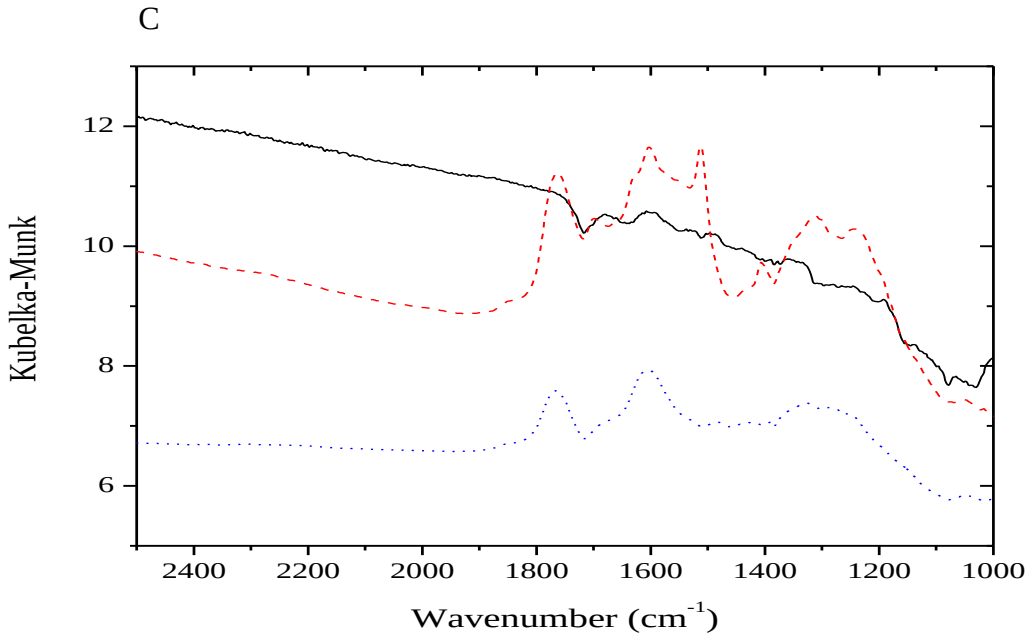

Figure 3.6 IR spectra for ACOXIDs (A: solid line – AC, dash line – 9 hours, dot line – 3 hours, dash dot line – 6 hours, dash dot dot line – 12 hours), ACREDUCTs (B: dash dot line – 9 hours, solid line – AC, dot line – 6 hours, dash line – 3 hours), and grafted ACs {C: solid line – AC, dash line – ACPDICD, dot line – AC-β-CD[1:10:10(9)]}

The aromatic C-H peak was not observed for tosyl-β-CD because of spectral overlap in the region (> 3,000 cm^{-1}) which is attributed with the strong vibrational band for hydroxyl groups of β-CD which cover a similar spectral region for tosyl-β-CD. The peak at 1,852 cm^{-1} from ACOXID could be an acid anhydride and one of its vibrational bands may be overlapped with the lactone peak. The strong peak at 1,760 cm^{-1} shows that AC was severely oxidized with HNO_3. The peak at 1,604 cm^{-1} from ACOXID can be assigned as an aromatic C=C or C=O for a highly conjugated system with an aromatic ring such as quinone. However, when ACOXID was reduced with $LiAlH_4$, this peak apparently increased with a red shift (~ 10 cm^{-1}). Therefore, it was identified as a quinone type because an aromatic C=C is not expected under these reaction conditions from a reduced form and the quinol type C=C, to the reduced form of a quinone, was gradually increased due to an inductive effect of the hydroxyl group in the quinol aromatic ring (Hydroquinone). The DRIFT spectra for AC-β-CDs are almost similar to AREDUCTs due to their similar IR activity arising from their

functional groups. However, AC-β-CD[1:10:1(3)], AC-β-CD[2:10:0.9(3)], and AC-β-CD[1:20:2 (6)] showed the characteristic imine peak at 1,677 cm^{-1}, whereas AC-β-CD[1:10:5(6)], AC-β-CD[1:10:10(9)], and AC-β-CD[1:10:20(9)] didn't show the imine peak. ACPDICD showed typical amine peaks (3,300 cm^{-1} and 3,400 cm^{-1}) urethane peaks (1,698 cm^{-1} for C=O and 1,512 cm^{-1} for amide II). (See DRIFT Spectra in APENDICES: A36 - AC, A37 - Tosyl-β-CD, A38 - ACOXID(3), A39 - ACOXID(6), A40 - ACOXID(9), A41 - ACREDUCT(3), A42 - ACREDUCT(6), A43 - ACREDUCT(9), A44 - AC-β-CD[1:10:1(3)], A45 - AC-β-CD[2:10:0.9(3)], A46 - AC-β-CD[1:20:2 (6)], A47 - AC-β-CD[1:10:5(6)], A48 - AC-β-CD[1:10:10(9)], A49 - AC-β-CD[1:10:20(9)], and A50 – ACPDICD)

3.2.10 Elemental Analysis

The content of nitrogen and oxygen was apparently changed as surface modification was applied to ACs. The results of the C, H, and N elemental analysis measurements are shown in Table 3.12. The content of oxygen and hydrogen was adjusted by taking the content of adsorbed water from TGA/DTG analysis because the nitrogen content in ACPDICD by XPS is considered high, although XPS result are available. Oxygen content was calculated assuming that aluminum content in the samples was zero even though residual elements other than C, H, and N were estimated to be less than 1 % for AC, ACOXID, and ACPDICD and ~ 6 % for ACREDUCT(9), AC-β-CD [1:10:10(9)] and AC-β-CD [1:10:20(9)].

Table 3.12 The results of elemental analysis (C, H, N)(*)

Name	C (%)	H (%)	N (%)	O (%)
AC	85.2	0.4	0.4	14.0
ACOXID(9)	70.0	0.7	1.2	28.1
ACREDUCT(9)	60.2	1.1	1.7	37.0
AC-β-CD [1:10:10(9)]	63.0	1.3	0.9	34.8
AC-β-CD [1:10:20(9)]	68.0	1.1	1.0	29.9
ACPDICD	68.1	1.4	6.0	24.5

(*) Values are corrected due to adsorbed water.

The presence of 1.2 % nitrogen in ACOXID(9) provides support that a nitro group was formed by oxidation with nitric acid. The use of PDI for grafting of β-CD to ACOXID resulted in an increase of the content of nitrogen because of the presence of N atoms in the PDI linker and the subsequent formation of a urethane bond via an additional reaction.

3.2.11 SEM

The SEM images for ACs showed bright spots caused by backscattered electrons and the arrows indicate the presence of metal components, as shown in Figure 3.7. Alkali, transition, and heavy metals (refer to the section 2.3.3.1 in Chapter 2 and 3.2.3 in Chapter 3) contained in the structure of AC during manufacturing processes are engaged to provide backscattered electrons and the image will be getting whiter as the atomic number of metal increases due to increased backscattering.

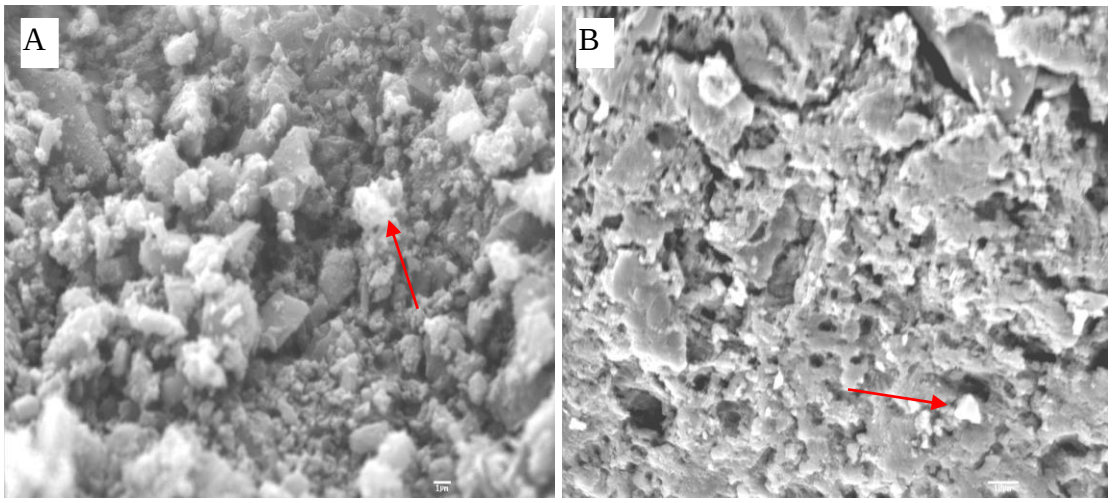

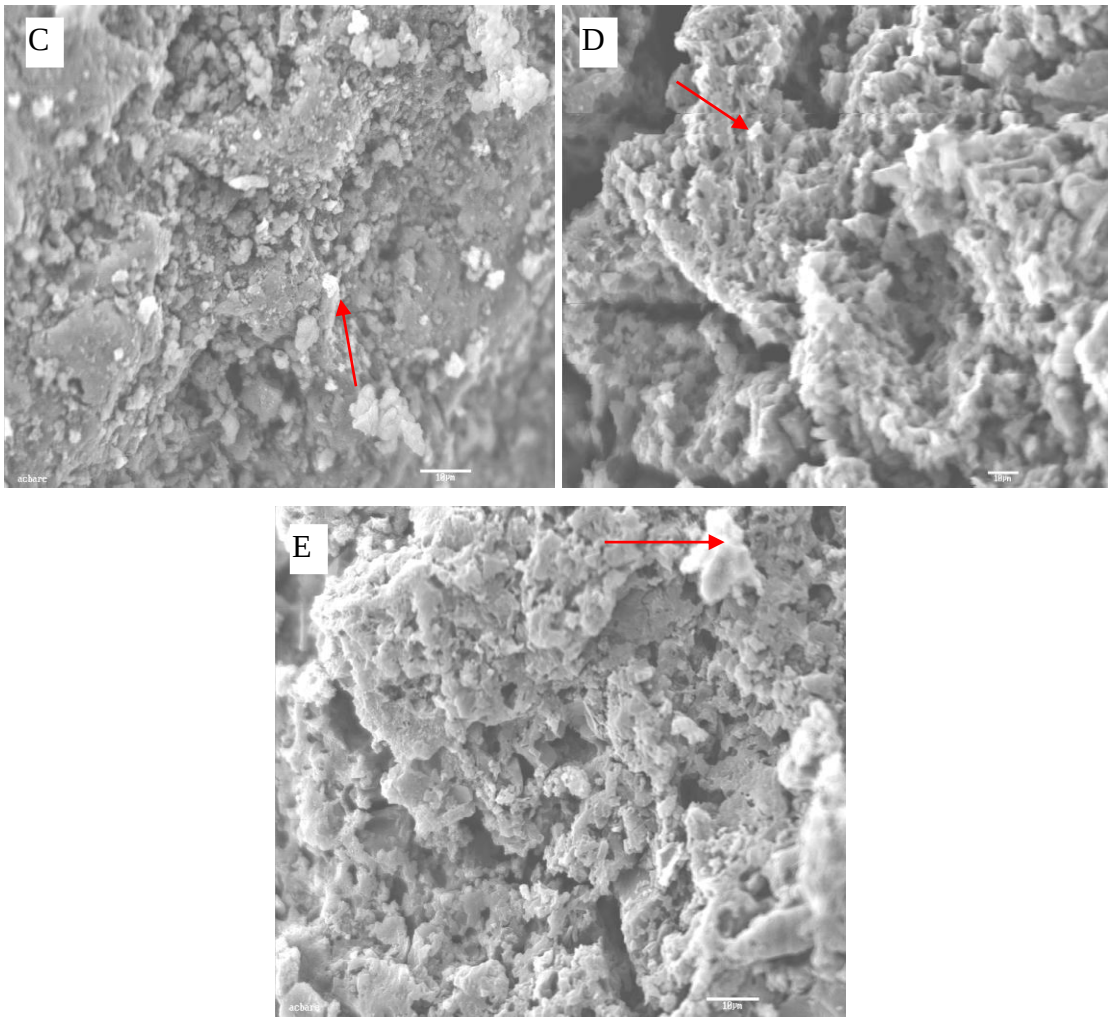

Figure 3.7 The images of SEM of ACs with different scale bars (A = 1 μm, B to E = 10 μm) obtained at 25 °C, where A = AC, B = ACOXID(9), C = ACREDUCT(9), D = AC-β-CD [1:10:10(9)], and E = ACPDICD

ACOXID(9) (B) had more wide pores than AC (A) and the surface appears to have been broken and eroded by the oxidation with nitric acid. ACREDUCT(9) (C) were concluded to be blocked and the appearance aggregates of bright metals (Li and Al). AC-β-CD [1:10:10(9)] (D) and ACPDICD (E) illustrate swollen textures with some pore structure.

3.2.12 XPS

Origin of C 1s, O 1s, and N 1s electron is from amorphous AC, surface functional groups (-C=O, -C-NO_2, -COOH, -OH, amine, and lactone or quinone), linkers (imine,

hemiacetal, and urethane bond), and grafted β-CD. All spectra for the fitted C 1s peaks were calibrated by 0.95 eV presuming that initial spectra from AC spectra is dominated by C-C and C-H bonding which is related to 285.0 eV binding energy. The chemical environment on the surface of AC and the grafted AC are very complex and the theoretical binding energy of C 1s, O 1s, and N 1s electron is much different than expected. The electron withdrawing groups next to C, O, and N atom and higher oxidation states of C, O, and N atom serve to increase the electron density of the individual atoms and can make its binding energy higher, whereas electron donating groups next to C, O, and N atom and lower oxidation states of C, O, and N atoms which decrease the electron density of the individual atom can make its binding energy attenuated due to the change of the net interaction energy between the nucleus and the core electrons accordingly. Neighboring atoms of oxygen and nitrogen atoms in AC and grafted ACs are all electron donating groups, whereas carbon atom is surrounded by electron donating groups (-C=C and –CH) or electron withdrawing groups (-C-O-C, -C=N, -C-OH, and $-CO_2$). For example, some peaks (284.2 eV from C=C and 283.4 eV from complex hydrocarbons, diamond or offset of C-H bonding with $O-CH_3$) were detected below 285.0 eV for C 1s electron and other peaks resulting from various oxidation states of carbon, e.g., C-O (286.4 eV) and C=O (282.2 eV), also involved over from 286.0 eV. Other atoms such as S and F (from impurities), Al (from $LiAlH_4$), and Na (from AC) were also detected. The quantitative analysis result of XPS is shown in Table 3.13. Note that abundant amounts of carbon in AC was detected, which shows deviation from EA result (Table 3.12) because there are many sources of carbon impurities such as trace organic compounds and CO_2. Aluminum and nitrogen content also shows deviation from AA results [6.0 % for ACREDUCT(9) in Table 3.4] and EA results (6.0 % for ACPDICD in Table 3.12), respectively, because the aluminum sample holder and atmospheric nitrogen might be possible error sources of detecting their signals.

Table 3.13 Quantitative analysis result of XPS for AC, AC-β-CD [1:10:10(9)], and ACPDICD

Name	Peak	Binding Energy (eV)	Mass Concentration (%)	Δ eV from Theoretical value (*)
AC	C 1s	284.0	94.1	- 0.1
	O 1s	532.0	5.0	- 11.1
	N 1s	400.5	0.2	- 9.4
	S $^2p_{1/2}$	163.5	0.5	- 0.1 (* = 163.6)
	Na 1s	1,071.0	0.2	+ 0.2 (* = 1,070.8)
AC-β-CD [1:10:10(9)]	C 1s	283.0	36.6	- 1.1
	O 1s	530.5	44.3	- 12.6
	N 1s	399.0	0.5	- 10.9
	Al $2p_{1/2}$	73.0	17.7	0
	Al 2s	117.5		0.3 (* = 117.8)
	S $2p_{1/2}$	167.5	0.6	+ 3.9
	F 1s	684.0	0.3	- 12.7 (* = 696.7)
ACPDICD	C 1s	283.0	60.1	- 1.1
	O 1s	530.5	27.3	- 12.6
	N 1s	398.0	12.6	- 11.9

The XPS spectra are also shown in Figure 3.8, where C 1s peaks for A, B, C, and D were calibrated by 0.95 eV.

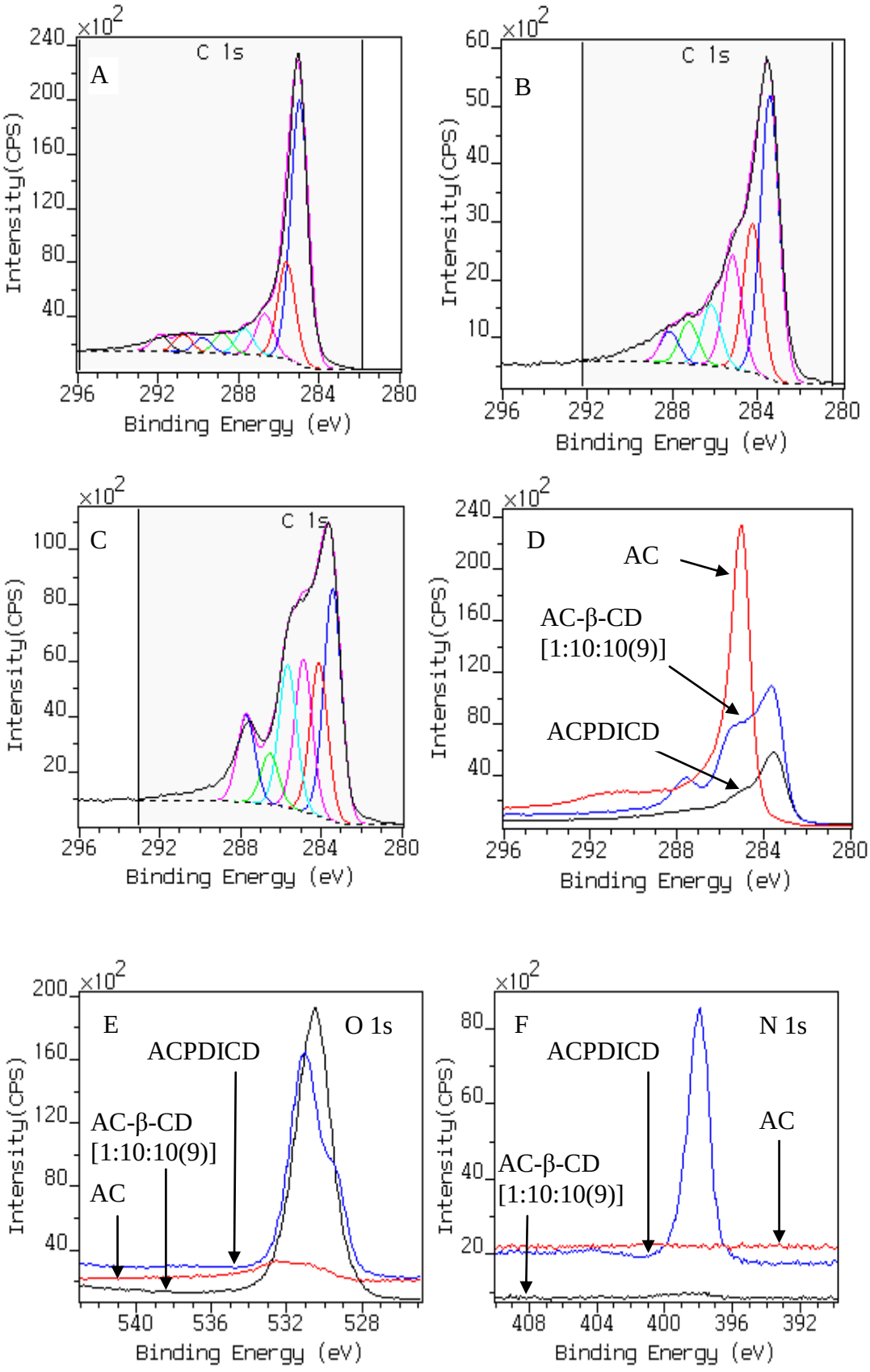
A
C 1s
×10^2
Intensity(CPS)
Binding Energy (eV)
B
C 1s
C
C 1s
D
AC
AC-β-CD
[1:10:10(9)]
ACPDICD
E
O 1s
ACPDICD
AC-β-CD
[1:10:10(9)]
AC
F
N 1s
ACPDICD
AC
AC-β-CD
[1:10:10(9)]

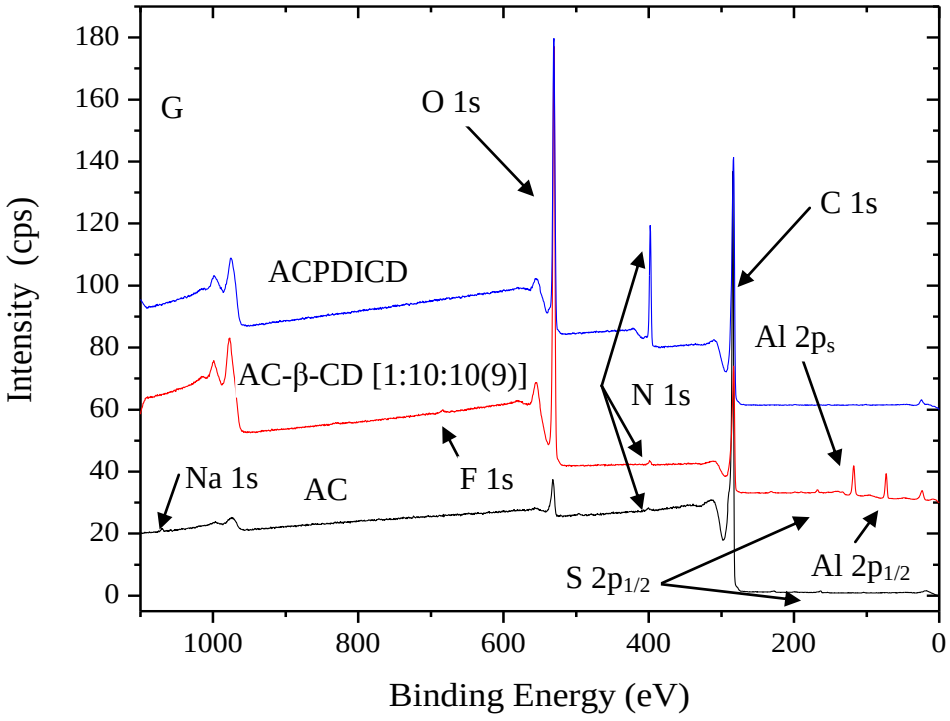

Figure 3.8 XPS spectra {A = AC C 1s, B = ACPDICD C 1s, C = AC-β-CD [1:10:10(9)] C 1s, D = Comparison of C 1s, E = O 1s, F = N 1s, G = Survey of AC, AC-β-CD [1:10:10(9)], and ACPDICD}

3.2.13 ^{1}H NMR Spectroscopy

The product identity of tosyl-β-CD was confirmed using ^{1}H NMR and is in agreement with data obtained from the literature,[111] which are shown in Table 3.14.

Table 3.14 Assignment of characteristic ^{1}H NMR peaks of tosyl-β-CD

Functional groups	Characteristic Peaks (ppm)	Literature values (ppm)[111]
CH_3	2.42 (s, 3H)	2.42 (s, 3H)
H-2	3.42~3.18 (m, overlap with HOD, 7H)	3.42~3.18 (m, overlap with HOD)
H-3,4,5	3.74~3.43 (m, 21H)	3.74~3.43 (m, 28H)
H-6a,b	4.55~4.13 (m, 14H)	4.55~4.13 (m, 6H)
H-1	4.76 (br, s, 7H)	4.76 (br, s, 3H)
OH-6	4.82 (br, s, 6H)	4.82 (br, s, 4H)
OH-2,3	5.87~5.58 (m, 14H)	5.87~5.58 (m, 14H)
Benzene (ortho)	7.42 (d, 2H)	7.42 (d, 2H)
Benzene (meta)	7.74 (d, 2H)	7.74 (d, 2H)

Note: s = singlet, m = multiplet, br = broad, and d = doublet. Solvent is DMSO-d_6 and spectrometer frequency is 500 MHz at 25 °C.

The mole ratio of β-CD:tosyl chloride in the tosyl-β-CD was 1:1 because the integration ratio of OH-6 of β-CD at δ 4.8 is 3.01 (3.01/6 = 0.50) and the integration ratio of the aromatic protons of tosyl chloride at δ 7.7 is 1.00 (1.00/2 = 0.50). With regard to proton numbers of tosyl-β-CD, the total number of protons 76 according to 1 tosyl group per β-CD. This value is the same as the synthesized compound [1 glucose unit = 10 protons, the grafted glucose unit to tosyl group = 9 protons, tosyl group = 7 protons, total = (10 × 6) + 9 + 7 = 76 protons]. However, the literature value showed only 62 protons and is suspected to be wrong. (See ^{1}H NMR spectrum: A51 - tosyl-β-CD)

3.3 Sorption Studies

3.3.1 Sorption isotherms for AC

Sorption isotherms are shown in Figure 3.9, where Q_e was measured as C_e varies for three types of conditions for studying sorption performance by pH and mass of adsorbent: A) variable concentration of PNP fixed mass of AC at pH = 6.00, B)

variable mass of AC with fixed concentration of PNP at pH = 6.00, and C) variable mass of AC with fixed concentration of PNP at pH = 10.00.

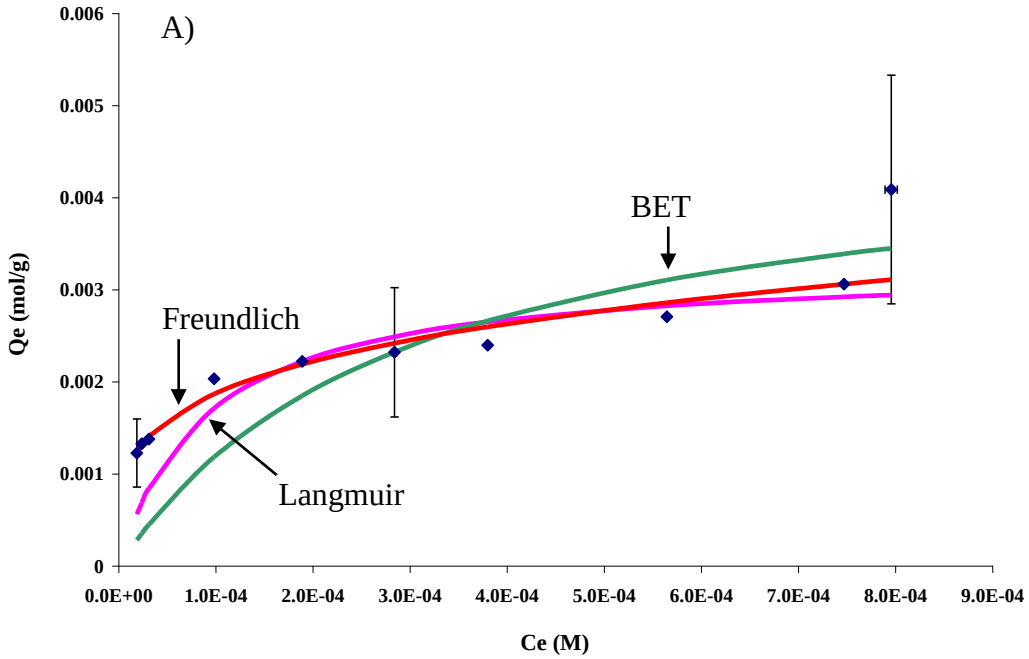

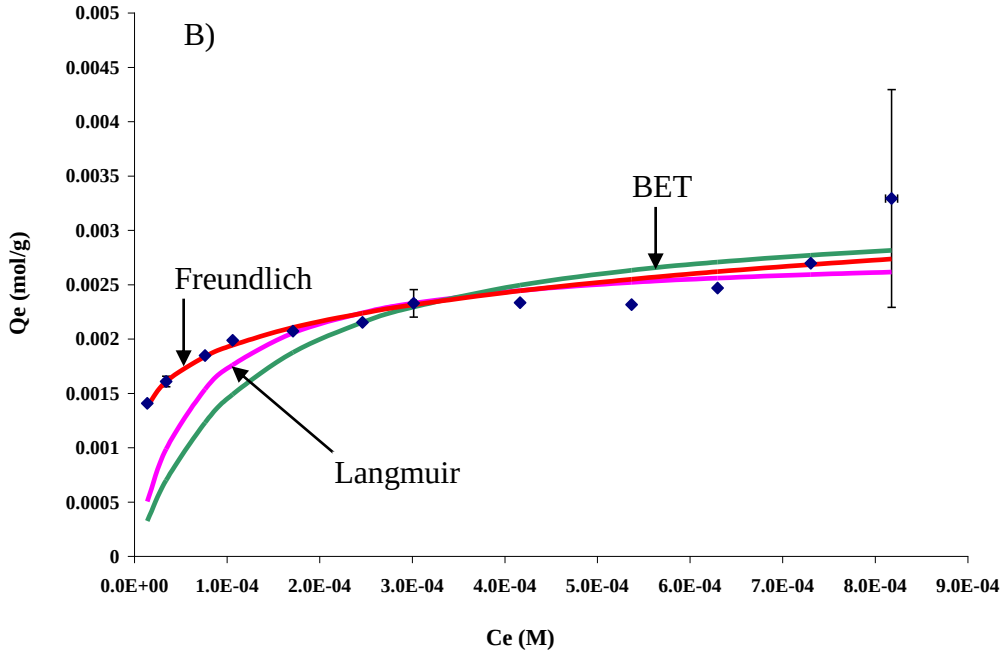

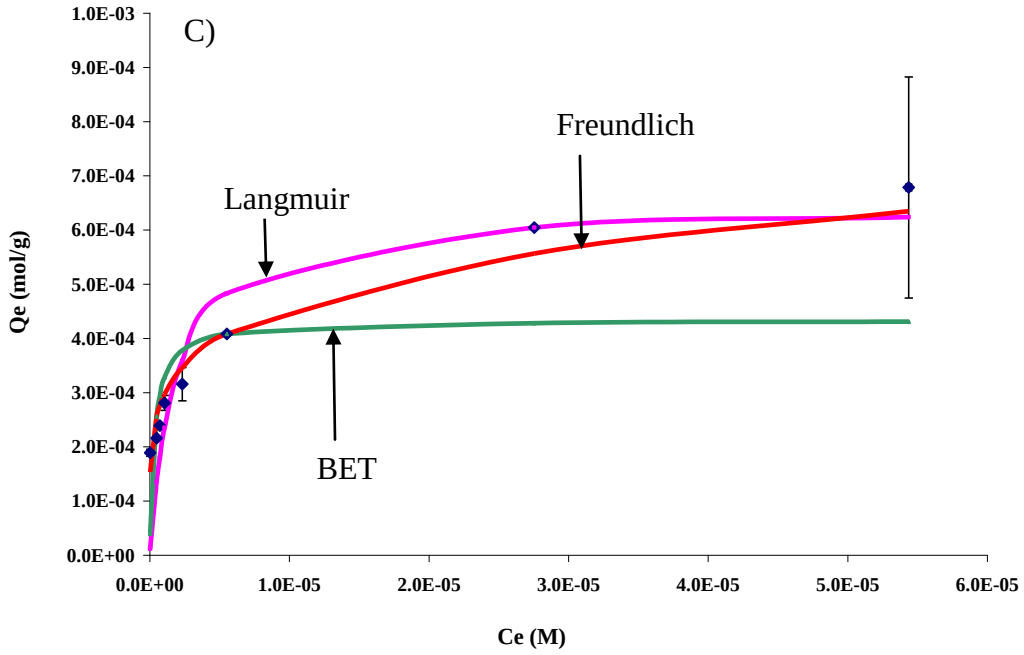

Figure 3.9 Sorption isotherms of AC at 25 °C: [A) variable concentration of PNP fixed mass of AC at pH = 6.00, B) variable mass of AC with fixed concentration of PNP at pH = 6.00, and C) variable mass of AC with fixed concentration of PNP at pH = 10.00]

The equilibrium parameters are shown in Table 3.15, where R^2 is the linear regression correlation coefficient and R_s is the dimensionless constant separation factor.[123]

Table 3.15 Equilibrium parameters as evaluated from linearized models of the sorption isotherms of AC with PNP

		pH of the solution of PNP(*)		
		6.00	6.00	10.00
Static Variable		1 mg (AC)	1.0×10^{-3} (PNP)	1.0×10^{-3} (PNP)
Langmuir	Surface Area (m^2/g)	1.04×10^{3}	891	204
	Q_m (mol/g)	3.27×10^{-3}	2.81×10^{-3}	6.50×10^{-4}
	K_L (g/mol)	1.12×10^{4}	1.57×10^{4}	5.40×10^{5}
	R^2	0.922	0.956	0.995
	R_s	-	6.08×10^{-2}	2.10×10^{-2}
BET	Surface Area (m^2/g)	1.49×10^{3}	1.02×10^{3}	137
	Q_m (mol/g)	4.72×10^{-3}	3.23×10^{-3}	4.30×10^{-4}
	K_{BET} (L/g)	3.41×10^{3}	8.04×10^{3}	2.90×10^{6}
	R^2	0.912	0.763	0.403
Freundlich	K_F (L/g)	1.77×10^{-2}	9.01×10^{-3}	4.22×10^{-3}
	n	4.11	5.97	5.18
	R^2	0.936	0.908	0.926
Error(**)	Q_e/C_e (%, ±)	30.3/0.8	9.7/0.8	13.0/0.4

(*) Literature values[113] for adsorption of PNP with AC at pH buffer = 6.00 and room temperature [Surface Area (m^2/g): 853, Q_m (mol/g): 2.37 x 10^{-3} , K_L (g/mol): 8.62 × 10^4] (**) Mean error of total errors calculated by standard error propagation method (refer to section 2.5.5 in Chapter 2)

The reason that a very high error range in Q_e involved was resulted from employing a less sensitive weighing balance ~ 0.1 mg sensitivity (4-place balance) for very small samples (~ 10 mg max.). If a 5-place balance (~ 0.01 mg sensitivity) for those small samples, the error will be approximately decreased by 1/10 of the error values.

The equilibrium parameter, R_s, is given by equation (3.3) and can be employed to identify Langmuir adsorption as being a suitable model or not;

$$R_s = 1/ (1+K_L C_o) \qquad (3.3)$$

where R_s is the dimensionless constant separation factor; K_L is the Langmuir constant; and C_o is the initial PNP concentration.

The R_s value can be identified according to the type of isotherm and is shown in Table 3.16.

Table 3.16 R_s values by types of isotherms

Values of R_s	Type of equilibrium (Langmuir -type)
$R_s > 1$	Unfavorable
$R_s = 1$	Linear
$0 < R_s < 1$	Favorable
$R_s = 0$	Irreversible

An unfavorable equilibrium is represented by $R_s > 1$ and can be seen in the desorption case.

The possibility of sorption of PNP with AC occurs in pores and with surface bound carbonyl groups. Physisorption was the major type of sorption process. All sorption isotherms were in agreement with a Langmuir model because its R^2 value was higher than that of BET and also in agreement with a Freundlich model because its R^2 value was higher. In cases where AC contains trace amounts of metals, chemisorption may occur between metals and PNP. However, all AC materials were thoroughly washed with HCl and HNO_3 and are anticipated to remove such trace metals.

The calculated Langmuir surface area at pH = 10.00 was 204 m^2/g by considering the cross-sectional area of neutral PNP (52.5 $Å^2$). In this case, Langmuir curve fitting was favorable because its R^2 was higher than that of BET. The surface area was much lower than as received AC (1,269 m^2/g) as determined by nitrogen gas sorption surface area estimates for an AC (powder) from porosimetry. However, the calculated surface area according to Langmuir estimates at pH = 6.00 with fixed mass of AC was 1,035 m^2/g; this value was in agreement (1,269 m^2/g) with the nitrogen gas sorption

surface area. In this case, PNP molecules exist primarily in their nonionized form because the pKa of PNP is 7.15.

To adequately explain these differences in the calculated surface areas between gas sorption and dye sorption, we may expect differences because of differences in the size of the adsorbates (N_2 = 16.2 $Å^2$, PNP = 52.5 $Å^2$), sorption temperature (e.g., porosimetry at 77 K and dye sorption at 25 °C), availability of sorption sites (solvent in dye sorption process may compete for surface sites), and pore filling because of the Kelvin effect. Nitrogen molecules are physisorbed more readily as the relative pressure increases until equilibrium reaches unity (refer to Figure 1.8 in Chapter 1) because the amount sorbed is proportional to the relative pressure. PNP can be physisorbed until equilibrium is reached as the adsorbate concentration increases because of its small molecular area and van der Waals and π-π stacking interactions between PNP and the hydrophobic surface of AC.

A diagram of the sorption on the surface of AC with N_2 and dyes can be illustrated as shown in Scheme 3.8, where adsorbates can be adsorbed on the surface of AC according to their molecular sizes and the accessible surface of the adsorbent.

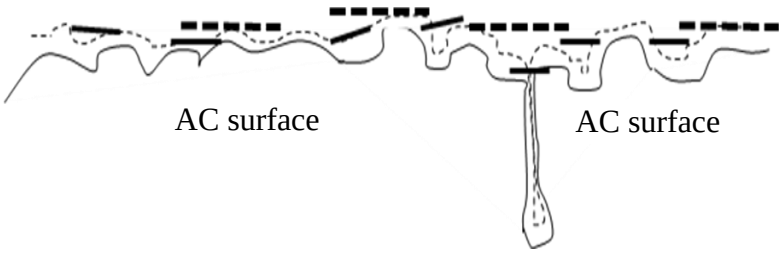

Scheme 3.8 A diagram of sorption on the surface of AC with different molecular sized adsorbates (dotted line = N_2, bold dashed line = PNP, and bold dotted line = MB)

Moreover, physisorption of PNP on the surface of AC at acidic and basic pH values can be possible and models of its mode of adsorption are shown in Scheme 3.9.

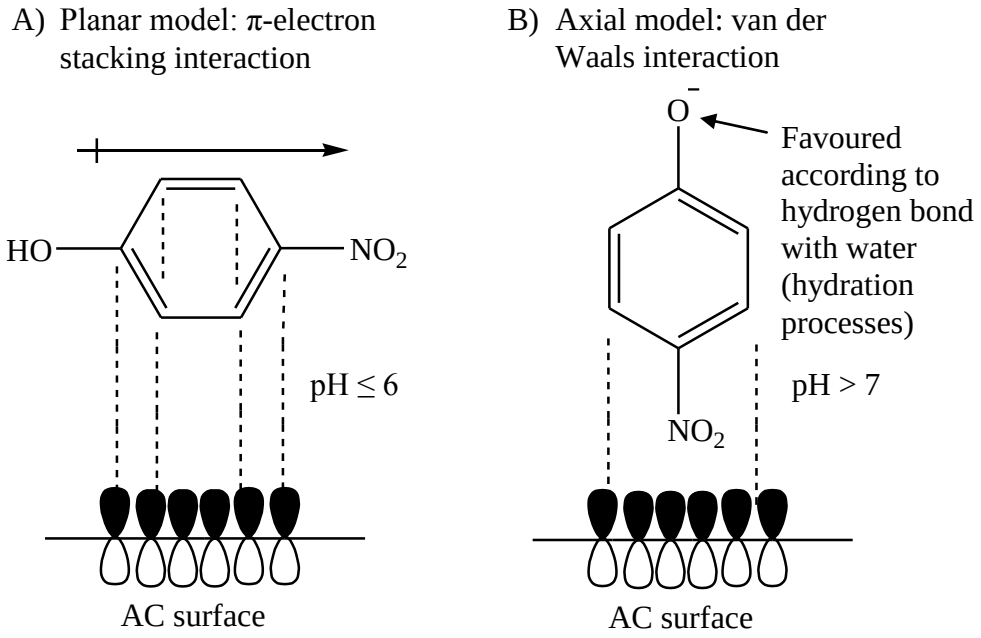

Scheme 3.9 Physisorption models of PNP on AC [A) Planar model at pH ≤ 6 and B) Axial model at pH > 7]

At acidic conditions, PNP molecules can be adsorbed in a planar orientation on the surface of AC with π-electron stacking interactions of the sp^2 orbitals between the aromatic ring of PNP and the basal planes of AC. This model might be favored by BET sorption model (Type A) in that the appearance of sorption isotherm looked like BET isotherm although the total number (10 ~ 12) of samples was not properly high. As well, the planar model would allow for subsequent layers of PNP molecules to interact through favorable π-π stacking interactions. However, the depronated PNP anions, at basic conditions, may be axially adsorbed on the surface of AC with van der Waals interactions between the depronated PNP anions and the basal planes of AC, where the phenoxide ion of PNP may be joined hydrogen bond formation with the surrounded water molecules. (cf. Scheme 3.9) This model might be favored by a Langmuir sorption model (Type I) in that the appearance of sorption isotherm looked like Langmuir isotherm and the total number (~ 10) of samples was not properly high. As well, the axial mode of adsorption would favor monolayer arrangement of PNP because π-π stacking would tend to occur within a monolayer as opposed to between

layers, as argued for planar stacking of PNP. The type of layer (mono- or multi-) can be further identified by thermodynamic parameters because monolayer is only possible in chemisorption with very high $\Delta_{ads}H$ values (~ 400 kJ/mol), whereas physisorption processes tend to display lower enthalpies of adsorption ($\Delta_{ads}H$ (< ~ 100 kJ/mol). Furthermore, we may expect favorable physisorption of PNP with the surface bound carbonyl groups of AC at pH = 6 and also electrostatic repulsion with the surface bound carbonyl groups of AC at pH = 10 which are illustrated as shown in Scheme 3.10.

A) Planar model: H-bond with the surface carbonyl groups

B) Axial model: electrostatic repulsion with the surface carbonyl groups

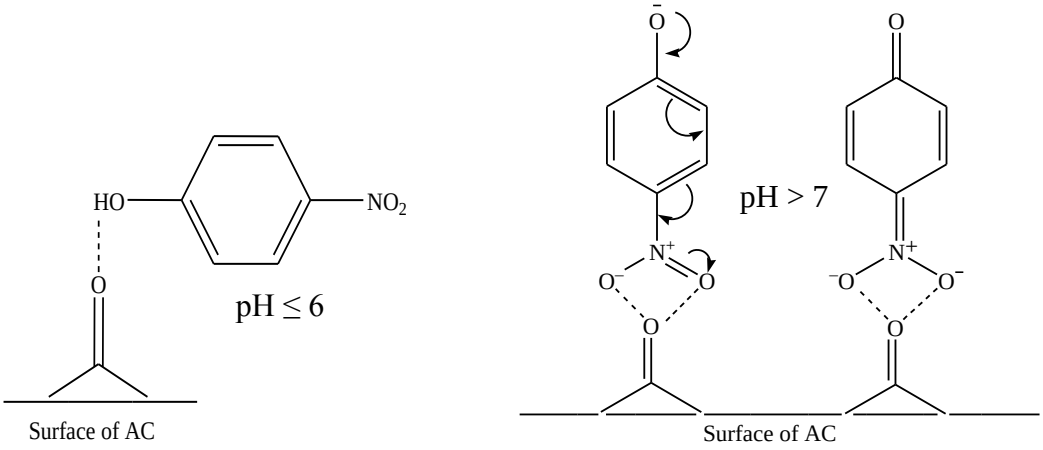

Scheme 3.10 Physisorption models of PNP with the surface bound carbonyl groups of AC [A) Planar model at pH ≤ 6 and B) Axial model at pH > 7]. The dashed line in B) represents a water- mediated H-bond (the water molecules are omitted for purposes of clarity)

The calculated surface area according to the Langmuir model at pH = 6.00 with fixed concentration of PNP (1×10^{-3} M) was 891 m^2/g which was lower than that of experiments using fixed mass of sorbent because at these high concentrations of dye, there might be more solute-solute dye interactions. The small mass of AC can affect the efficiency of sorption processes because the UV absorbance of PNP solution after equilibrium ranged from 7.40 to 0.126 absorbance units as the mass of AC ranged from 1.0 mg to 14.0 mg. This equilibrium effects can be understood according to equilibrium processes dominated by Langmuir type equilibrium because a relative

excess of PNP to AC will force a greater degree of sorption onto the surface of AC compared to the opposite (i.e., AC >> PNP) case.

The R_s value of the Langmuir isotherm at pH = 10.00 and pH = 6.00 is 0.0210 and 0.0608, respectively. Therefore, those sorption equilibrium processes are favorable Langmuir conditions according to the R_s values listed in Table 3.15. (See Sorption equilibrium parameters in the APENDICES: A52: AC with PNP at pH = 6.00 and 25 °C, A53: AC with PNP at pH = 6.00 and 25 °C, and A54: AC with PNP at pH = 10.00 and 25 °C)

3.3.2 Sorption isotherms for grafted ACs

The sorption isotherms with a fixed mass of grafted ACs are shown in Figures 3.10 to 3.13 plotted by the best fit sorption model which has the greatest linear regression value to unity. Figure 3.10 was carried out for AC-β-CD [1:10:10(9)] with PNP at pH buffer = 6.00 and room temperature, Figure 3.11 was carried out for AC-β-CD [1:10:10(9)] with MB at pH buffer = 8.40 and room temperature, and Figure 3.12 was carried out for ACPDICD with PNP at pH buffer = 6.00 and room temperature, and Figure 3.13 was carried out for ACPDICD with MB at pH buffer = 8.40 and room temperature. The equilibrium parameters are shown in Table 3.17.

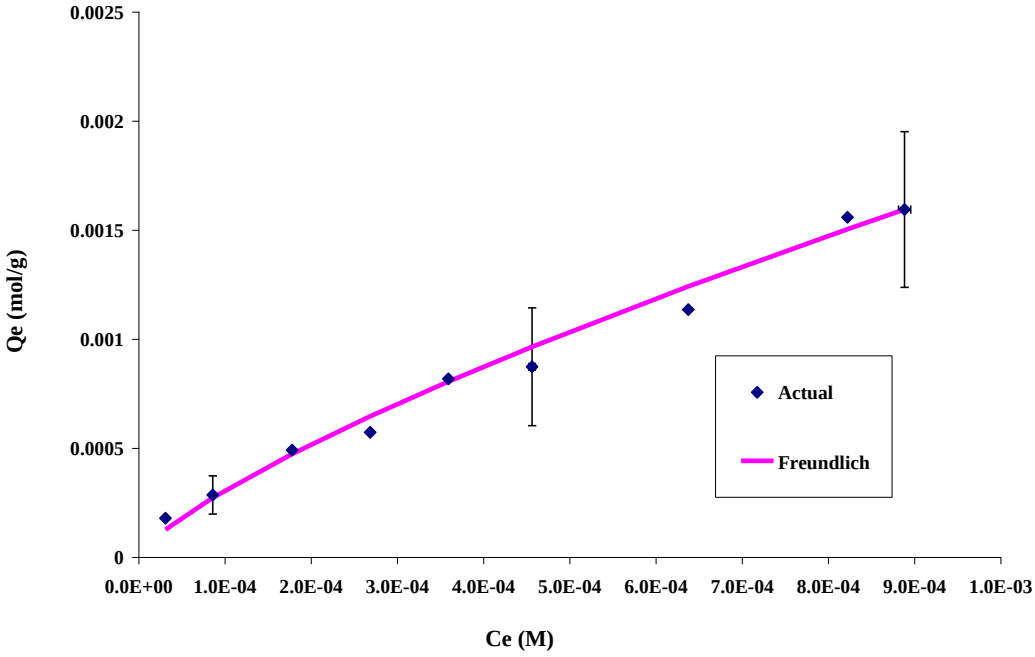

Figure 3.10 Sorption isotherm of AC-β-CD [1:10:10(9)] with variable concentrations of PNP at pH = 6.00 and room temperature

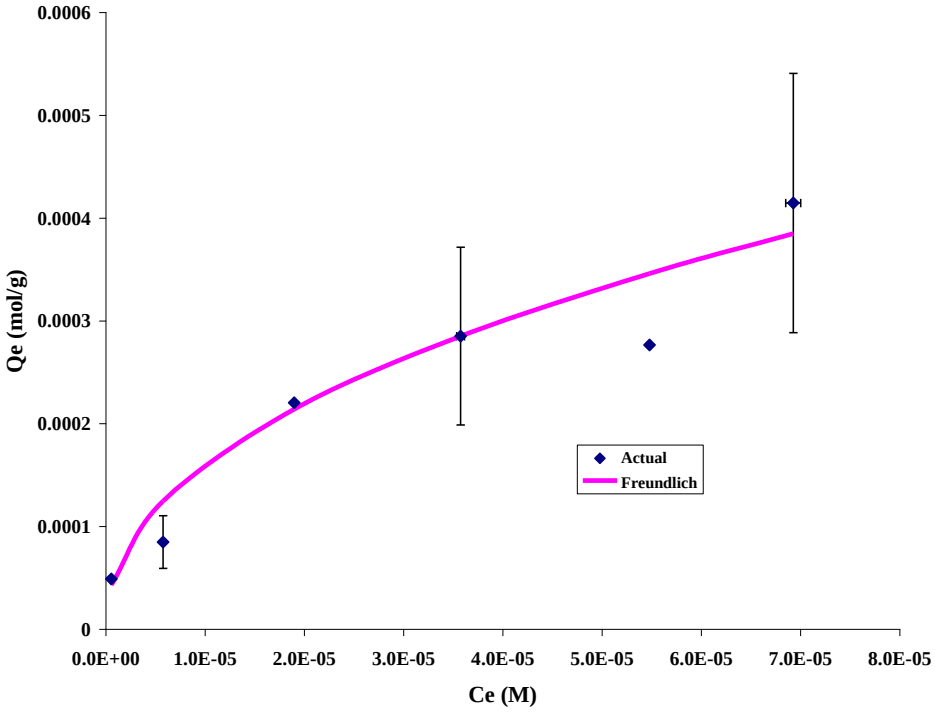

Figure 3.11 Sorption isotherm of AC-β-CD [1:10:10(9)] with variable concentrations of MB at pH = 8.40 and room temperature

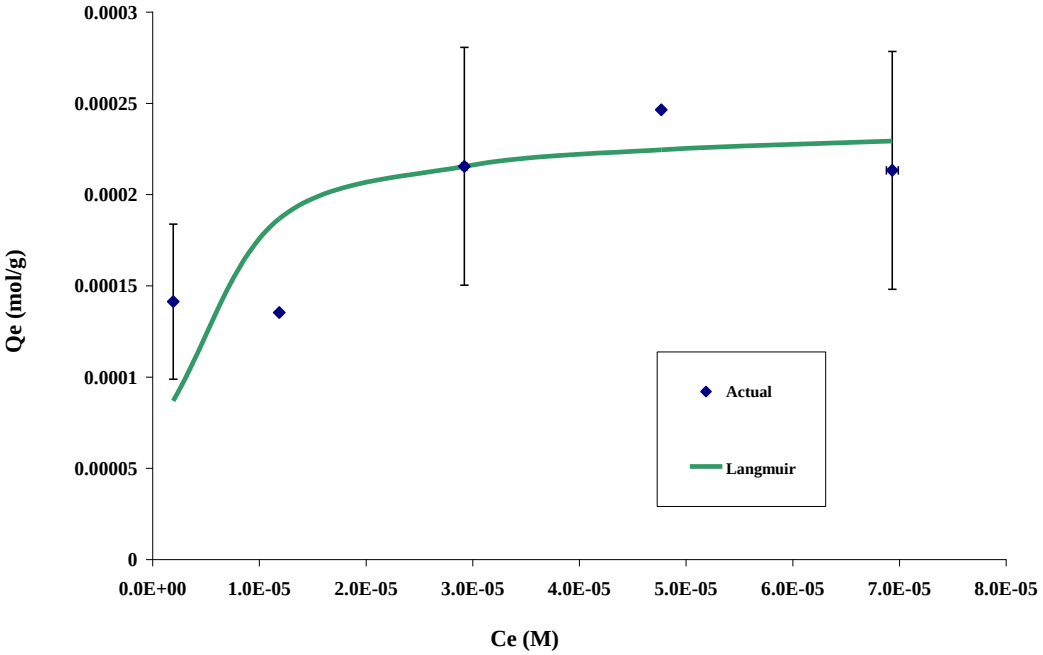

Figure 3.12 Sorption isotherm of ACPDICD with variable concentrations of PNP at pH = 6.00 and room temperature

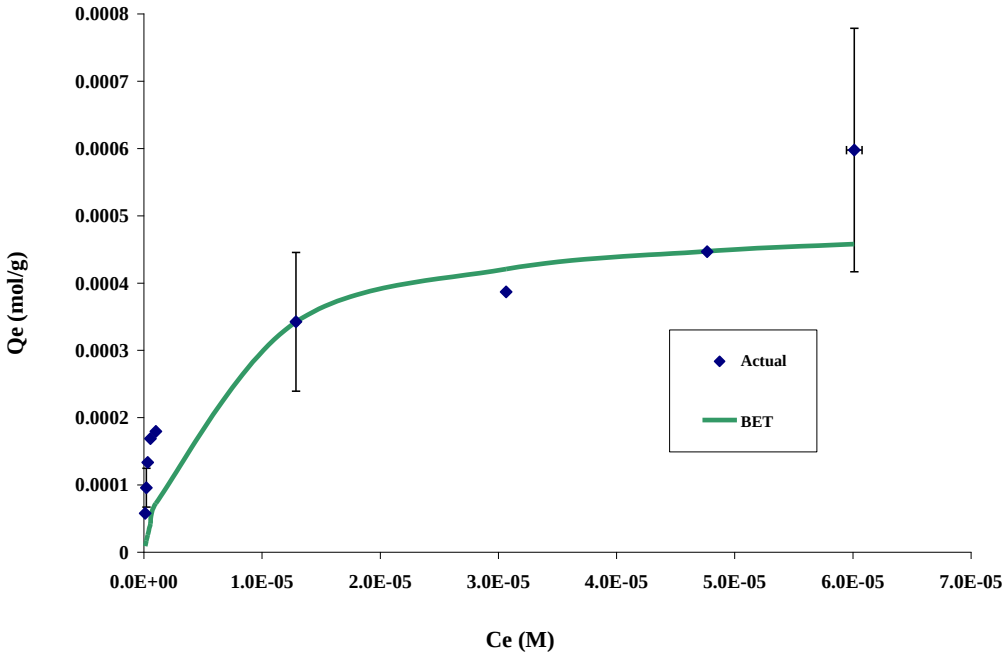

Figure 3.13 Sorption isotherm of ACPDICD with variable concentrations of MB at pH = 8.40 and room temperature

Table 3.17 Equilibrium parameters obtained from equilibrium sorption isotherms of grafted ACs at 25 °C

		AC-β-CD [1:10:10(9)]		ACPDICD	
Solution of adsorbate		PNP	MB	PNP	MB
		pH = 6.00	pH = 8.40	pH = 6.00	pH = 8.40
Static variable		1 mg (grafted ACs)			
Langmuir	Surface Area (m^2/g)	8.14×10^2	130	76	171
	Q_m (mol/g)	2.58×10^{-3}	4.11×10^{-4}	2.41×10^{-4}	4.74×10^{-4}
	K_L (g/mol)	1.30×10^3	6.11×10^4	2.92×10^5	3.44×10^5
	R^2	0.741	0.864	0.974	0.949
BET	Surface Area (m^2/g)	1.67×10^3	147	92	182
	Q_m (mol/g)	5.28×10^{-3}	4.64×10^{-4}	2.92×10^{-4}	5.04×10^{-4}
	K_{BET} (L/g)	4.86×10^2	4.48×10^4	9.62×10^4	1.64×10^5
	R^2	0.937	0.838	0.413	0.985
Freundlich	K_F (L/g)	3.20×10^{-1}	2.96×10^{-2}	1.11×10^{-3}	1.02×10^{-2}
	n	1.33	2.21	6.39	3.32
	R^2	0.984	0.943	0.675	0.945
Error(*)	Q_e/C_e (%, ±)	28.6/0.8	29.8/1.1	29.6/0.8	30.2/1.1

(*) Mean error of total errors calculated by standard error propagation method (refer to section 1.3.4 in Chapter 1)

The physisorption of PNP on AC-β-CD [1:10:10(9)] and ACPDICD may occur in the pores, interior β-CD, and with surface functional and linker groups (hemiacetal linker and urethane linker), which was the major mode of sorption. Physisorption for AC-β-CD [1:10:10(9)] was achieved by H-bond with PNP at different sites of two different hemiacetal linker groups (one from –CH_2OH/GA/β-CD and one from –OH/GA/β-CD) and free surface functional groups such as phenols, amine, and β-CD. Physisorption for ACPDICD was achieved primarily by H-bonding interactions at lower concentration of PNP. At high PNP concentrations (from 1×10^{-3} to 9×10^{-5} M with absorbance from 7.98 to 0.78), solute-solute dye interaction was more predominant rather than solute-substrate (carboxylic acid and phenol groups in AC, secondary amines in the linker, and hydroxyl groups in β-CD) interaction until the interactions

are reversed and adsorption commenced. This equilibrium effects can be understood according to Langmuir adsorption because a relative excess of PNP to ACPDICD will force a greater degree of sorption onto the surface of ACPDICD compared to the opposite (i.e., ACPDICD >> PNP) case. As the degree of surface coverage goes to zero, the distribution coefficient increases dramatically and the opposite observed as the surface coverage approaches unity. In this sorption process, the surface area was calculated in the limited range of concentration of PNP (8.0×10^{-5} to 9.0×10^{-6} M).

The sorption of MB on AC-β-CD [1:10:10(9)] and ACPDICD may occur in pores and cavities of β-CD by physisorption caused by van der Waals interactions as well as hydrophobic effects. β-CD/MB inclusion complex is possible, however, MB can not form H-bonds with AC-β-CD [1:10:10(9)] and ACPDICD because it does not have any H-bond donors or acceptors. The proposed adsorption scheme of PNP with the surface of AC-β-CD [1:10:10(9)] and ACPDICD are shown in Scheme 3.11, where adsorption of PNP with ACPDICD is possible only at low concentrations of PNP.

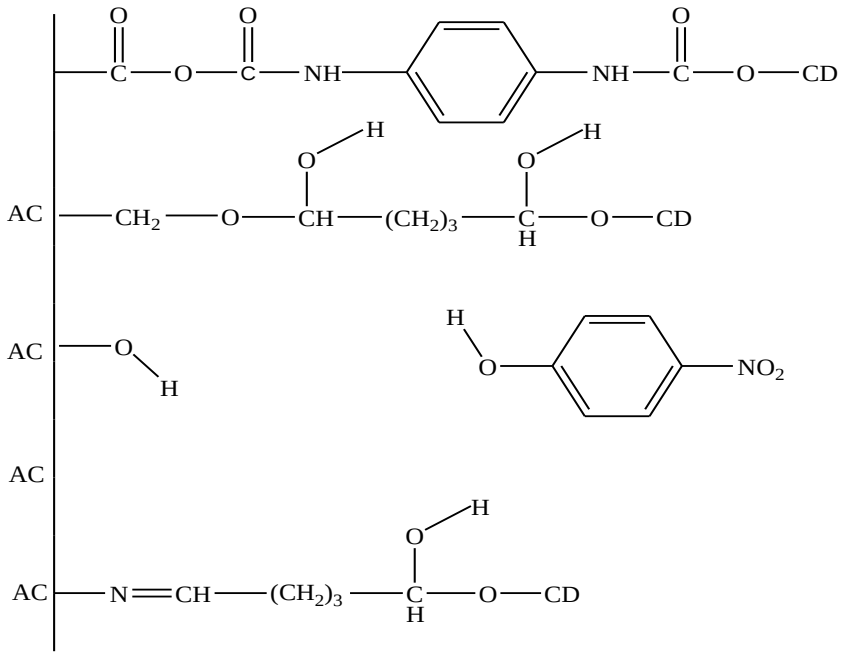

Scheme 3.11 Available adsorption sites scheme on the surface of AC-β-CD [1:10:10(9)] and ACPDICD. Note the availability of H-bond donor and acceptor

groups according to the nature of the surface bound groups on AC. The surface of AC is denoted by the vertical line.

Physisorption onto grafted ACs occurred with in the mesopores. Therefore, MB was more favorable than PNP. π-π stacking interactions on the surface of AC were concluded for the sorption of AC with PNP, and interaction was also found with MB.

Differences in the favorability of sorption isotherm models were also observed by different dyes. AC-β-CD [1:10:10(9)] was favored to bind both dyes according to the BET model, whereas ACPDICD did not show any preference to a given model because it had almost same surface areas uisng PNP or MB. However, ACPDICD was favored to bind MB more than PNP because MB was larger than PNP with ACPDICD due to the mesoporosity of ACPDICD.

Considering the molecular surface area of PNP (4.58 Å wide and 11. 46 Å long) and MB (8.39 Å wide and 14.31 Å long), PNP can be included within 1 molecule of β-CD, whereas MB[82] can be complexed with 2 or more β-CD molecules because of its greater size. For example, if we assume that β-CD, PNP, and MB form a cylindrical shape, then the volume of β-CD, PNP, and MB are approximately 240 $Å^3$, 189 $Å^3$, and 790 $Å^3$ respectively (for β-CD, volume = ¼ × π × $(0.62)^2$ × 0.79 = 0.24 nm^3 = 240 $Å^3$) (refer also to Table 1.3 in Chapter). Therefore, PNP is more strongly bound on average as compared to MB because it is fully included in the cavity of β-CD which is supported by its greater binding constant as observed for β-CD-HDI polymers (5 × 10^9 M^{-1}). (See Sorption equilibrium parameters in APENDICES: A55: AC-β-CD [1:10:10(9)] with PNP at pH = 6.00 and 25 °C, A56: ACPDICD with PNP at pH = 6.00 and 25 °C, A57: AC-β-CD [1:10:10(9)] with MB at pH = 8.40 and 25 °C, and A58: ACPDICD with MB at pH = 8.40 and 25 °C)

CHAPTER 4

CONCLUSIONS AND FUTURE WORK

4.1 Conclusions

Surface modification of AC with β-CD was accomplished by oxidation with nitric acid, reduction with lithium aluminum hydride, and grafting with linkers of GA and PDI for the attachment of β-CD. The maximum amount of surface acid groups and surface base groups were achieved by a 9 hour oxidation and its subsequent reduction. The presence of the grafted β-CD was supported by experimental evidence from DRIFTS, TGA/DTG, MALDI, Raman, and XPS. Characterization by those methods showed evidence for concluding that β-CD was covalently bonded to ACs. A characteristic instrumental DRIFTS results is that the imine bond at 1,660 cm^{-1}, decomposition temperatures from 312 °C to 323 °C with TGA/DTG, the presence of a molecular fragment ion of 1,157 and 1,173 with MALDI TOF MS, several Raman peaks of H-bond of β-CD and bound water (3,400 cm^{-1}), methylene bond (2,800 cm^{-1} ~ 3000 cm^{-1}), G band (~ 1,600 cm^{-1}), D band (~ 1,340 cm^{-1}), deformation vibration of CH-OH (1,478 cm^{-1} and 1,338 cm^{-1}), stretching vibration of C-O-C (1,109 cm^{-1}, 1,093 cm^{-1}, and 1,052 cm^{-1}), skeletal vibration (946 cm^{-1}, 848 cm^{-1}, and 475 cm^{-1}) with the associated =C-H stretching (~ 3,060 cm^{-1} from imine) and the urethane bond (3,306 cm^{-1} and 1,633 cm^{-1}) with Raman spectroscopy, and O 1s electron (530.5 eV) for AC-β-CD [1:10:10(9)] and O 1s electron (530.5 eV) and N 1s electron (398.0 eV) for ACPDICD with XPS.

The sorption study for AC was done based on different pH values (i.e., pH= 6.00 and pH= 10.00) of adsorbate solution and different mass of adsorbent. The mass effect may slightly affected surface area, but in a limited manner. However, the pH effect was sufficient to change the sorption performance by altering chemical structure of the adsorbate and interaction between the sorbate and the sorbent. The sorption study for

the grafted AC was done based on different adsorbates with different pH values of the adsorbate solution with a similar mass of adsorbent. The sorption study for AC with a fixed mass of PNP at pH = 6.00 showed similar surface areas (1,035 m^2/g with the Langmuir model and 1,491 m^2/g with the BET model) as that (1,269 m^2/g with the Langmuir model and 956 m^2/g with the BET model) by nitrogen porosimetry. Large differences in the surface areas between aqueous sorption and porosimetry may be attributed to the synergistic effect of physisorption from surface functional groups, the linker, and the cavity of β-CD. The calculated surface areas for grafted ACs with PNP and MB was varied by the incorporation of the linker bond and surface functional groups. Grafting with GA showed about 2 to 5 times the difference of surface areas from aqueous sorption with nonlinear curve-fitting models: 814 m^2/g with the Langmuir model and 1,669 m^2/g with the BET model for PNP and 264 m^2/g with the Langmuir model and 1,019 m^2/g with the BET model for MB. PNP was preferred over MB in terms of providing more reasonable estimates of the surface areas. Grafting with PDI showed about two times the difference of surface areas from aqueous sorption with dyes, but almost the same surface areas with nonlinear curve-fitting models: 76 m^2/g with the Langmuir model and 92 m^2/g with the BET model for PNP and 171 m^2/g with the Langmuir model and 182 m^2/g with the BET model for MB. MB was better than PNP in terms of providing more reasonable estimates of surface areass because of its appropriate molecular size to fit within the mesoporosity of ACPDICD. Considering the calculated surface areas obtained from the sorption isotherm with dyes from aqueous solution, grafted AC with GA provided more binding affinity for dyes than grafted AC with PDI. This results is related to the more efficient surface functional groups for forming H-bonds with AC-β-CD [1:10:10(9)] involved to physisorption, although the surface areas of both grafted ACs were similar (103 m^2/g for AC-β-CD [1:10:10(9)] and 95 m^2/g for ACPDICD).

The total surface areas in gas adsorption was dramatically decreased from over 1,000 m^2/g to below 100 m^2/g by modifying the surface structure of AC due to severe oxidation of AC and following chemical treatments and surface modification. These chemical modifications result in the widening and blocking of pores with metals and

surface bound compounds. However, the decrease in surface areas was dramatically recovered from below 100 m^2/g to over 1,000 m^2/g by the sequential processes of surface modification grafted β-CD, as shown by its sorption efficiency toward dye molecules in solution. The surface area estimates obtained from dye sorption in aqueous solution are given in Table 3.5 for ACs from gas sorption and Table 3.17 for grafted ACs from dye sorption. Therefore, the surface modified AC with β-CD can be used for industrial applications involving adsorption of organic contaminant molecules which may be found in water, soil, and air. For example, the manufacturing of high purity silicon requires ultra high pure water. Surface modified AC materials as described in this thesis are anticipated to be useful for removal of organic contaminants, e.g., environmental remediation of water, because of their high surface areas and strong sorption affinities.

4.2 Future Work

Two possible future studies will be pursued for surface modification and evaluation of sorption performance. To obtain better surface modification and higher sorption performance of AC, microwave-assisted synthesis can be applied to attach surface functional groups. This strategy can avoid the significant decrease of surface area which was shown in the oxidation process with nitric acid and following chemical modifications. Without a linker, direct surface modification can be possible if enough mole ratio of ACREDUCT or ACAMID to tosyl-β-CD is applied under an inert atmosphere. To evaluate sorption performance more systematically, detailed thermodynamic and kinetic studies will provide a better understanding of the sorption performance of the grafted ACs. The use of advanced statistical methods includes weighted $(1/error^2)$ non-linear fittings and this will provide more consistent parameters. In other words, microwave-assisted synthesis with AC can provide optimal synthesis for achieving sorption performance and its systematic evaluation of sorption performance can open the door of industrial applications because both CD and AC are good sequestrants for harmful organic molecules and metals in aquatic environments. Materials of this type can address health and environment concerns through the development of innovative remediation processes.

REFERENCES

1. Kinoshita, K., "*Carbon: Electrical and Physicochemical Properties"*, John Wiley & Sons, Inc., New York, **1988**, p. 10.
2. NORIT Americas Inc., *Understanding Activated Carbons*, Jul **2005**, 00-010-TP
3. Do. D.D., *Chemical Engineering Science*, **1996**, 51, 17, 4145-4158
4. Sing, K.S.W, Everett, D.H., Haul, R.A.W., Moscou, L., Pierotti, R.A., Rouquerol, J., Siemieniewska, T., *Pure Appl. Chem.*, **1985**, 57, 603
5. Abe, I., Fukuhara, T., Kawasaki, N., Hitomi, M., Kera, Y., *Journal of Colloid and Interface Science*, **2000**, 229, 615-619
6. http://www.prominentinc.com/literature-activated_carbon_terms.html (accessed 25/07/07)
7. Manocha, S.M., *Sādhanā*, **2003**, 28, parts 1 & 2, pp. 335-348
8. Datasheet of NORIT ROX 0.8, NORIT Americas Inc., No. 3342, Apr. **2003**
9. Moreno-Castilla, C., Ferro-Garcia, M.A., Joly, J.P., Bautista-Toledo, I., Carrasco-Marin, F., Rivera-Utrilla, J., *Langmuir*, **1995**, 11, 4386-4392
10. Otake, Y., Jenkins, R.G., *Carbon*, **1993**, 31, 109-121
11. Saha, B., Tai, M.H., Streat, M., *Trans IChemE*, **2001**, 79, Part B, 211-217
12. Silva, A. R., Freire, C., Castro, B. de., Freitas, M. M. A., A., Figueriredo, J. L., *Microporous and Mesoporous Materials*, **2001**, 46, 211-221
13. Ishifune, M. Suzuki, R., Mima, Y., Uchida, K., Yamashita, N., Kashimura, S., *Electrochimica Acta*, **2005**, 51, 14-22
14. Lennox, J.C., Murray, R.W., *J. Am. Chem. Soc*, **1978**, 100, 3710-3714
15. Delamar, M., Desarmot, G., Fagebaume, O., Hitmi, R., Pinson. J., Saveant, J.M., *Carbon*, **1997**, 35, 801-807
16. Mawhinney, D.B., Naumenko, V., Kuznetsova, A., Yates, Jr. J.T., *J. Am. Chem. Soc*, **2000**, 122, 2383-2384
17. Vinke, P., Van der Eijk M., Verbree, M., Voskamp, A.F., Van Bekkum, H., *Carbon*, **1994**, 32, 675-686
18. Trahnovsky, W.S., "*Oxidation in Organic Chemistry"*, New York, Academic Press, **1978**, p. 301
19. Turney, T.A., "*Oxidation Mechanisms"*, London, Butterworths, **1965**, p. 84
20. Fanning, P.E., Vannice, A., *Carbon*, **1993**, 31, 5, 721-730
21. Kinoshita, K., "*Carbon: Electrical and Physicochemical Properties"*, John Wiley & Sons, Inc., New York, **1988**, p. 87-88.
22. Boehm, H.P., *Carbon*, **1994**, 32, 759-769
23. Noh, J.S., Schwarz, J.A., *Carbon*, **1990**, 28, 675-682
24. Boehm, H.P. In *Advances in Catalysis*; Eley, D.D., Pines, H., Weisz, P.B., Eds.; Academic Press: New York, **1966**, Vol. 16, p. 183
25. Tamai, H., Shiraki, K., Shiono. T., Yasuda, H., *Journal of Colloid and Interface Science*, **2006**, 295, 299-302
26. Silva, A. R., Martins, M., Castro, B. de., Freitas, M. M. A., Freire, C., Valente, A., Figueriredo, J. L., *Microporous and Mesoporous Materials*, **2002**, 55, 275-284
27. Alves, J. A. C., Freire, C., Castro, B. de., Figueriredo, J. L., *Colloids and Surfaces A: Physicochem. Eng. Aspects*, **2001**, 189, 75-84

28. Pompeo, F., Resasco, D.E., *Nano Lett*., **2002**, 2, 4, 369-373
29. Budarin, V.L., Clark, J.H., Gorlova, A.A., Boldyreva, N.A., Yatsimirsky, V.K., *J. Therm. Anal. Cal*., **2000**, 62, 349-352
30. Fan, X., Yuan, K., Hao, C., Li, N., Tan, G., Yu, X., *OPPI BRIEFS*, **2000**, 32, 3, 287-290
31. Budarin, V.L., Clark, J.H., Tavener, S.J., Wilson, K., *Chem. Commun*., **2004**, 2736-2737
32. Michael, D., Mingos, P., Baghurst, D.R., *Chem. Soc. Rev*., **1991**, 20, 1-47
33. Perreux, L., Loupy, A., *Tetrahedron*, **2001**, 57, 9199-9223
34. Bahr, J.L., Tour, J.M., *J. Mater. Chem*., **2002**, 12, 1952-1958
35. Balasubramanian, K., Burghard, M., *Small*, **2005**, 1, 2, 180-192
36. Hirsch, A., Vostrowsky, O., *Top Curr. Chem*., **2005**, 245, 193-237
37. Tasis, D., Tagmatarchis, N., Bianco, A., Prato, M., *Chem. Rev*. **2006**, 106, 1105-1136
38. Diallo, M.S., Christie, S., Swaminathan, P., Johnson, J.H., Goddard, W.A., *Eviron. Sci. Technol.*, **2005**, 39, 1366-1377
39. Salipira, K.L, Mamba, B.B., Krause, R.W., Malefetse, T.J., Durbach, S.H., *Environ Chem Lett*, **2007**, 5, 13-17
40. Constantin, M., Fundueanu, G., Bortolotti, F., Cortesi, R., Ascenzi, P., Menegatti, E., *International Journal of Pharmaceutics*, **2004**, 285, 87-96
41. Abay, I., Denizli, A., Biskin, E., Salih, B., *Chemosphere*, **2005**, 61, 1263-1272
42. Belyakova, L.A., Kazdobin, K.A., Belyakov, V.N., Ryabov, S.V., Danil de Namor, A.F., *Journal of Colloid and Interface Science*, **2005**, 283, 488-494
43. Schollmeyer, E., Buschmann, H.-J., Jansen, K., Wego, A., *Progr. Colloid Polym. Sci*. **2002**, 121, 39-42
44. Connors, K.A., *Chem. Rev.*, **1997**, 97, 1325-1357
45. Szejtli, J., *Chem. Rev*. **1998**, 98, 1743-1753
46. http://jindrich.org/CD/sbcdcon2.gif (accessed 13/06/07)
47. Crini, G., Morcellet, M., *J. Sep. Sci*., **2002**, 25, 789-813
48. Yamamura, H., Fujita, K., *Chem. Pharm. Bull*. **1991**, 39, 10, 2505-2508
49. McNaughton, M., Engman, L., Birmingham, A., Powis, G., Cotgreave, I.A., *J. Med. Chem.* **2004**, 47, 233-239
50. Sebesta, R., Salisova, M., *Enantiomer*, **1999**, 4, 271-277
51. Khan, A.R., Forgo, P., Stine, K.J., D'Souza, V.T., *Chem. Rev*. **1998**, 98, 1977-1996
52. Jue, C.K., Lipke, P.N., *J. Biochem. Biophys. Methods*, **1985**, 11, 109-115
53. Ma, M. , Li, D., *Chem. Mater*., **1999**, 11, 872-874
54. Schneider, H., Hacket, F., Rüdiger, V., Ikeda, H., *Chem. Rev*. **1998**, 98, 1755-1785
55. Chen, M., Daio, G., Zhang, E., *Chemosphere*, **2006**, 63, 522-529
56. Voncina, B., Marechal, M.L., *Journal of Applied Polymer Science*, **2005**, 96, 1323-1328
57. Crini, G., *Bioresource Technology*, **2003**, 90, 193-198
58. Egyed, O., *Vibrational Spectroscopy*, **1990**, 1, 225-227
59. Janus, L., Carbonnier, B., Deratani, A., Bacquet, M., Crini, G., Laureyns, J., Morcellet, M., *New J. Chem*., **2003**, 27, 307-312
60. Huq, R., Mercier, L., *Chem. Mater*., **2001**, 13, 4512-4519

61. Park, C., Lee, I.H., Lee, S., Song, Y., Rhue, M., Kim, C., *PNAS*, **2006**, 103, 1199-1203
62. Tomasik, P. "*Chemical and functional properties of food saccharides*," CRC Press, New York, **2004**, p. 282-284, 287
63. Buschmann, H.J., Knittel, D., Schollmeyer, E., *Journal of Inclusion Phenomena and Macrocyclic Chemistry*, **2001**, 40, 169-172
64. Denter, U., Schollmeyer, E.., *Journal of Inclusion Phenomena and Molecular Recognition in Chemistry*, **1996**, 25, 197-202
65. Martel, B., Morcellet, M., Ruffin, D., Ducoroy, L., Weltrowski, M., *Journal of Inclusion Phenomena and Macrocyclic Chemistry*, **2002**, 44, 443-446
66. Hedges, A.R., *Chem. Rev*. **1998**, 98, 2035-2044
67. http://www.claire.co.uk/pdf_usr/Summer2003Web.pdf (accessed 13/06/06)
68. http://cals.arizona.edu/pubs/general/resrpt2003/article2_2003.pdf (accessed 13/06/06)
69. Challa, R., Ahuja, A., Ali, J., Khar, R.K., *AAPS PharmSciTech*, **2005**, 6, 2, Article 43, E329-E357
70. Zettlemoyer, A.C., *Chem. Rev*., **1959**, 59, 6, 937-981
71. Laszlo, K., Podkoscielny, P., Dabrowski, A., *Applied Surface Science*, **2006**, 252, 5752-5762
72. Allen, T., *"Particle Size Measurement"*, 3rd Ed., Chapman and Hall, New York, **1981**, p. 523-525
73. Inel, O., Tumsek, F., *Turk. J. Chem*., **2000**, 24, 9-19
74. Gregg, S.J., Sing, K.S., *"Adsorption, Surface Area and Porosity"*, 2nd Ed., Academic Press, New York, **1982**, p. 4
75. Brauner, S., Deming, L.S., Deming, E., Teller, E., *J. Am. Chem. Soc*., **1940**, 62, 1723-1732
76. Singleton, J.H., Halsey, G.D., "*Symposium on Problems Relating to the Adsorption of Gases by Solids*", **1954**, Sep., 10-11, Kinston, Ontario
77. Lynam, M.M., Kilduff, J.E., Weber, W.J., *J. Chem. Edu*. **1995**, 72, 80-84
78. Fjeld, C., Denu, J.M, *J. Biol. Chem*., **1999**, 274, 29, 20336-20343
79. Giles, C.H., MacEwan, T.H., Nakhwa, S.N., Smith, D., *J. Chem. Soc*, **1960**, 3973-3993
80. Fetterolf, M.L., Patel, H.V., Jennings, J.M., *J. Chem. Eng. Data*, **2003**, 48, 831-835
81. Li, D., Ma, M., *Clean Products and Processes*, **2002**, 2, 112-116
82. Zhao, G-C., Zhu, J-J., Chen, H-Y., *Spectrochimica Acta Part A*, **1999**, 55, 1109-1117
83. Boehm, H.P. In *Advances in Catalysis*; Eley, D.D., Pines, H., Weisz, P.B., Eds.; Academic Press: New York, **1966**, Vol. 16, p. 185-191
84. Boehm, H.P., *Carbon*, **1994**, 32, 759
85. Bandosz, T.J., Jagiello, J., Schwarz, J., *Langmuir*, **1996**, 12, 6480-6486
86. Kinoshita, K., "*Carbon: Electrical and Physicochemical Properties"*, John Wiley & Sons, Inc., New York, **1988**, p. 94.
87. Jagiello, J., *Langmuir*, **1994**, 10, 2778-2785
88. Provencher, S.W., *Computer Physics Communication*, **1982**, 27, 213-227; 229-242

89. Bandosz, T.J., Jagiello, J., Putyera, K., Schwarz, J.A., *J. Chem. Soc. Faraday Trans*. **1994**, 90, 23, 3573-3578
90. Venter, J.J., Vannice, M.A., *Carbon*, **1988**, 26, 889-902
91. Reffner, J.A., Wihlborg W.T., *American Laboratory*, **1990**, Apr. , 27-34
92. Brimmer, P.J., Griffiths, P.R., *Anal. Chem.*, **1986**, 58, 2179-2184
93. Baker, S.E., Cai, W., Lasseter, T.L., Weidkamp, K.P., Hamers, R.J., *Nano Lett*., **2002**, 2, 12, 1413-1417
94. Blyth, R.I.R., Netzer, F.P., Buqa, H., Ramsey, M.G., Besenhard, J.O., Golob, P., Winter, M., *Applied Surface Science*, **2000**, 167, 99-106
95. Ramanathan, T., Fisher, F.T., Ruoff, R.S., Brinson, L.C., *Chem. Mater*. **2005**, 17, 1290-1295
96. Sherwood, P.M.A., *Journal of Electron Spectroscopy and Related Phenomena*, **1996**, 81, 319-342
97. Dranca, I., Lupascu, T., Vogelsang, K., Monahova, L., *J. Therm. Anal. Cal*. **2001**, 64, 945-953
98. Figueiredo, J.L, Pereira, M.F.R., Freitas, M.M.A, Orfao, J.J.M., *Carbon*, **1999**, 37, 1379-1389
99. Pan, C., Xu, S., Zou, H., Guo, Z., Zhang, Y., Guo, B., *J. Am. Soc. Mass Spectrom*., **2005**, 16, 263-270
100. Yadav, L.D.S., "*Organic Spectroscopy*", Kluwer Academic Publishers, Boston, **2005**, p. 107-129
101. Shimodaira, N., Masui, A., *Journal of Applied Physics*, **2002**, 92, 2, 902-909
102. Filik, J., *Spectroscpopy Europe*, **2005**, 17, 5, 10-17
103. Li, Z-M., Zhang, N., Li, F-T., *Applied Surface Science*, **2006**, 253, 2870-2874
104. Kinoshita, K., "*Carbon: Electrical and Physicochemical Properties"*, John Wiley & Sons, Inc., New York, **1988**, p. 123-131
105. Villar-Rodil, S., Martinez-Alonso, A., Tascon, J.M.D., *J. Therm. Anal. Cal*., **2005**, 79, 529-532
106. Khezami, L., Chetouani, A., Taouk, B., Capart, R., *Powder Technology*, **2005**, 157, 48-56
107. Pescia, J., *J. Phys*., **1966**, 27, 782
108. Yadav, L.D.S., "*Organic Spectroscopy*", Kluwer Academic Publishers, Boston, **2005**, p. 152
109. Bahr, J.L and Tour, J.M. *J. Mater. Chem***. 2002**, 12, 1952-1958
110. Liu, J., Rinzler, A.G., Dai, H., Hafner, J.H., Bradley, R.K., Boul, P.J., Lu, A., Iverson, T., Shelimov, K., Huffman, C.B., Rodriguez-Macias, F.S., Lee, Y.S., Randall, T., Colbert, D.T., Smalley, R.E., *Science*, **1998**, 280, 5367, 1253-1256
111. Petter, R. C., Salek, J. S., Sikorski, C. T., Kumaravel, G., and Lin, F. *J. Am. Chem. Soc*. **1990**, 112, 3860-3868
112. Weast, R., Astle, M.J., "*CRC Handbook of Chemistry and Physics*", 63rd Ed., CRC Press, Florida, **1982-1983**, p. D-155
113. Lynam, M.M., Kilduff, J.E., Weber, W.J., *J. Chem. Edu*. **1995**, 72, 80-84
114. Ogata, Y., Tezuka, H., Kamei, T., *The Journal of Organic Chemistry*, **1969**, 34, 4, 845-847
115. Salame, I.I., Bandosz, T.J., *J. Colloid and Interface Sci*, **2001**, 240, 252-258
116. Zoltai, S.C., *Water, Air, and Soil Pollution*, **1988**, 37, 217-228

117. Behler, K., Osswald, S., Ye, H., Dimovski, S., Gogotsi, Y., *Journal of Nanoparticle Research*, **2006**, 8, 615-625
118. Long, D.A., "*Raman Spectroscopy*", McGraw-Hill, Inc., London, **1977**, p. 158
119. Ponchel, A., Abramson, S., Quartararo, J., Bormann, D., Barbaux, Y., Monflier, E., *Microporous and Mesoporous Materials*, **2004**, 75, 261-272
120. Mahmud, S.T., "*Synthesis of Cyclodextrin Functionalized Silica Materials*", M.Sc. thesis at University of Saskatchewan, Aug., 2007, SK, Canada, Section 3.2.4
121. Zhuang, Q-L., Kyotani, T., Tomita, A., *Energy & Fuels*, **1994**, 8, 714-718
122. Guibal, E., Milot, C., Eterradossi, O., Gauffier, C., Domard, A., *Int. J. Biol. Macromolecules*, **1999**, 24, 49-59
123. Hall, K.R, Eagleton, L.C., Acriros, A., Vermeulen, T., *I & EC Fundamentals*, **1966**, 5, 212-223

APPENDICES

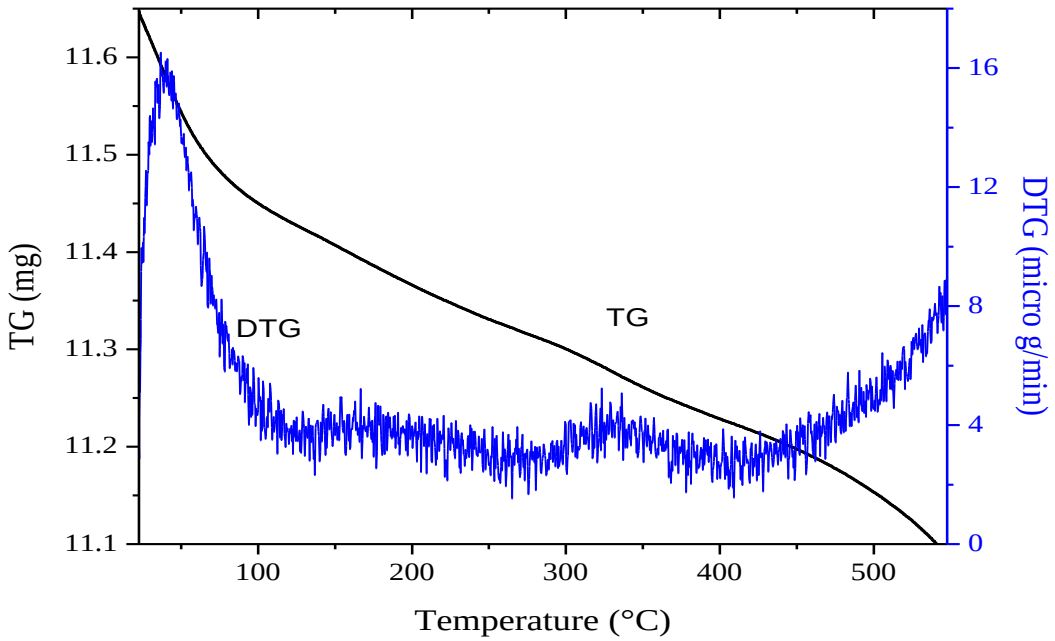

A1: TGA/DTG Thermogram - AC

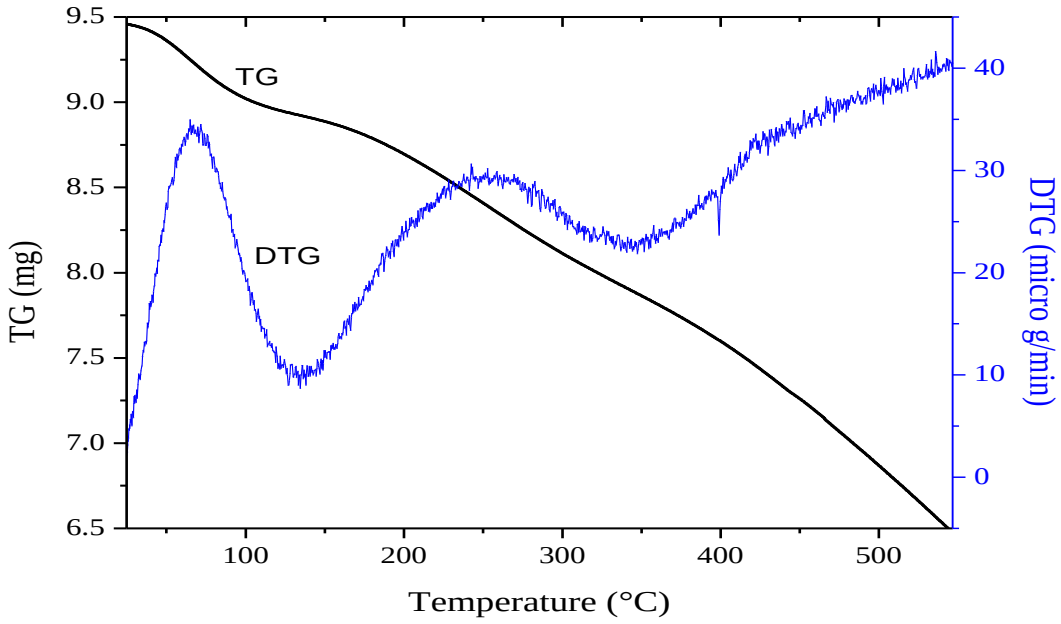

A2: TGA/DTG Thermogram - ACOXID(9)

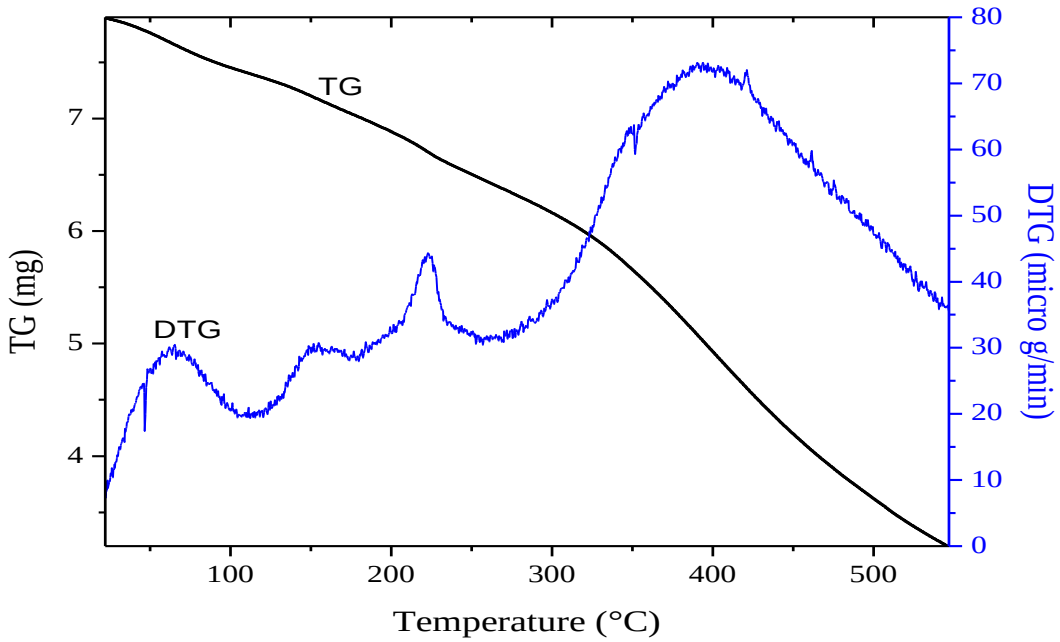

A3: TGA/DTG Thermogram - ACREDUCT(9)

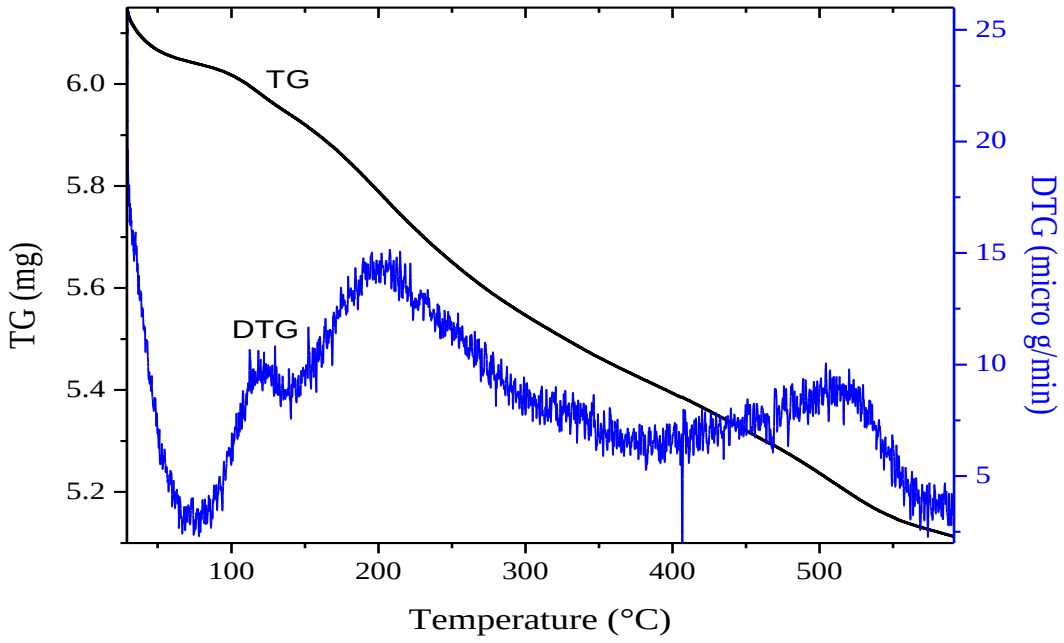

A4: TGA/DTG Thermogram - ACGAP(10)

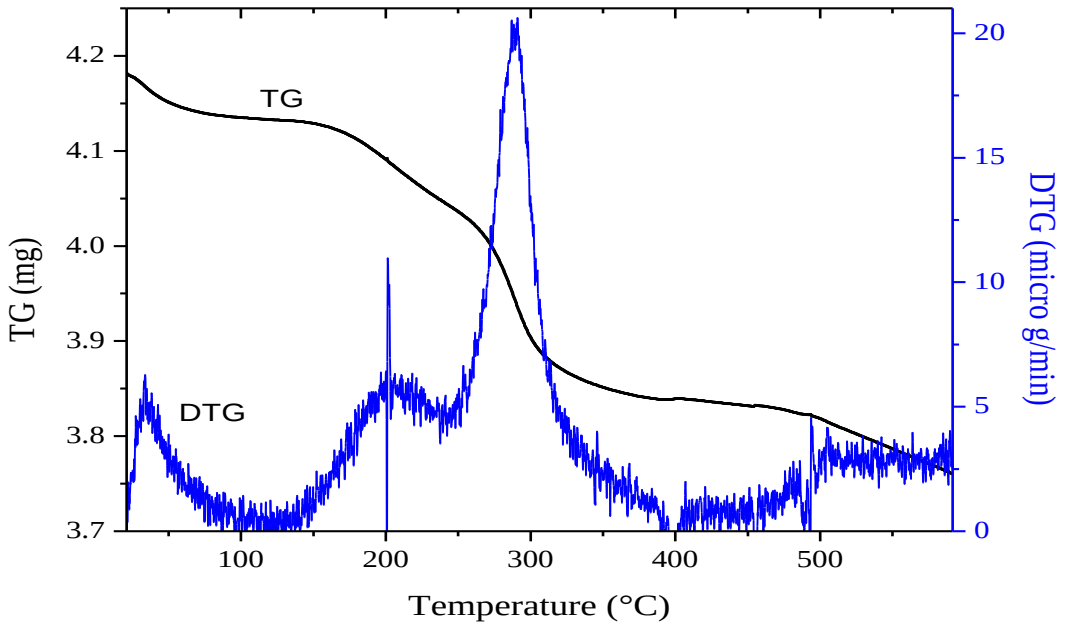

A5: TGA/DTG Thermogram - ACCDP(10)

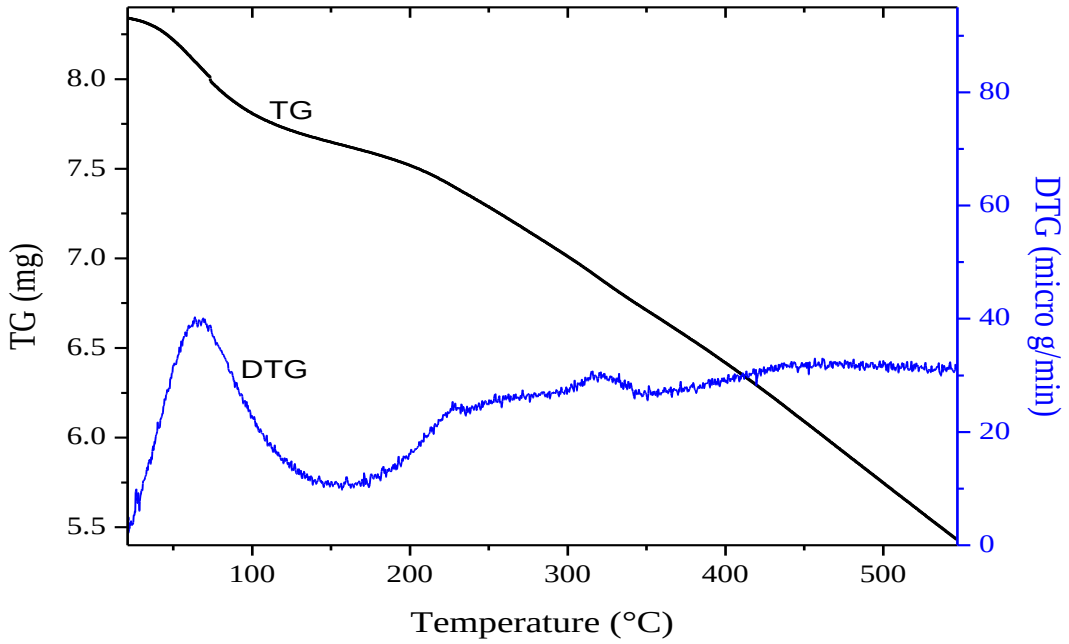

A6: TGA/DTG Thermogram - AC-β-CD [1:10:10(9)]

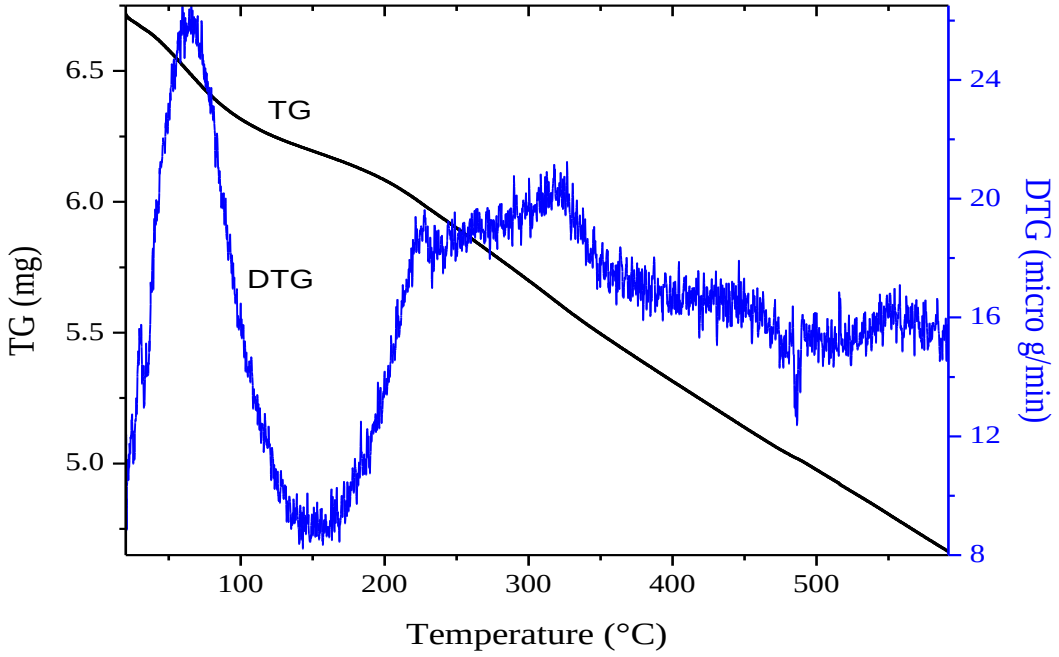

A7: TGA/DTG Thermogram - AC-β-CD [1:10:20(9)]

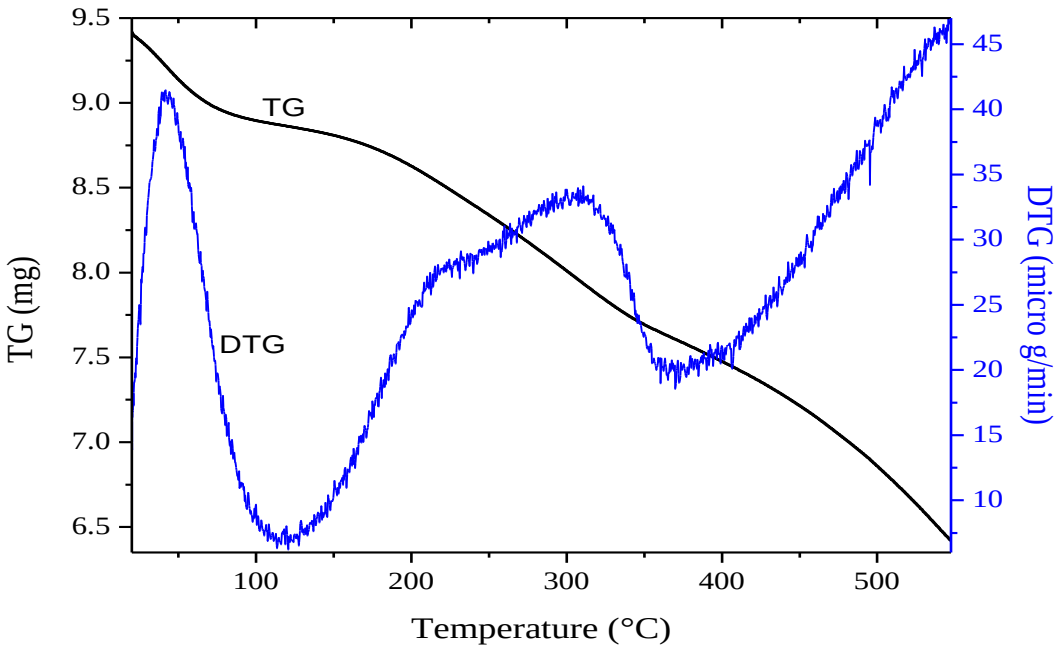

A8: TGA/DTG Thermogram - ACPDICD

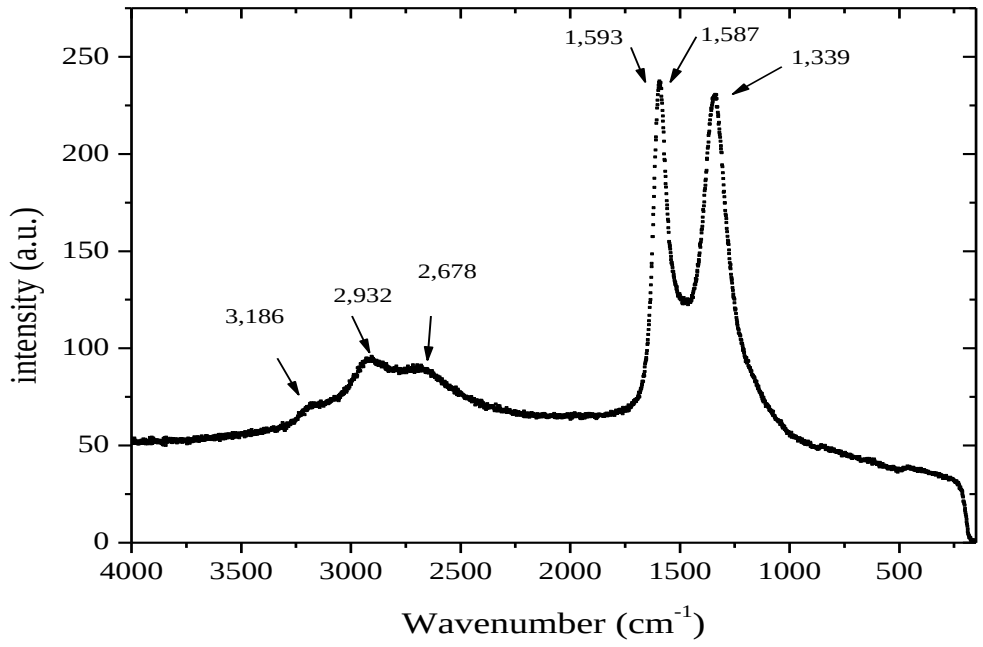

A9: Raman Spectra - AC at 25 °C

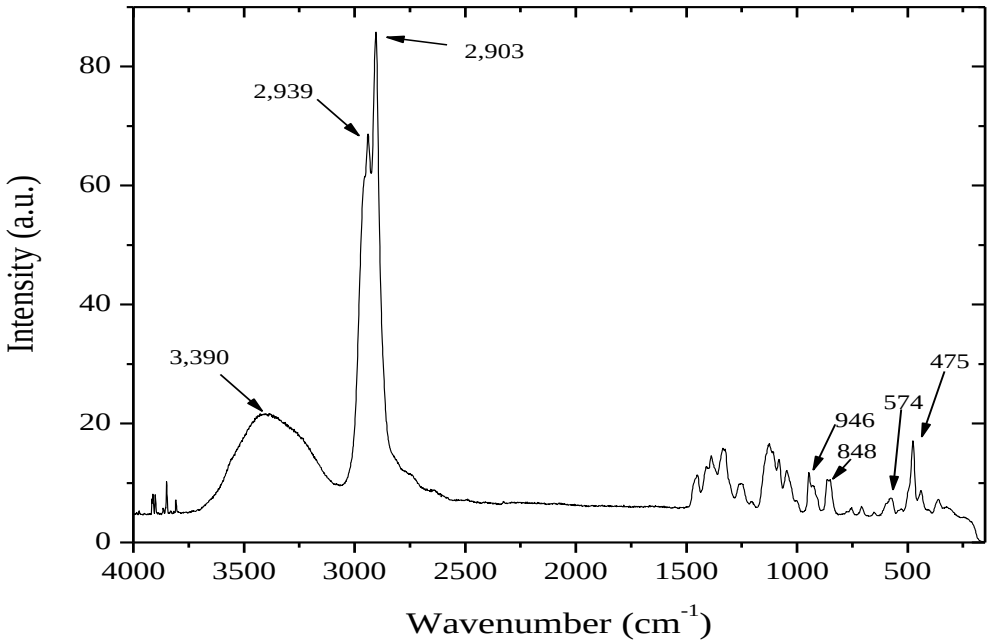

A10: Raman Spectra - β-CD at 25 °C

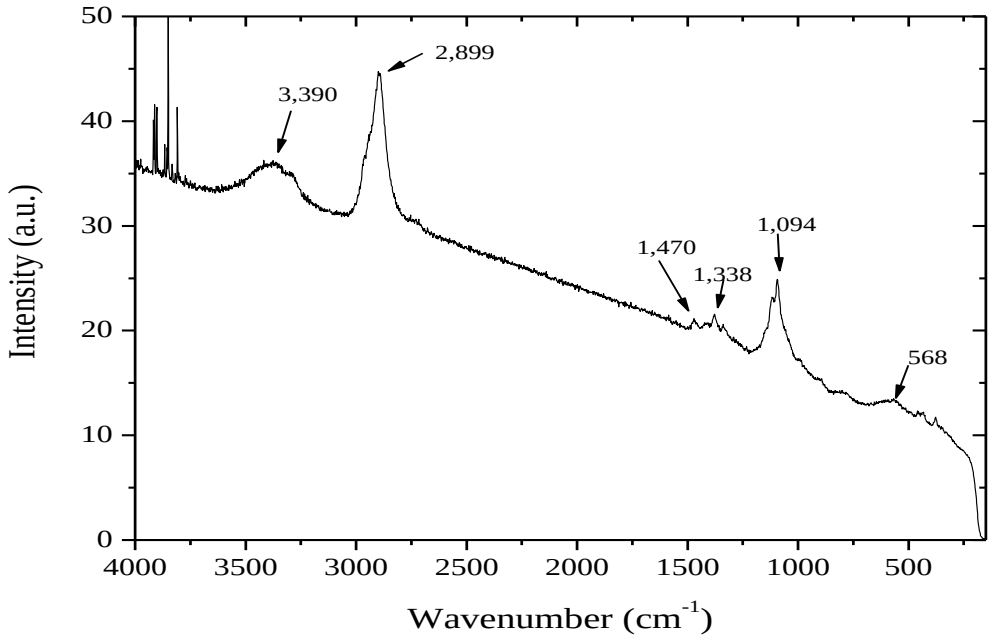

A11: Raman Spectra - ACCDP(10) at 25 °C

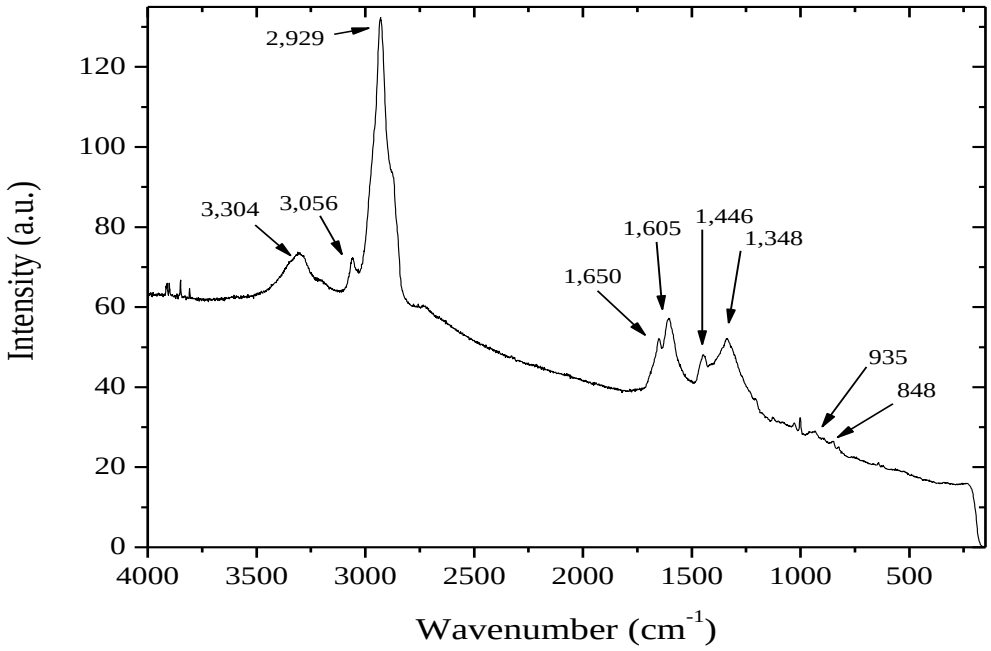

A12: Raman Spectra - AC-β-CD [1:10:1(3)] at 25 °C

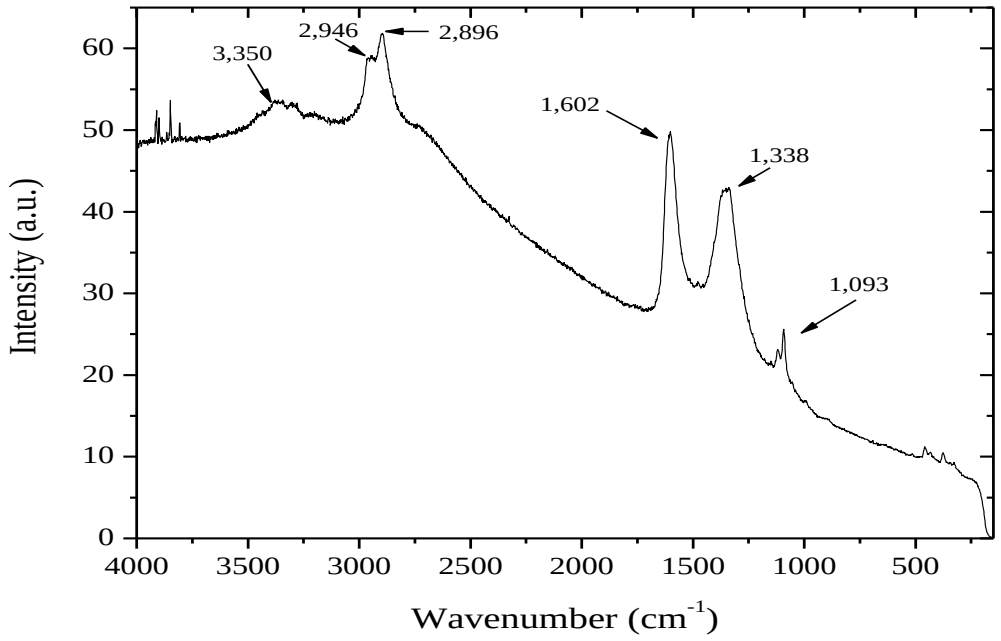

A13: Raman Spectra - AC-β-CD [1:10:5(6)] at 25 °C

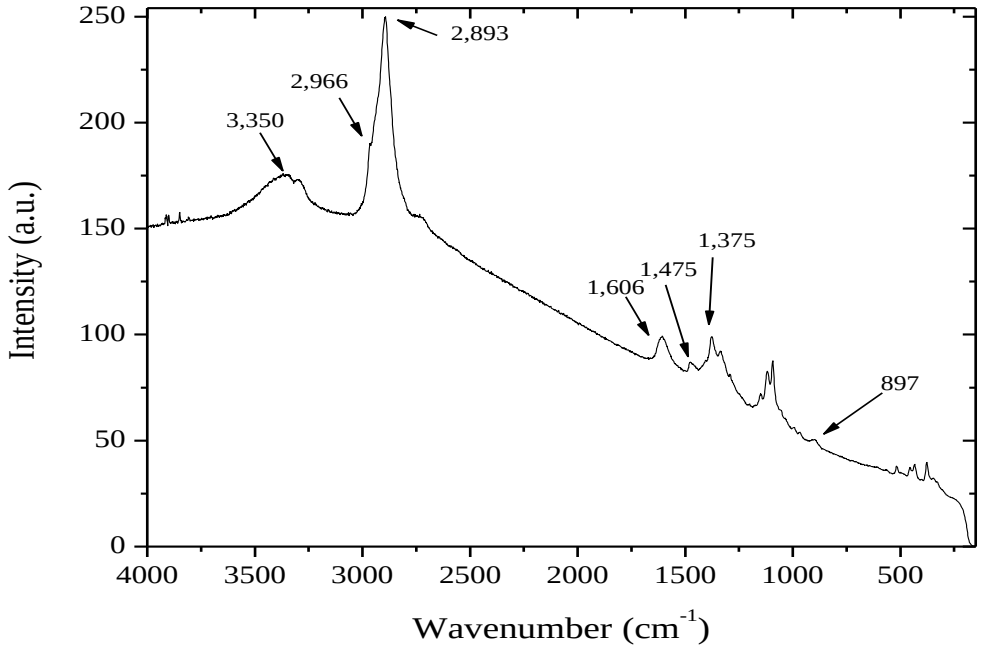

A14: Raman Spectra - AC-β-CD [1:10:10(9)] at 25 °C

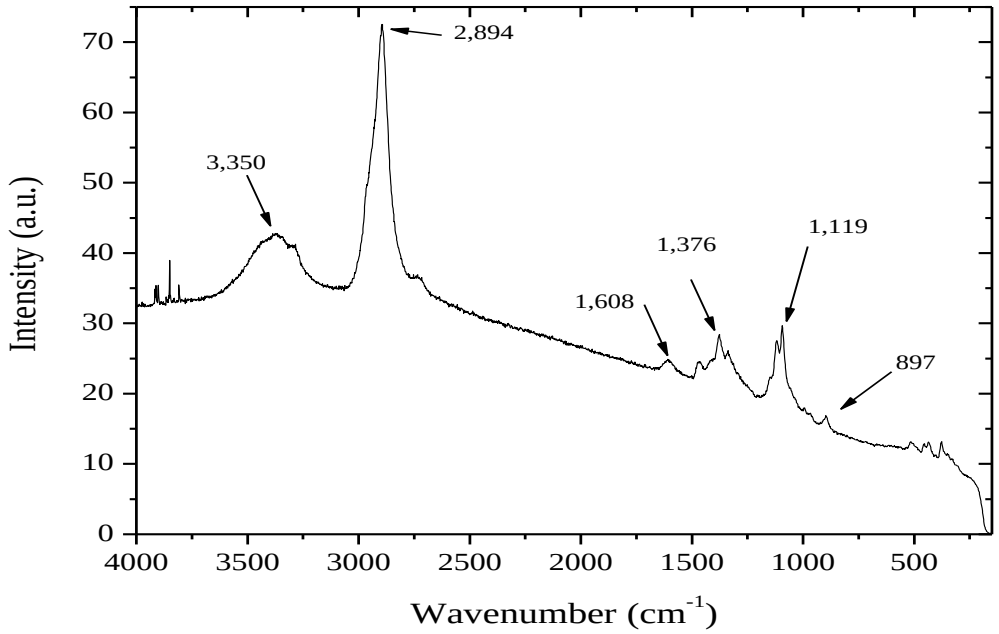

A15: Raman Spectra - AC-β-CD [1:10:20(9)] at 25 °C

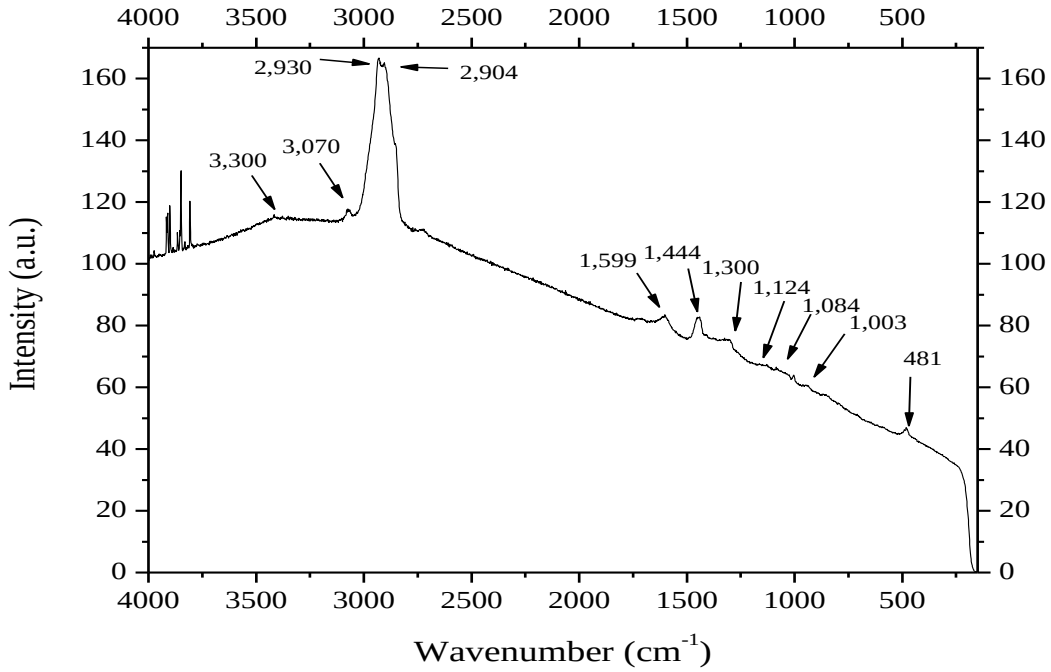

A16: Raman Spectra - AC-β-CD [2:10:0.9(3)] at 25 °C

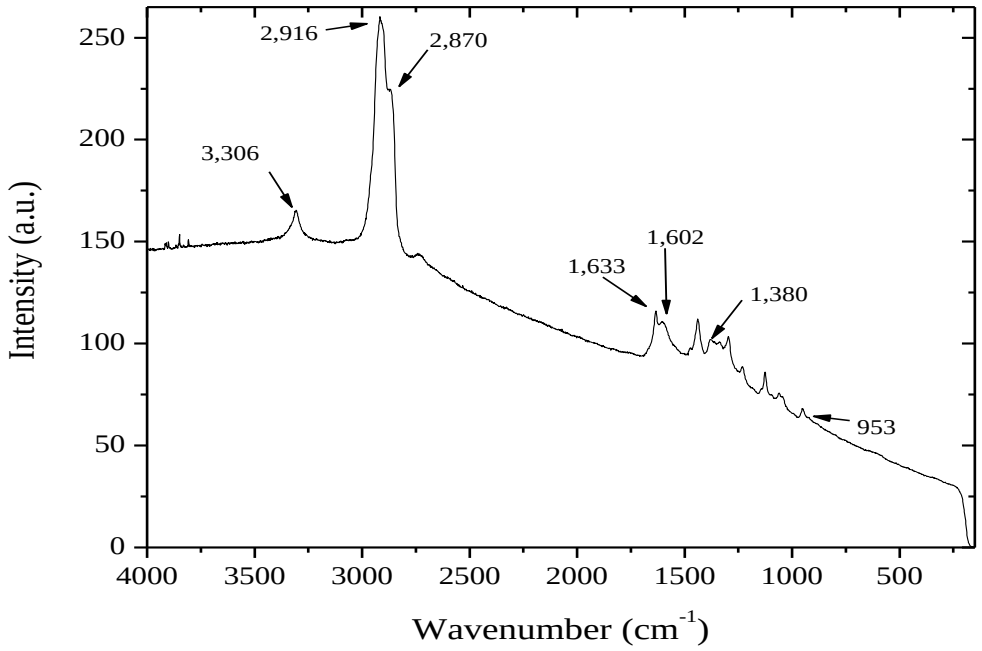

A17: Raman Spectra - ACPDICD at 25 °C

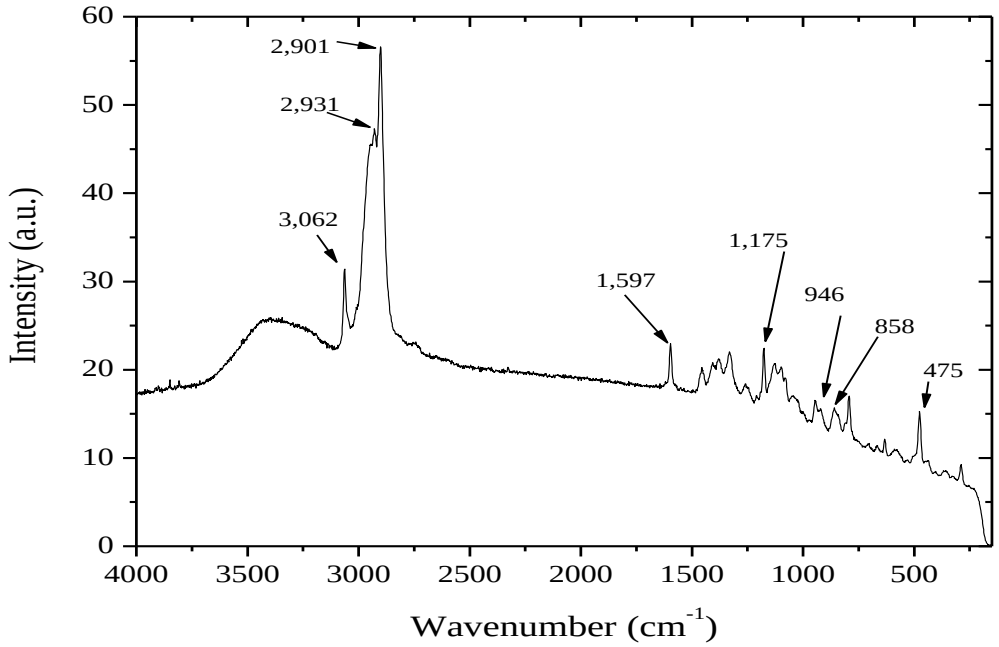

A18: Raman Spectra – Tosyl-β-CD at 25 °C

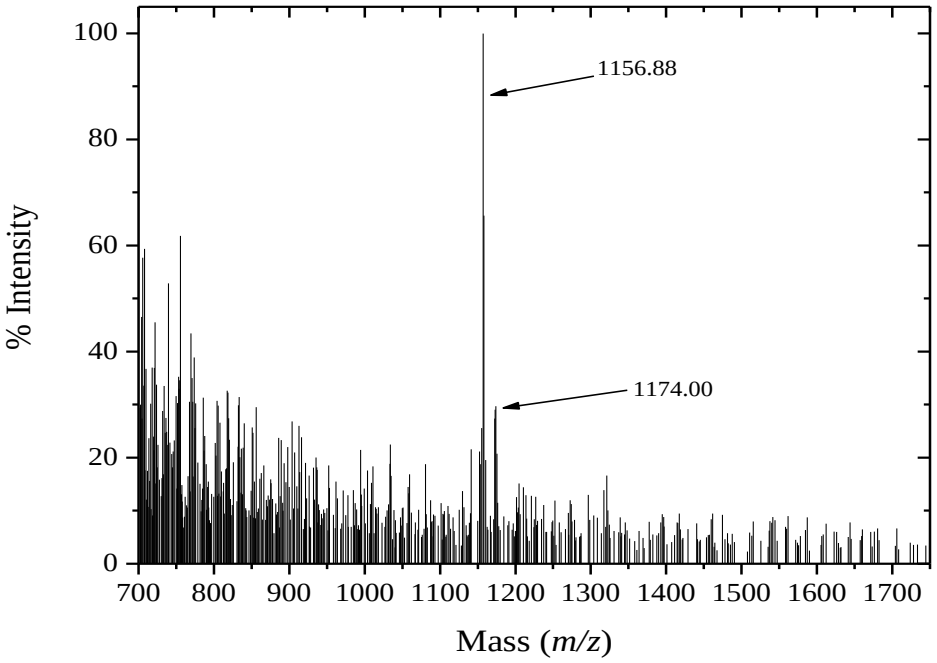

A19: MALDI TOF MS Spectra - AC-β-CD [1:10:1(3)]

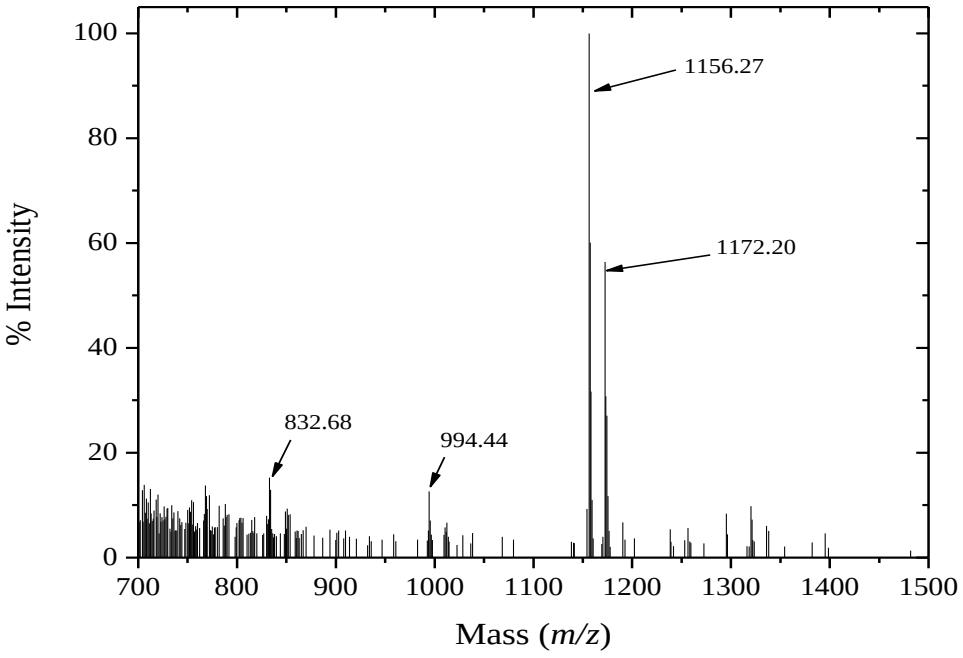

A20: MALDI TOF MS Spectra - AC-β-CD [1:10:5(6)]

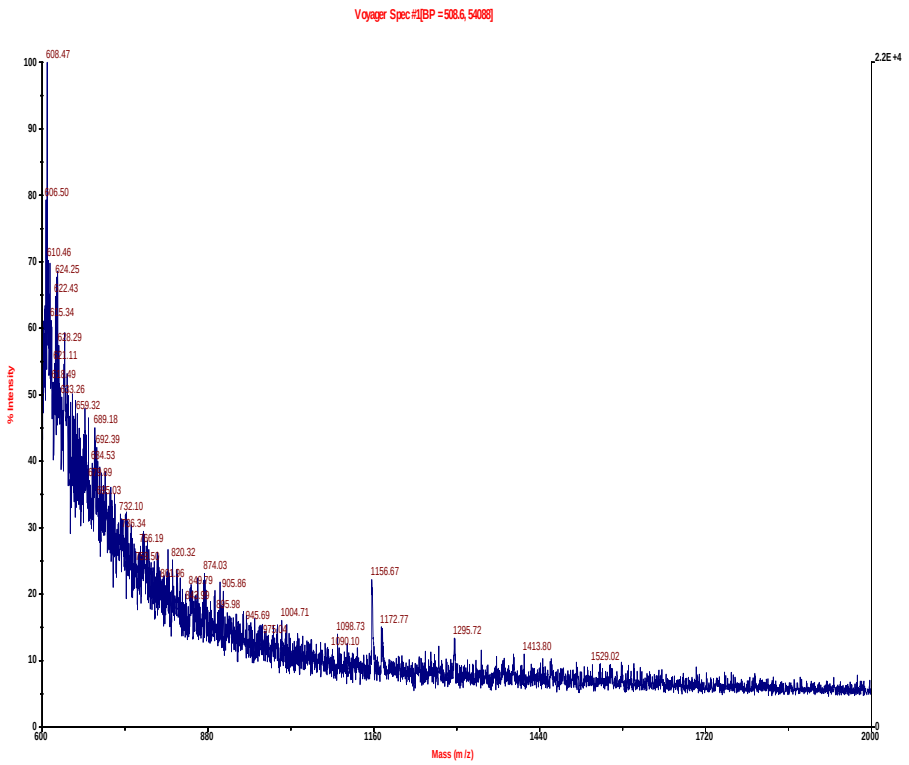

A21: MALDI TOF MS Spectra - AC-β-CD [1:10:10(9)]

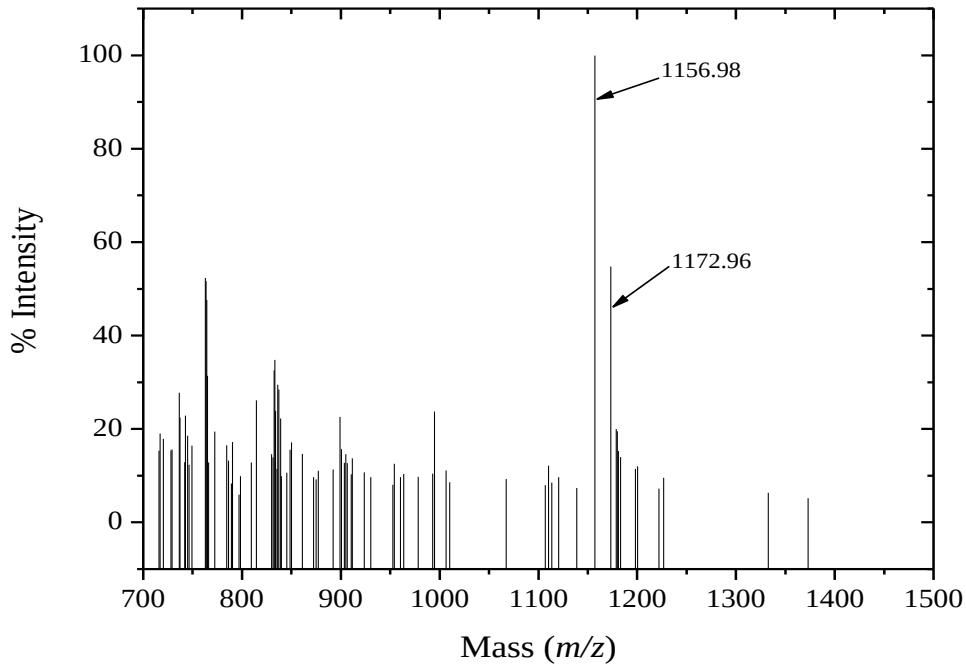

A22: MALDI TOF MS Spectra - AC-β-CD [1:10:20(9)]

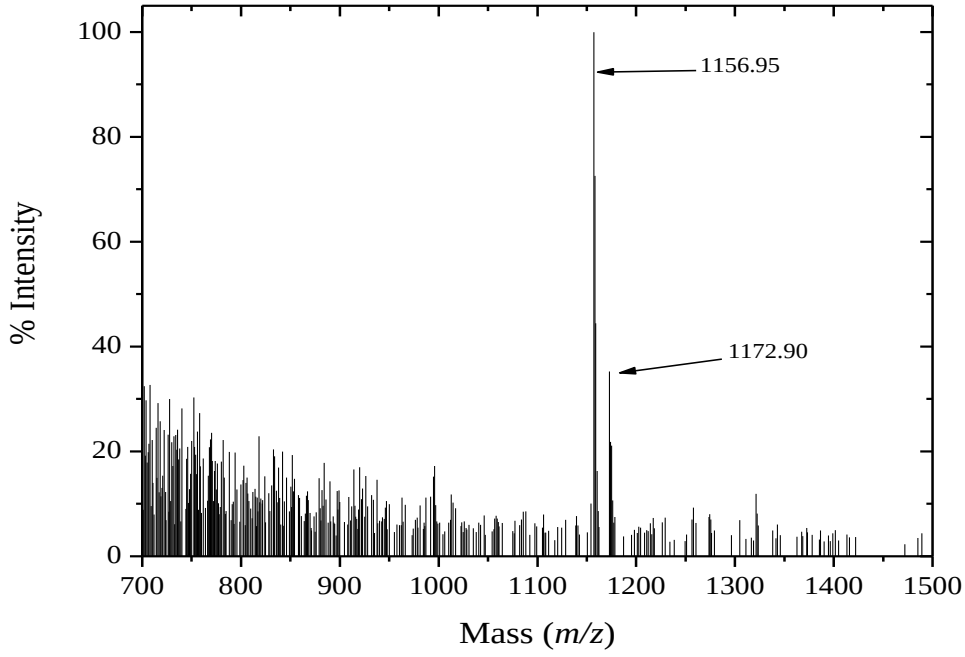

A23: MALDI TOF MS Spectra - AC-β-CD [2:10:0.9(3)]

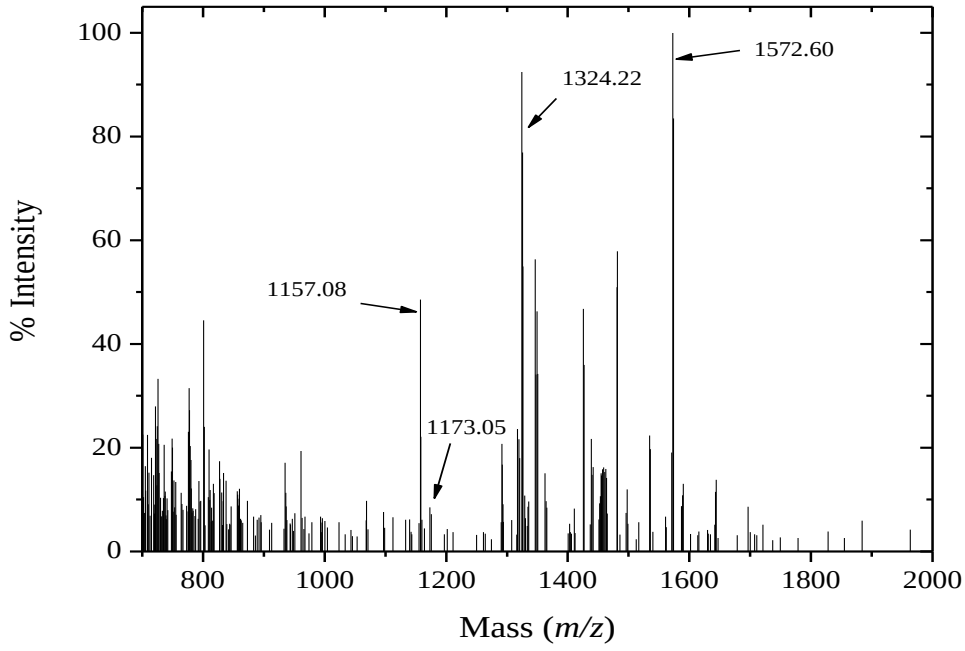

A24: MALDI TOF MS Spectra - ACPDICD

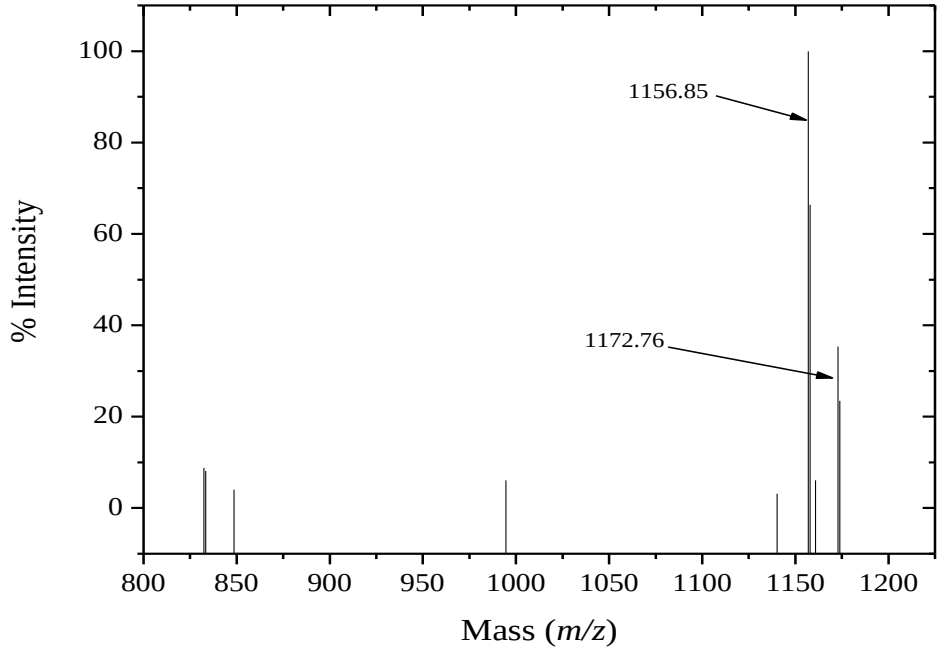

A25: MALDI TOF MS Spectra - ACCDP(10)

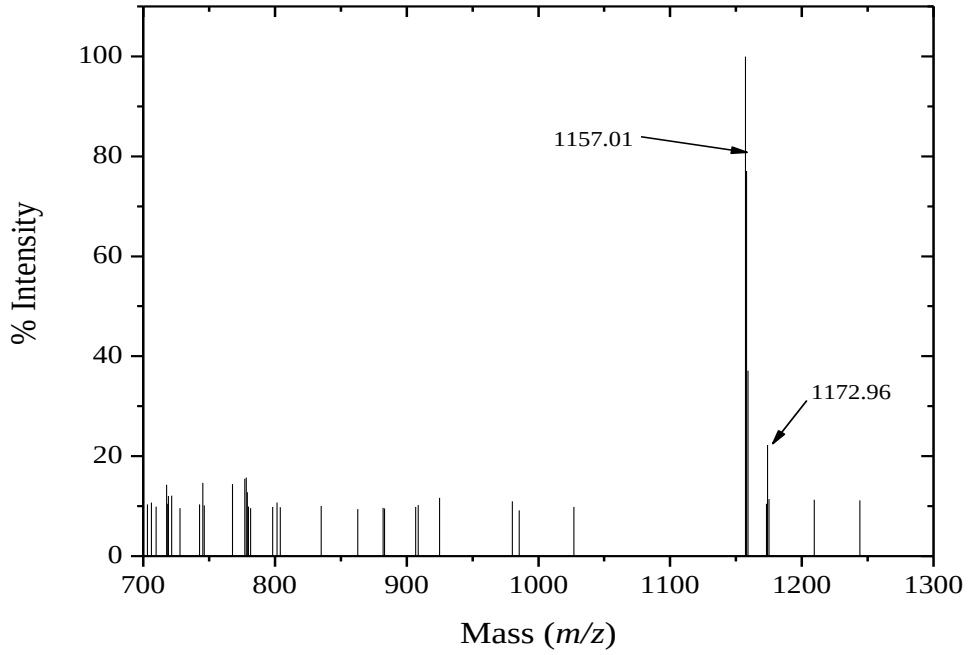

A26: MALDI TOF MS Spectra - β-CD

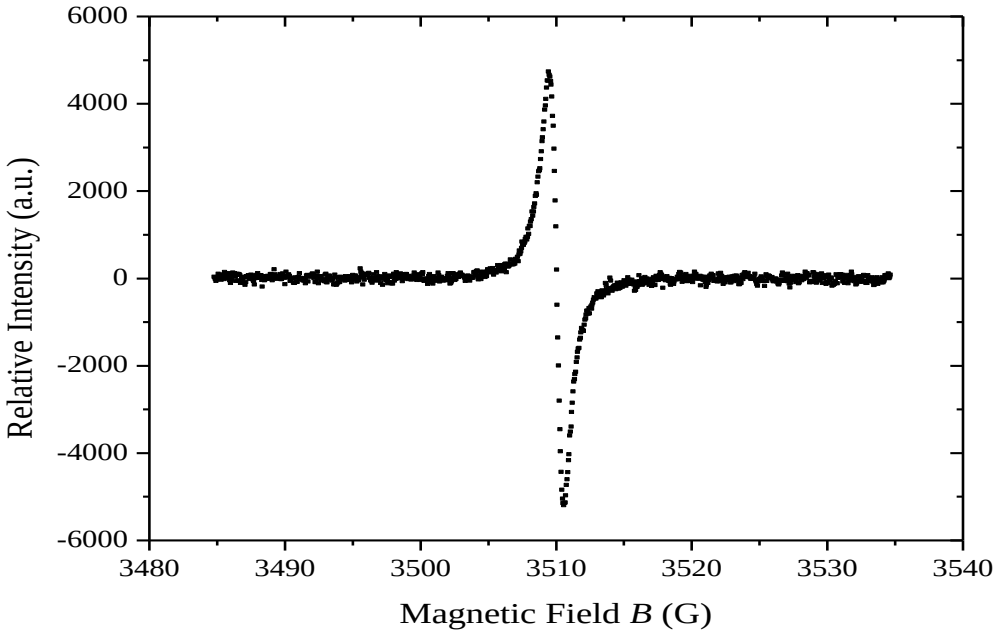

A27: ESR Spectra - DPPH at 25 °C

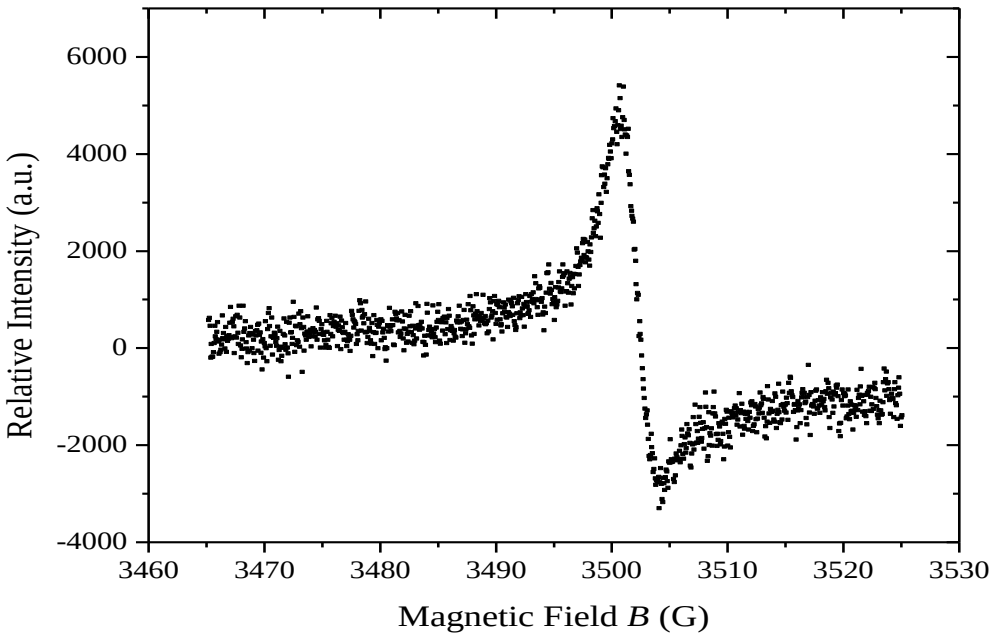

A28: ESR Spectra - ACOXID(6) at 25 °C

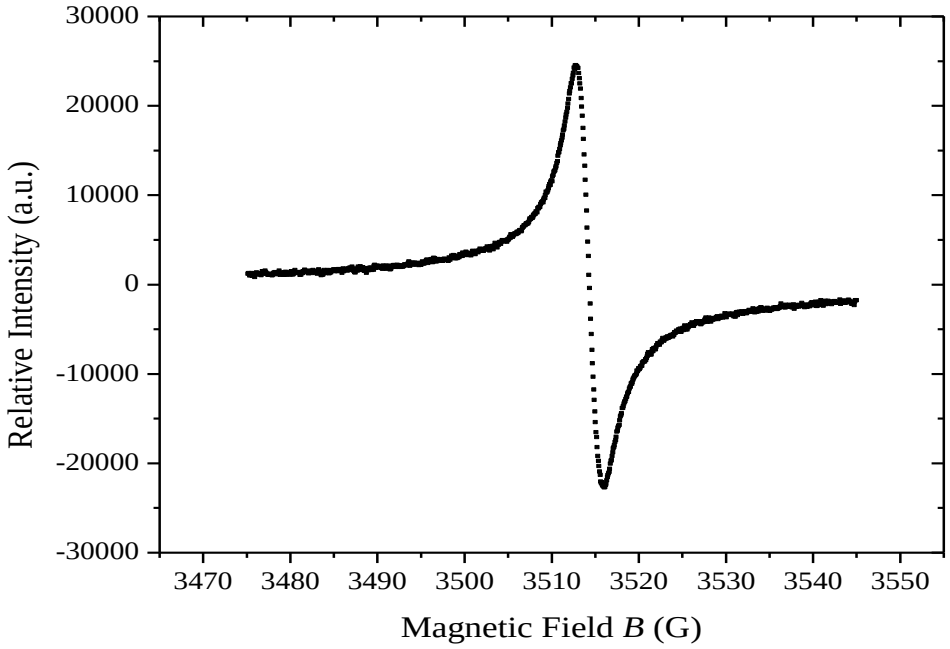

A29: ESR Spectra - ACOXID(12) at 25 ℃

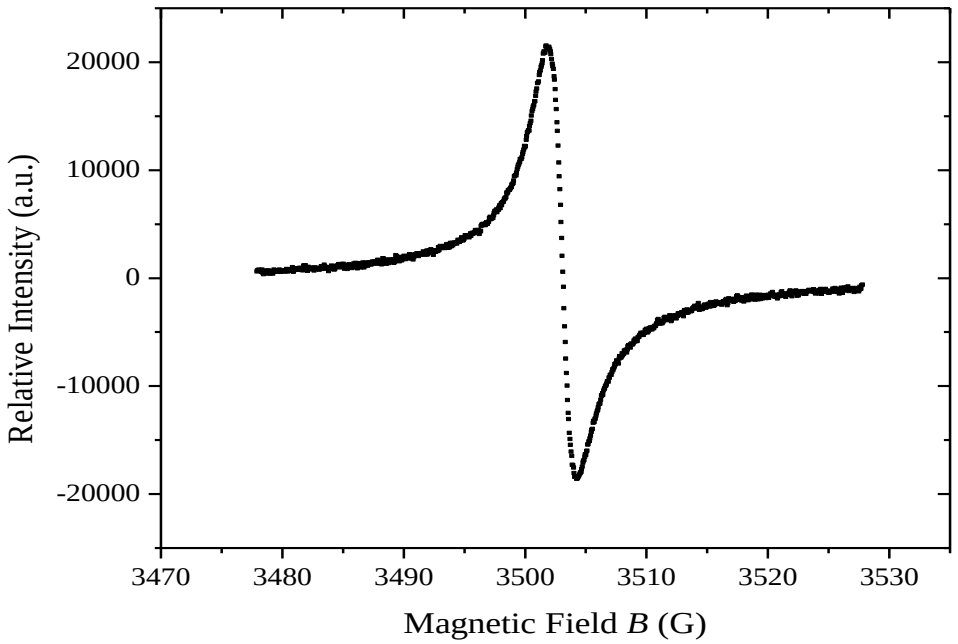

A30: ESR Spectra - ACPDICD at 25 ℃

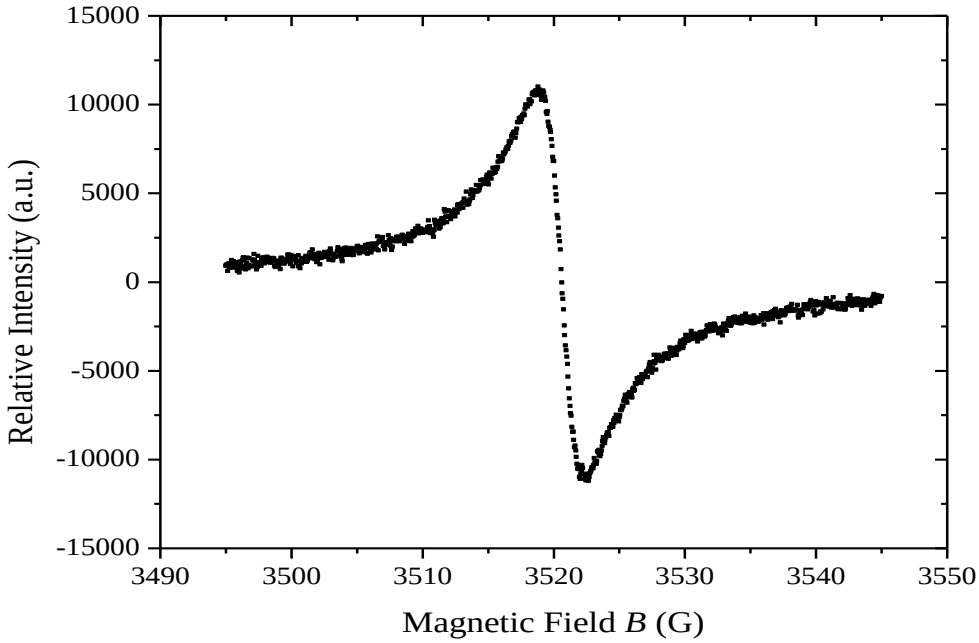

A31: ESR Spectra - AC-β-CD [1:10:20(9)] at 25 °C

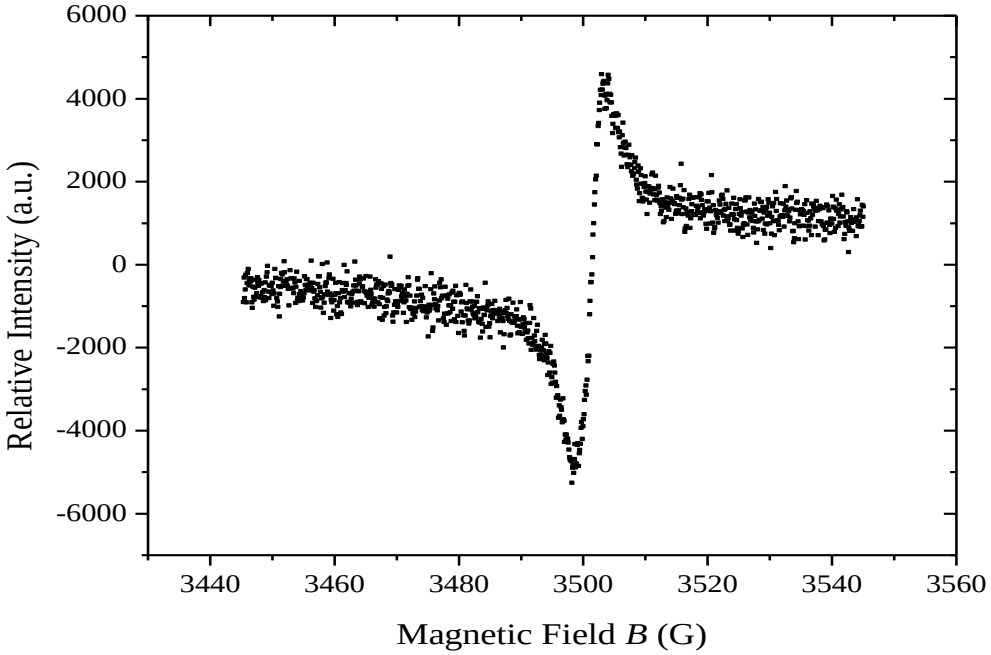

A32: ESR Spectra - ACREDUCT(6) at 25 °C

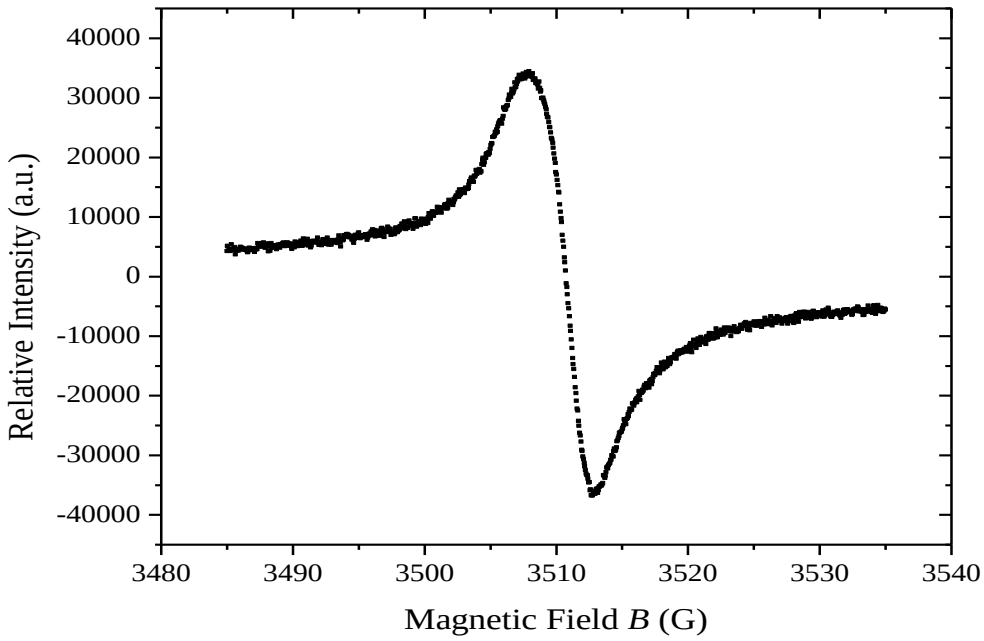

A33: ESR Spectra - ACREDUCT(9) at 25 ℃

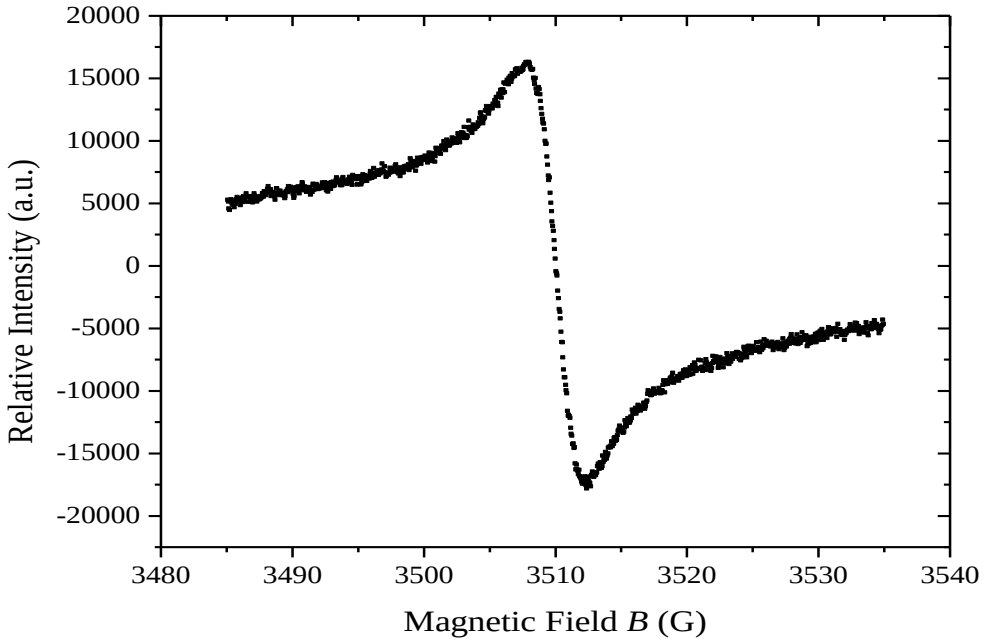

A34: ESR Spectra - AC-β-CD [1:10:10(9)] at 25 ℃

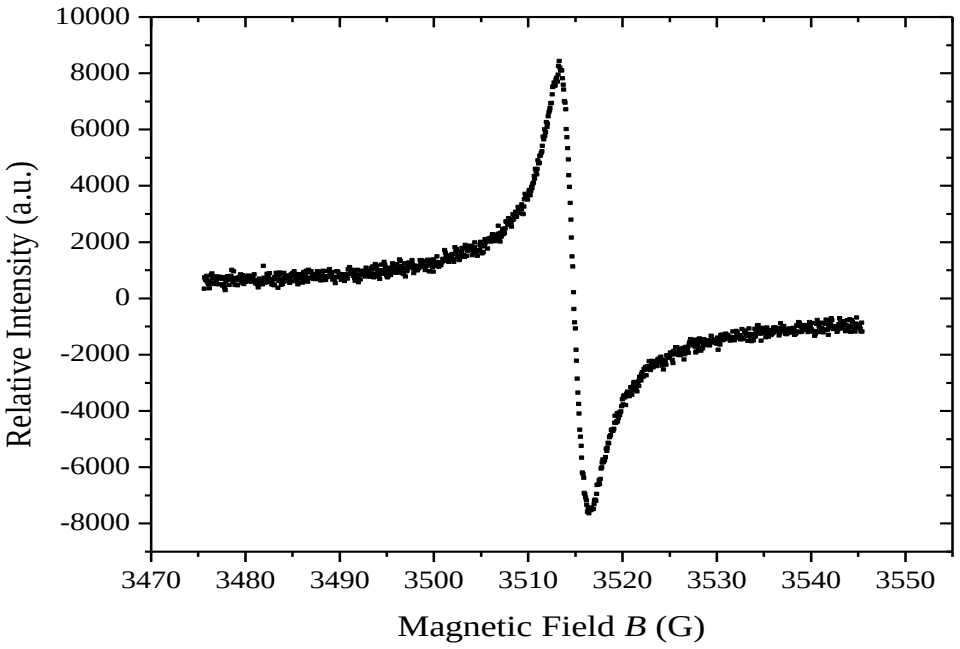

A35: ESR Spectra - ACOXID(9) at 25 °C

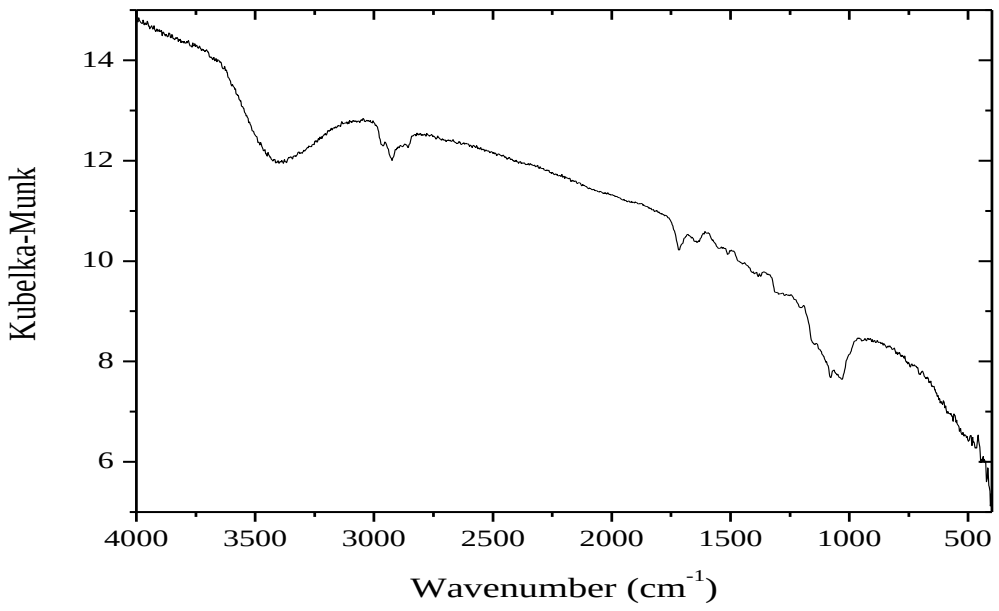

A36: DRIFT Spectra - AC at 25 °C with KBr

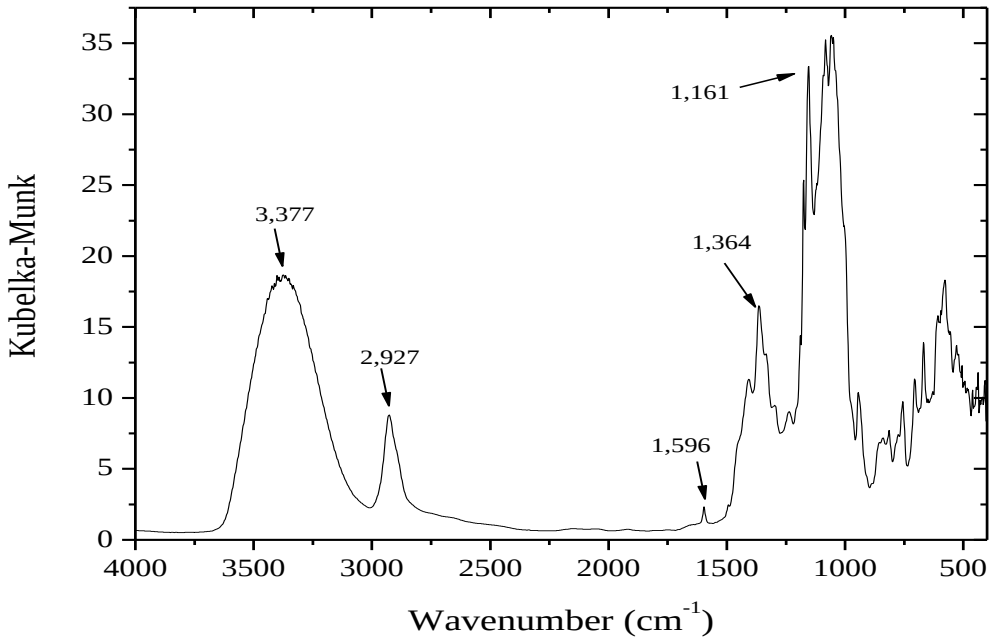

A37: DRIFT Spectra - Tosyl- β-CD at 25 °C with KBr

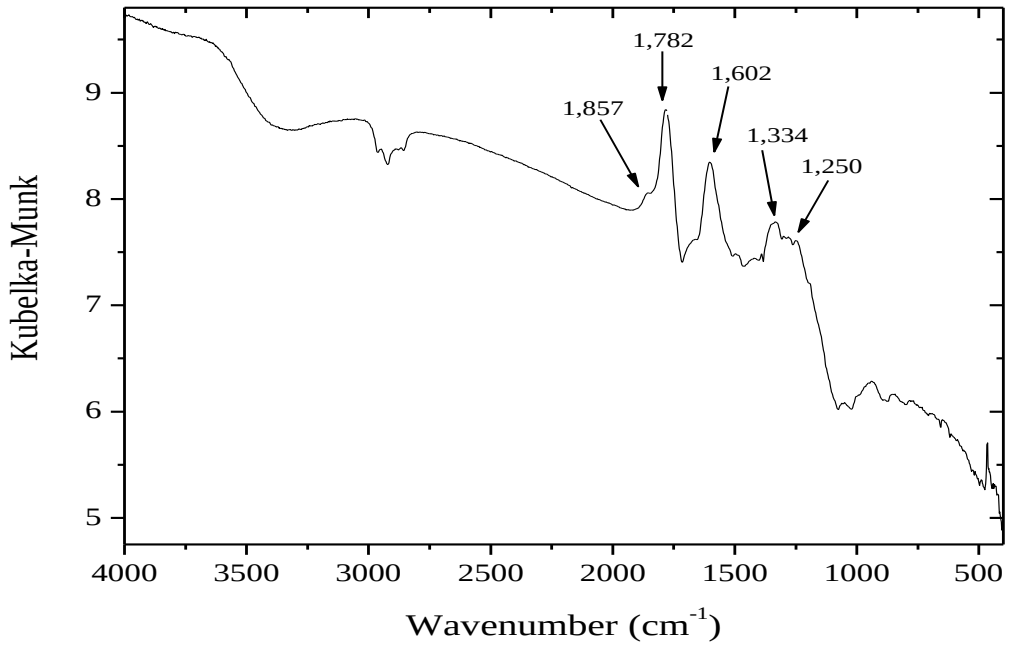

A38: DRIFT Spectra - ACOXID(3) at 25 °C with KBr

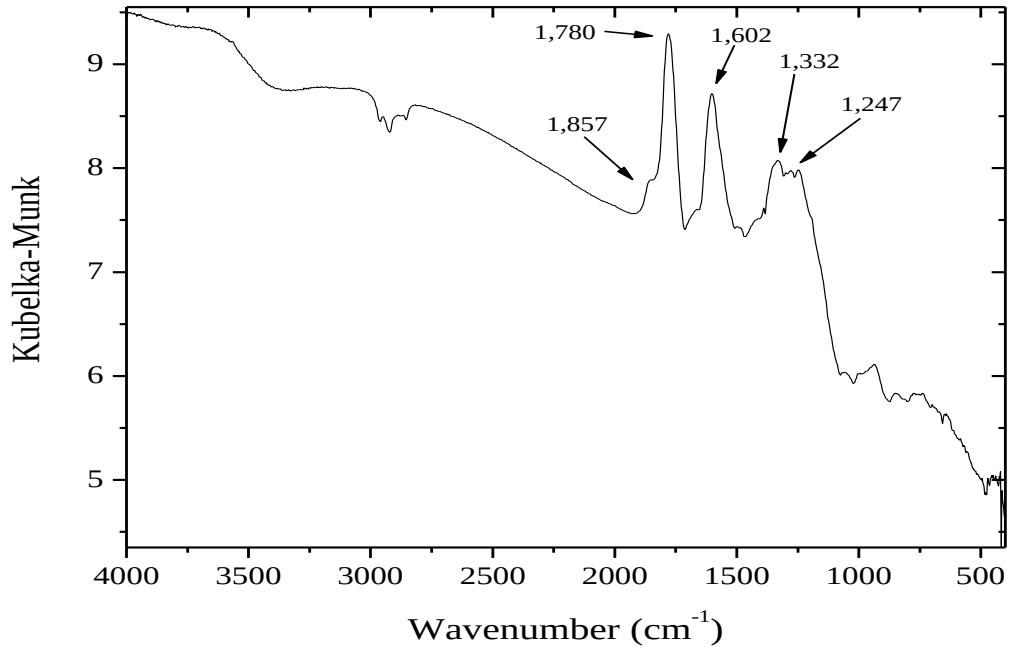

A39: DRIFT Spectra - ACOXID(6) at 25 °C with KBr

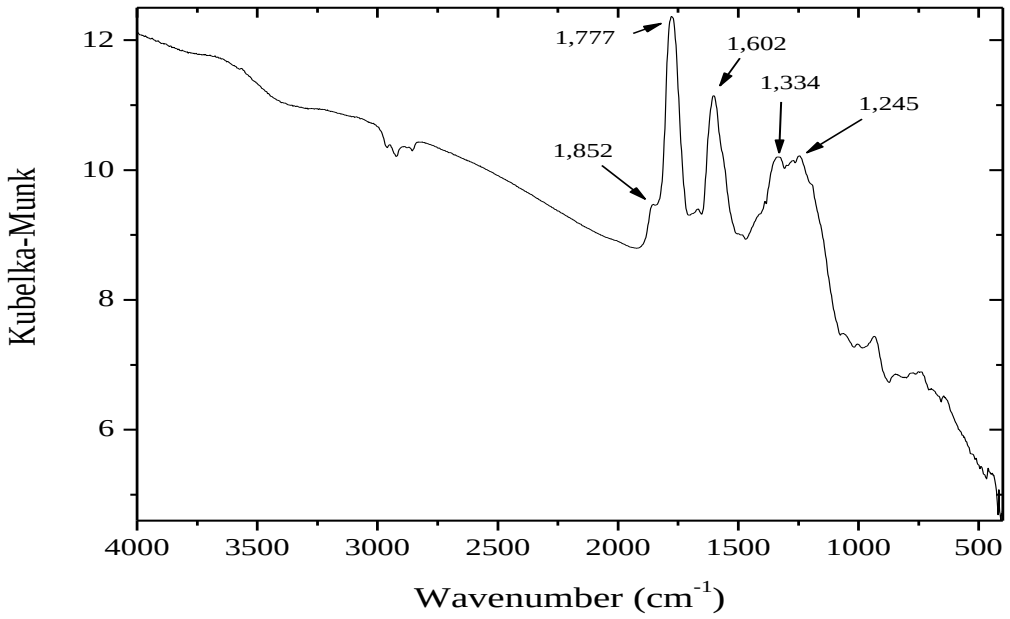

A40: DRIFT Spectra - ACOXID(9) at 25 °C with KBr

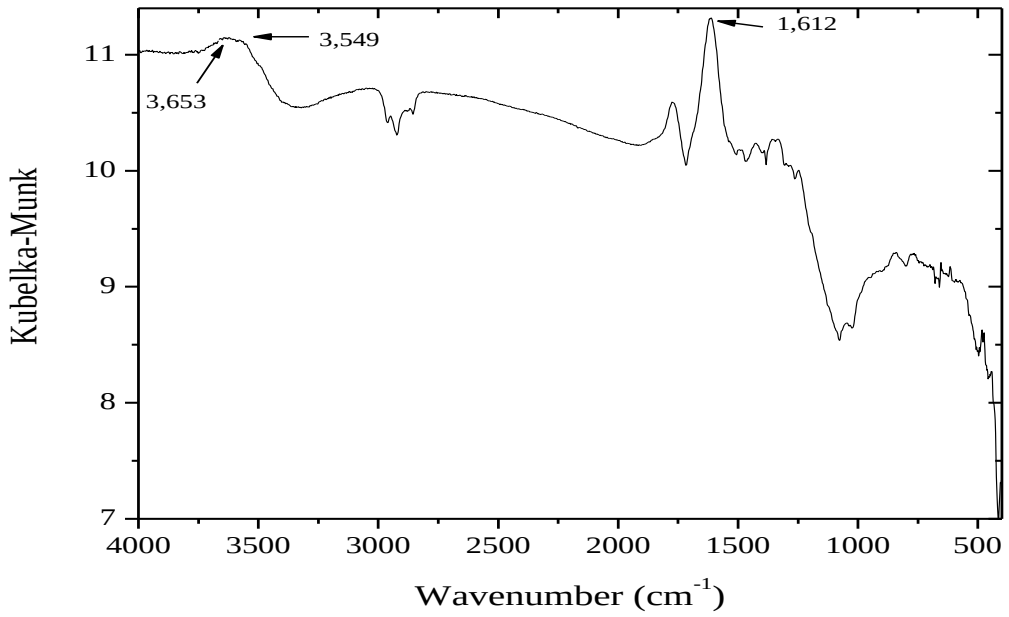

A41: DRIFT Spectra - ACREDUCT(3) at 25 °C with KBr

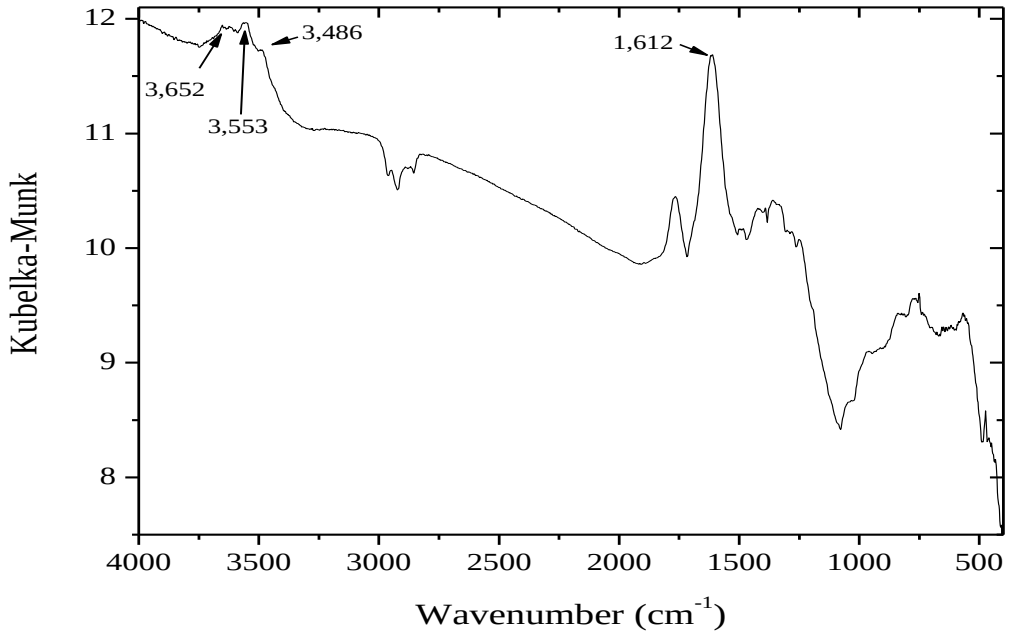

A42: DRIFT Spectra - ACREDUCT(6) at 25 °C with KBr

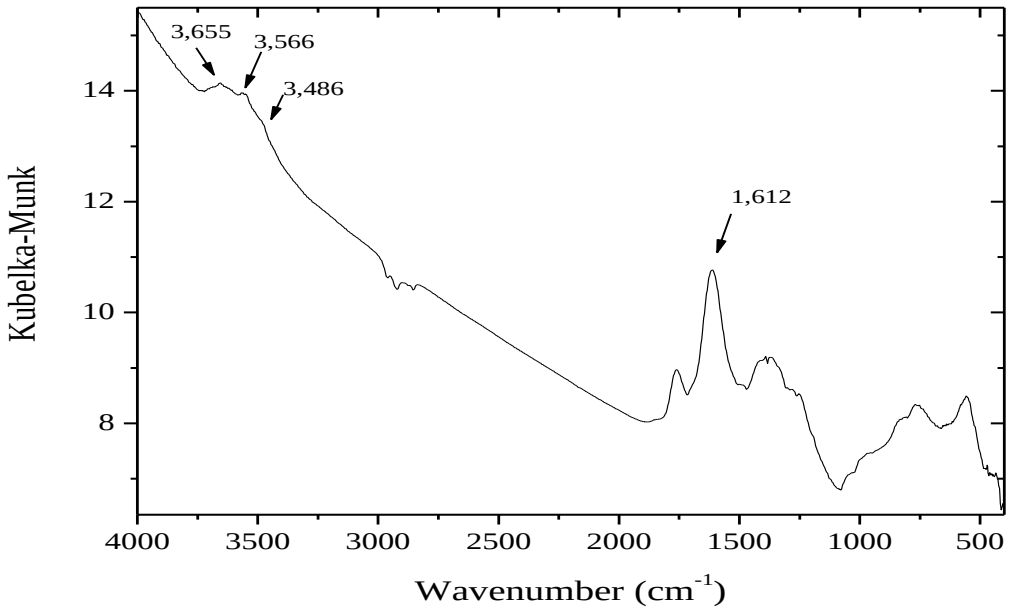

A43: DRIFT Spectra - ACREDUCT(9) at 25 °C with KBr

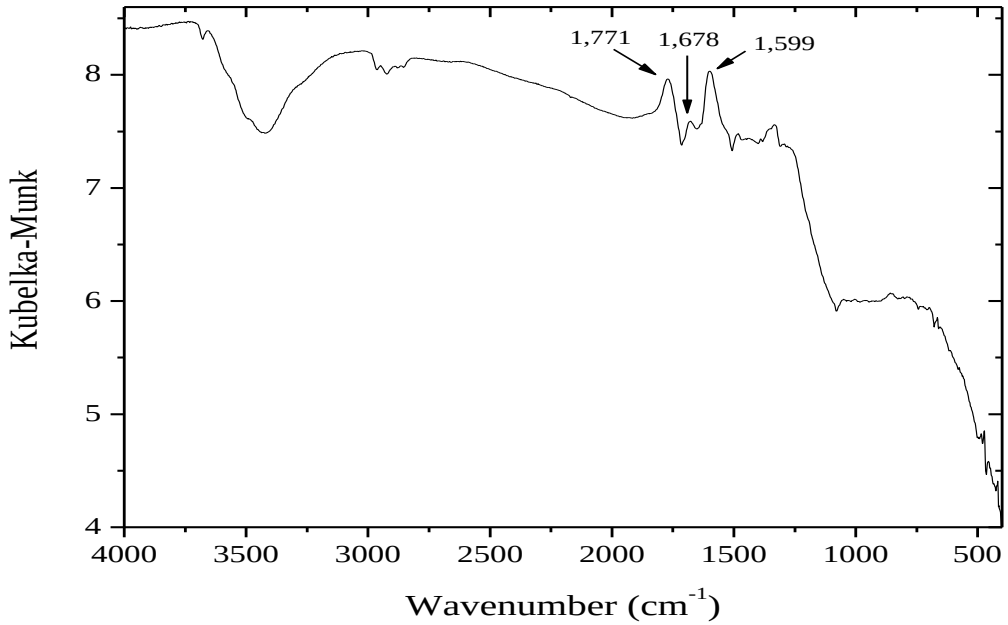

A44: DRIFT Spectra - AC-β-CD [1:10:1(3)] at 25 °C with KBr

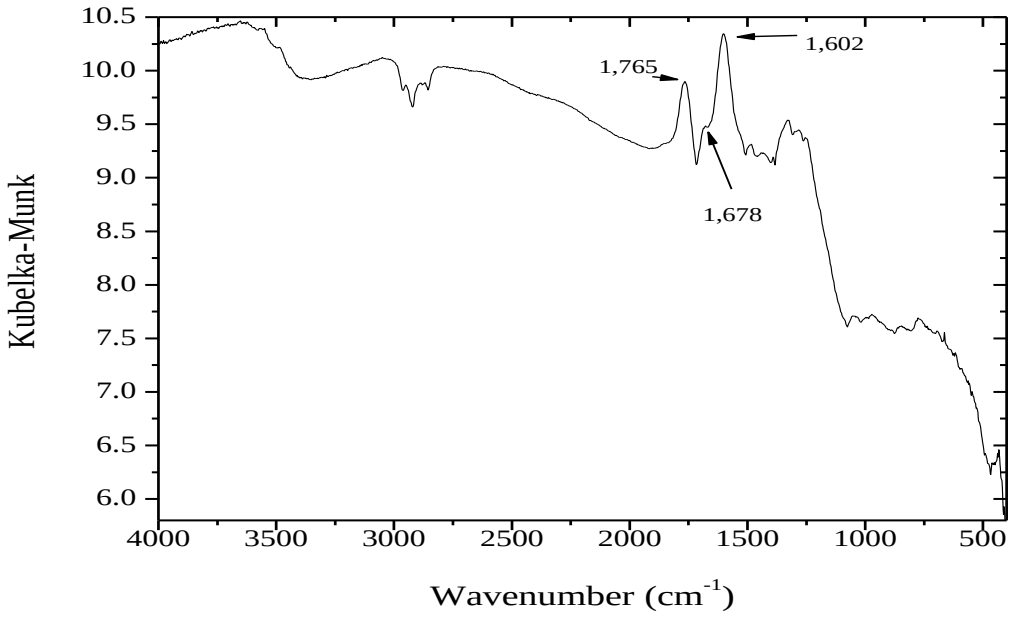

A45: DRIFT Spectra - AC-β-CD [2:10:0.9(3)] at 25 °C with KBr

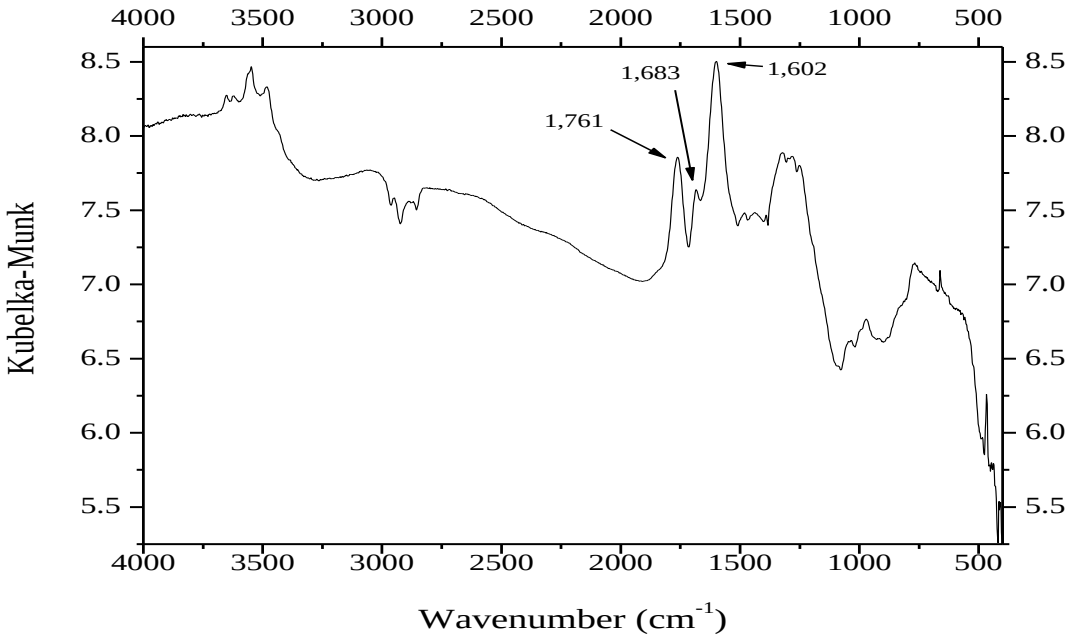

A46: DRIFT Spectra - AC-β-CD [1:20:2(6)] at 25 °C with KBr

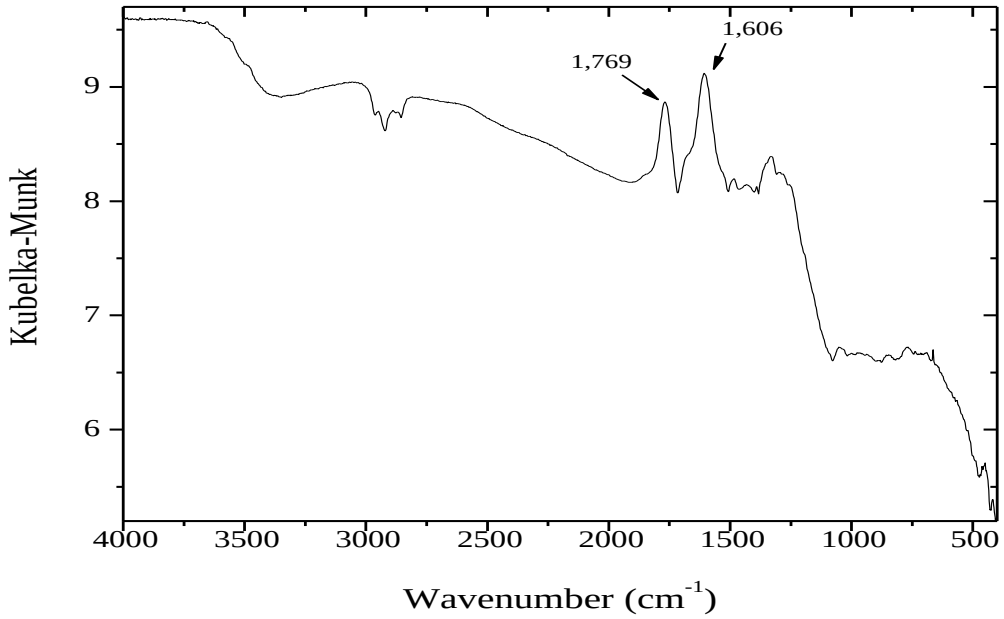

A47: DRIFT Spectra - AC-β-CD [1:10:5(6)] at 25 °C with KBr

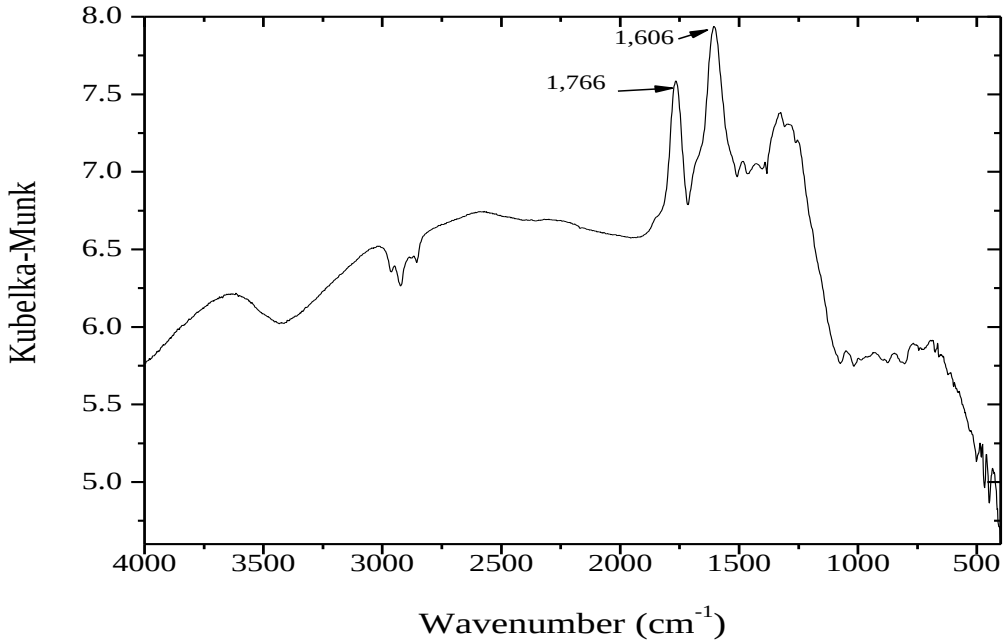

A48: DRIFT Spectra - AC-β-CD [1:10:10(9)] at 25 °C with KBr

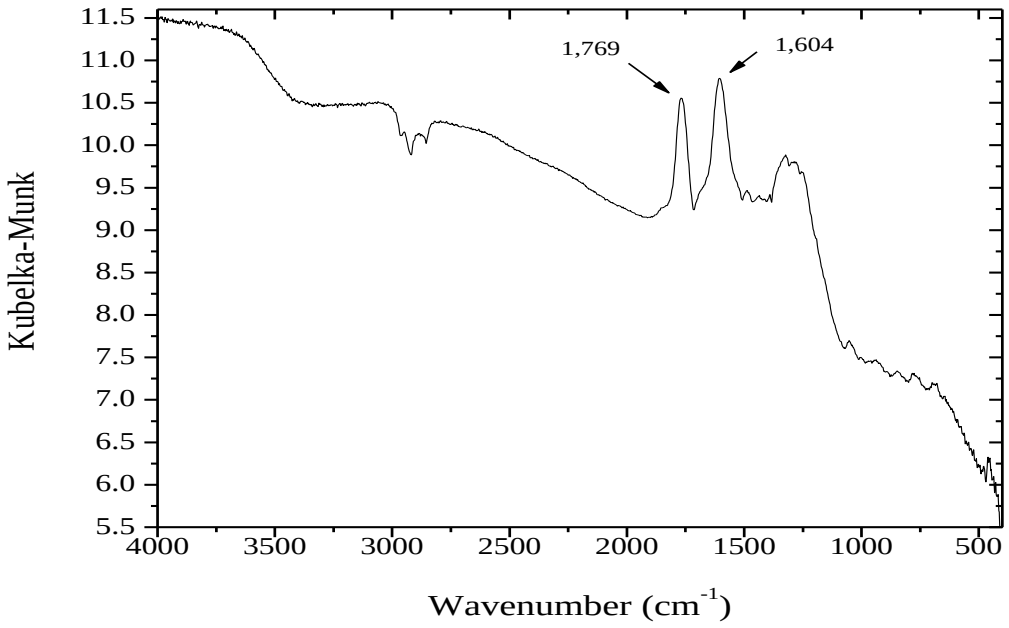

A49: DRIFT Spectra - AC-β-CD [1:10:20(9)] at 25 °C with KBr

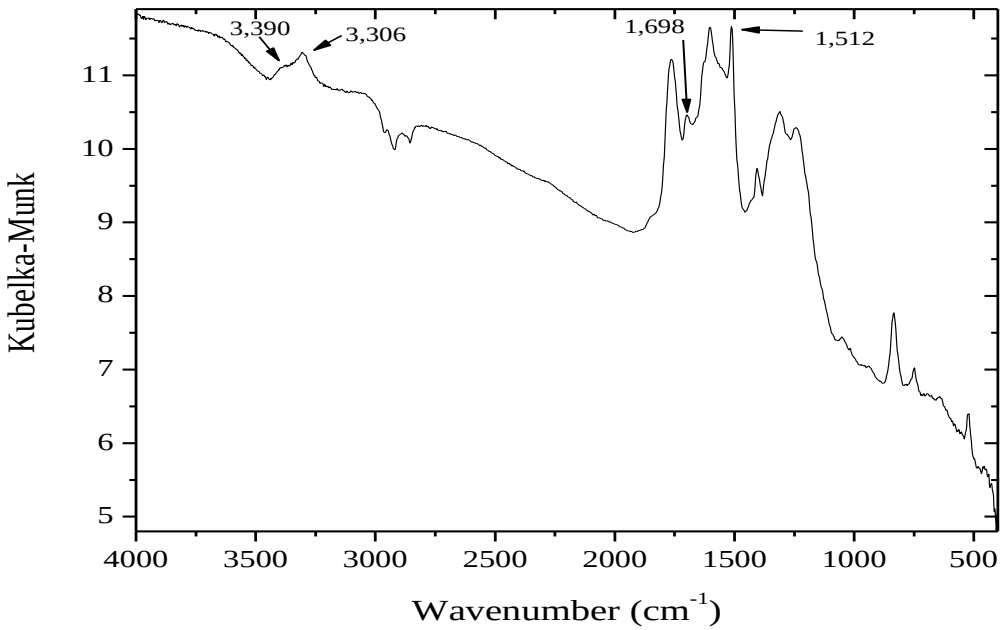

A50: DRIFT Spectra - ACPDICD at 25 °C with KBr

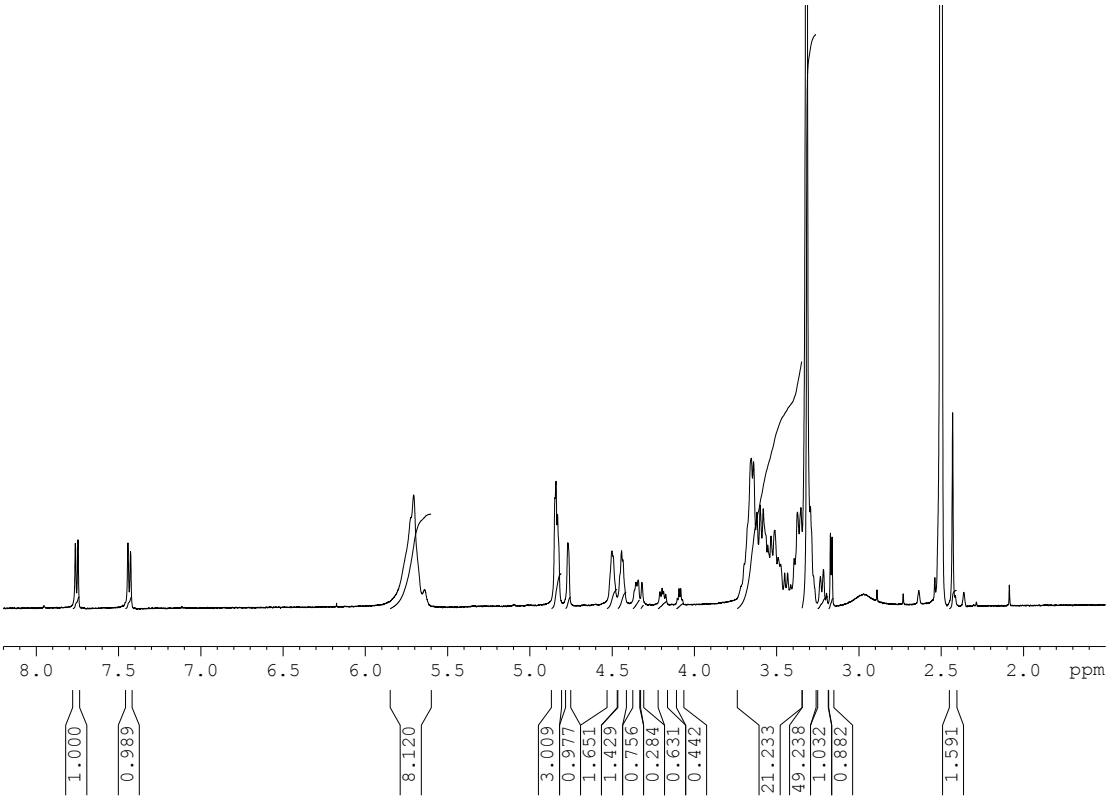

A51: ^{1}H NMR Spectrum - Tosyl-β-CD at 25 °C with DMSO-d_6 solvent and 128 scans obtained at a 500 MHz spectrometer frequency

Name / sorbate / pH	Mass (*) (mg)	Sorption equilibrium parameters			
		Absorbance	Q_e (mol/g)	C_e (M)	C_o(M)
AC/ PNP/ 6.00	1.0	7.20	4.09E-03	7.96E-04	1.00E-03
	1.0	6.76	3.06E-03	7.47E-04	9.00E-04
	1.0	5.11	2.71E-03	5.65E-04	7.00E-04
	1.0	3.44	2.40E-03	3.80E-04	5.00E-04
	1.0	2.57	2.32E-03	2.84E-04	4.00E-04
	1.0	1.71	2.22E-03	1.89E-04	3.00E-04
	1.0	0.890	2.03E-03	9.83E-05	2.00E-04
	1.0	0.281	1.38E-03	3.10E-05	1.00E-04
	1.0	0.214	1.33E-03	2.36E-05	9.00E-05
	1.0	0.169	1.23E-03	1.86E-05	8.00E-05

(*) measured to ± 0.1 mg sensitivity

A52: Sorption equilibrium parameters for AC with PNP at pH = 6.00 and 25 °C

Name / sorbate / pH	Mass (*) (mg)	Sorption equilibrium parameters			
		Absorbance	Q_e (mol/g)	C_e (M)	C_o(M)
AC / PNP /6.00	1.0	7.40	3.29E-03	8.18E-04	9.82E-04
	2.0	6.61	2.70E-03	7.30E-04	1.00E-03
	3.0	5.70	2.47E-03	6.30E-04	1.00E-03
	4.0	4.86	2.32E-03	5.37E-04	1.00E-03
	5.0	3.77	2.33E-03	4.17E-04	1.00E-03
	6.0	2.73	2.33E-03	3.02E-04	1.00E-03
	7.0	2.23	2.15E-03	2.46E-04	1.00E-03
	8.0	1.55	2.07E-03	1.71E-04	1.00E-03
	9.0	0.960	1.99E-03	1.06E-04	1.00E-03
	10.0	0.690	1.85E-03	7.62E-05	1.00E-03
	12.0	0.311	1.61E-03	3.43E-05	9.99E-04
	14.0	0.126	1.41E-03	1.39E-05	9.99E-04

(*) measured to ± 0.1 mg sensitivity

A53: Sorption equilibrium parameters for AC with PNP at pH = 6.00 and 25 °C

Name / sorbate / pH	Mass (*) (mg)	Sorption equilibrium parameters			
		Absorbance	Q_e (mol/g)	C_e (M)	C_o(M)
AC / PNP /10.00	1.0	0.950	6.78E-04	5.44E-05	8.83E-05
	2.0	0.481	6.05E-04	2.75E-05	8.80E-05
	4.0	0.096	4.08E-04	5.53E-06	8.80E-05
	5.4	0.040	3.16E-04	2.32E-06	8.80E-05
	6.2	0.018	2.81E-04	1.06E-06	8.80E-05
	7.3	0.012	2.39E-04	7.21E-07	8.80E-05
	8.1	0.008	2.16E-04	4.92E-07	8.80E-05
	9.3	0.000	1.89E-04	3.43E-08	8.80E-05

(*) measured to ± 0.1 mg sensitivity

A54: Sorption equilibrium parameters for AC with PNP at pH = 10.00 and 25 °C

Name / sorbate / pH	Mass (*) (mg)	Sorption equilibrium parameters			
		Absorbance	Q_e (mol/g)	C_e (M)	C_o(M)
AC-β-CD [1:10:10(9)] / PNP /6.00	1.4	8.04	1.60E-03	8.88E-04	1.00E-03
	1.0	7.44	1.56E-03	8.22E-04	9.00E-04
	1.1	5.77	1.14E-03	6.38E-04	7.00E-04
	1.0	4.13	8.74E-04	4.56E-04	5.00E-04
	1.0	3.25	8.19E-04	3.59E-04	4.00E-04
	1.1	2.43	5.74E-04	2.68E-04	3.00E-04
	0.9	1.61	4.92E-04	1.78E-04	2.00E-04
	1.0	0.776	2.86E-04	8.57E-05	1.00E-04

(*) measured to ± 0.1 mg sensitivity

A55: Sorption equilibrium parameters for AC-β-CD [1:10:10(9)] with PNP at pH = 6.00 and 25 °C

Name / sorbate / pH	Mass (*) (mg)	Sorption equilibrium parameters			
		Absorbance	Q_e (mol/g)	C_e (M)	C_o(M)
ACPDICD / PNP /6.00	1.0	0.628	2.13E-04	6.93E-05	8.00E-05
	1.0	0.432	2.46E-04	4.77E-05	6.00E-05
	1.0	0.265	2.15E-04	2.92E-05	4.00E-05
	1.2	0.108	1.35E-04	1.19E-05	2.00E-05
	1.0	0.018	1.41E-04	1.93E-06	9.00E-06

(*) measured to ± 0.1 mg sensitivity

A56: Sorption equilibrium parameters for ACPDICD with PNP at pH = 6.00 and 25 °C

Name / sorbate / pH	Mass (*) (mg)	Sorption equilibrium parameters			
		Absorbance	Q_e (mol/g)	C_e (M)	C_o(M)
AC-β-CD [1:10:10(9)] / MB /8.40	1.0	5.46	4.15E-04	6.93E-05	9.00E-05
	1.1	4.32	2.77E-04	5.48E-05	7.00E-05
	1.0	2.82	2.85E-04	3.57E-05	5.00E-05
	1.0	1.50	2.20E-04	1.90E-05	3.00E-05
	1.0	0.459	8.48E-05	5.76E-06	1.00E-05
	1.0	0.049	4.89E-05	5.55E-07	3.00E-06

(*) measured to ± 0.1 mg sensitivity

A57: Sorption equilibrium parameters for AC-β-CD [1:10:10(9)] with MB at pH = 8.40 and 25 °C

Name / sorbate / pH	Mass (*) (mg)	Sorption equilibrium parameters			
		Absorbance	Q_e (mol/g)	C_e (M)	C_o(M)
ACPDICD / MB /8.40	1.0	4.74	5.98E-04	6.0E-05	9.00E-05
	1.0	3.76	4.46E-04	4.8E-05	7.00E-05
	1.0	2.42	3.87E-04	3.1E-05	5.00E-05
	1.0	1.02	3.42E-04	1.3E-05	3.00E-05
	1.0	0.086	1.80E-04	1.0E-06	1.00E-05
	1.0	0.049	1.69E-04	5.5E-07	9.00E-06
	1.0	0.031	1.33E-04	3.3E-07	7.00E-06
	1.0	0.022	9.58E-05	2.1E-07	5.00E-06
	1.0	0.014	5.78E-05	1.1E-07	3.00E-06

(*) measured to ± 0.1 mg sensitivity

A58: Sorption equilibrium parameters for ACPDICD with MB at pH = 8.40 and 25 °C